論文 / 著書情報
Article / Book Information

題目(和文)	Bay-位置に側鎖をもつ液晶性円盤状液晶 -合成と液晶性、電荷輸送特性の評価-
Title(English)	Self-organizing Organic Semiconductors based on Bay-substituted Discotic Liquid Crystals -Synthesis and Characterization of Liquid Crystallinity and Charge Carrier Transport Properties-
著者(和文)	劉旭影
Author(English)	Liu Xu-Ying
出典(和文)	学位:博士(工学), 学位授与機関:東京工業大学, 報告番号:甲第9651号, 授与年月日:2014年9月25日, 学位の種別:課程博士, 審査員:半那　純一,宗片　比呂夫,梶川　浩太郎,石川　謙,飯野　裕明,清水　洋
Citation(English)	Degree:Doctor (Engineering), Conferring organization: Tokyo Institute of Technology, Report number:甲第9651号, Conferred date:2014/9/25, Degree Type:Course doctor, Examiner:,,,,,
学位種別(和文)	博士論文
Type(English)	Doctoral Thesis

Self-organizing Organic Semiconductors based on Bay-substituted Discotic Liquid Crystals

-Synthesis and Characterization of Liquid Crystallinity and Charge Carrier Transport Properties-

Liu Xu-Ying

Interdisciplinary Graduate School of Science and Engineering
Dept. of Electronics and Applied Physics
Tokyo Institute of Technology

2014.8

TABLE OF CONTENTS

Chapter 1

General introduction

Inorganic Si-based and Ge-based semiconductors, SiO_2 insulators, and metals such as Al and Cu have been the backbone of the semiconductor industry over the past 40 years.[1] However, from the end of the last century, facing the problems of high-cost and resource exhaustion, such inorganic semiconductors are experiencing the inevitable low ebb.

In recent two decades, consideration of requirement of large-area electronics, a growing research effort has been made in amorphous oxide-semiconductor systems (like In-Ga-Zn-O) [2] and organic electronics [3]. The former prepared by pulse laser deposition exhibits the mobility of 0.1 - 10 cm^2/Vs (higher than a-silicon), leading a big progress in modern electronics, while the lateral also was considered to improve the semiconducting, conducting, and light emitting properties of organics (polymers, oligomers) and hybrids (organic–inorganic composites) by using novel preparation strategies and self-organization techniques.[3] Performance improvements, coupled with the ability to process these “active” materials at low temperatures over large areas on materials such as plastic or paper, may provide unique technologies and generate new applications and form factors to address the growing needs for pervasive computing and enhanced connectivity. [4]

There are, basically, two reasons for this phenomenon: on the applied research side, organic semiconductors, specifically like π-conjugated materials, have seen significant development owing to their potential application to future-generation ultrathin, large-area, and/or flexible devices consisting of, for instance, organic field-effect transistors (OFETs), [5] organic light-emitting diodes (OLEDs), [6] and organic photovoltaics (OPVs), [7] which can be fabricated by low-cost and low-energy processes and thus offer novel features that are different from those of conventional silicon technologies; on the basic research side, π-conjugated materials are

fascinating systems in which a rich variety of new concepts have been uncovered to exploit the interplay between their π -electronic structure and their geometric structure so as to improve device's performance. In particular, the most essential parameter is the charge carrier mobility in these materials, which determinates in a high degree the successful application of the compounds, which is also formidable tool to probe the basic structure–performance relationships that govern the physics and chemistry of organic semiconductors. [8]

At the beginning, let's briefly review the development of organic semiconductors, namely, category based on molecular weight and crystal type. In fact, it is easy to understand that a clear cut-edge emerged when people found organic semiconductors with self-organization property, such as liquid crystals. In contrast to self-organizing semiconductors, conventional organic semiconductors don't have any such property.

1-1 Conventional organic semiconductors

In the early time, organic semiconductor, anthracene, firstly as photoconductor was used in Xerographic copier. However, according to the actual standard, such organic semiconductor didn't have absorbance in visible region, so led to low efficiency. Here, the reported photogeneration efficiency was 10^{-4}. The first commercial organic photoconductor was based on a charge-transfer complex between poly (vinylcarbazole) and trinitrofluorenone. Subsequently, Kodak produced a thiapyrylium salt, opening the door of developing an aggregated photoconductor. In practice, high performance devices require not only good electrical property, and also stable thermal property. Some of large π -conjugated systems, like metal-containing phthalocyanines (such as CuH_2P), can meet the stringent demands for the practical application. Moreover, phthalocyanines exhibit very wide optical absorption even up to 800nm, and have fast photoresponse, thus acting as an IR photoconductor for diode laser printers.

Generally speaking, conventional organic semiconductors can be broadly

classified into two categories: small molecules or oligomers (usually processed in vacuum) and polymers (usually processed by wet chemical techniques), as shown in Figure 1-1. However, lots of evidences have proved these materials can't be applied in industrial process. For instances, small molecules, even if showing high mobility over $1cm^2V^{-1}s^{-1}$, have to be deposited using vacuum sublimation techniques, which prevents from fabrication of large-area electronics, [9] while polymers just exhibit mobility ranging from 10^{-6} to 10^{-4} $cm^2V^{-1}s^{-1}$, hardly meeting the requirement of modern electronic devices. [10]

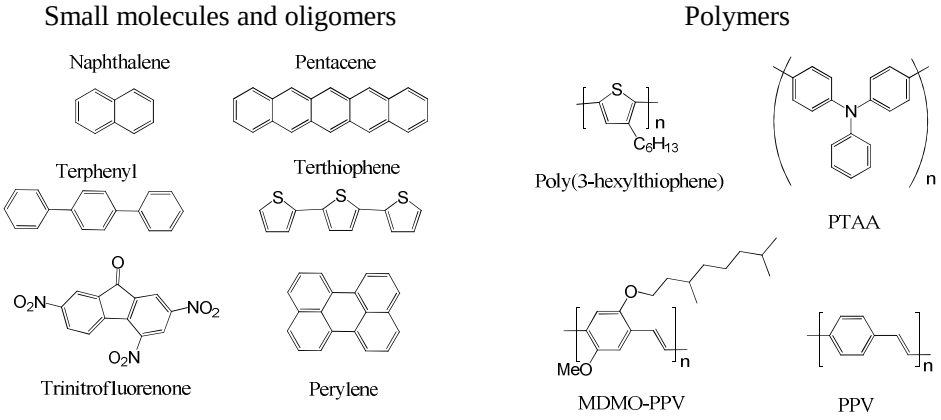

Figure 1-1 Examples of conventional organic semiconductors: small molecules and oligomers, and polymers.

1-1-1 Small molecules and oligomers

In the earlier researches, small molecular organic semiconductors mainly were studied and used to form thin films through vacuum sublimation, thus leading to the formation of molecular single crystals or amorphous state. The materials mainly include naphthalene, anthracene, tetracene, triphenylamines, perylenes, tetrathiafulvalenes, and fullerenes, and so on. Charge carrier transport mobility strongly depends on not only the nature of molecules themselves, and also the order of molecular arrangement.

Actually, the low-temperature results have shown that the possibility of band-like

transport occurred in this highly ordered single crystal. Take an instance, at low temperature about 10K, single crystal naphthalene exhibited much higher intrinsic hole mobility even up to 400$cm^2V^{-1}s^{-1}$ under 3KV/cm shown in Figure 1-2. Electron mobility was detected to be 24.5$cm^2V^{-1}s^{-1}$ at 22.5K, which didn't exhibit any electric field dependence. These properties clearly confirm the presence of a band-like transport in such single crystals.

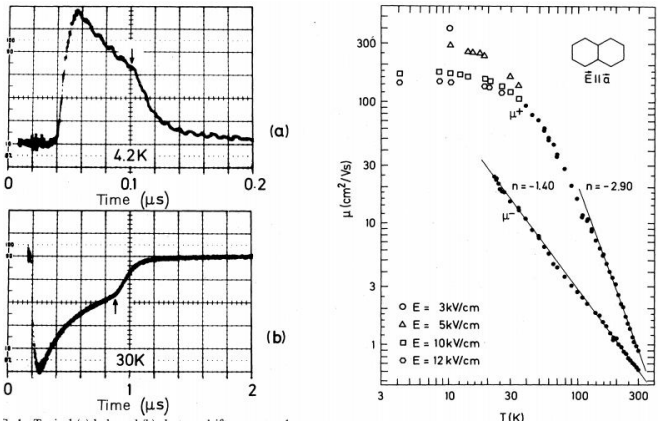

Figure 1-2 Typical positive at 4.2K and negative at 30K photocurrent (left) and temperature-dependent mobility (right)

In contrast to high mobility in single crystal, charge carrier mobility in amorphous compounds, due to slow hopping rate between the adjacent molecules, was found to be quite low, as described above. As one of famous organic semiconductors, triphenylamine-based compounds, such as the prototypical 4, 4'-bis(N-m-tolyl-N- phenylamino) biphenyl (TPD) molecule, have been researched for long period as organic photoconductors in the Xerox industry. They have already been extensively employed in OLED as hole-transporting materials, in which the amorphous film was formed through vacuum-deposited method. The figure 1-3 shows that the hole mobility was estimated to be 2-3$\times 10^{-3}$ cm^2/Vs at room temperature. [11]

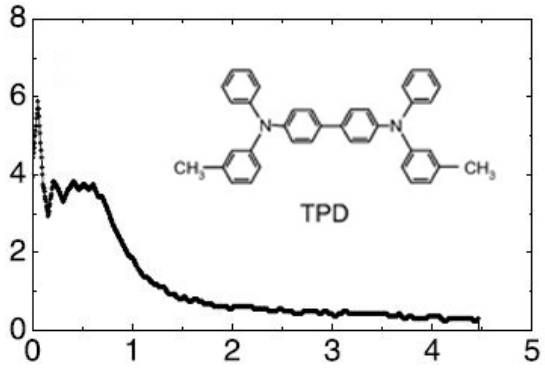

Figure 1-3 Molecular structures of TPD and typical transient photocurrent

Similarly, n-type perylene diimide derivatives are typical organic semiconductors for electron-transporting, due to quite low LOMO energy level around 4eV. The title compound N, N-bis(2-phenethyl)-perylene- 3,4:9, 10-bis(dicarboximide) (PECI) was sublimated to substrate to form a thin film, where the electron transport mobility was measured by TOF technique. In the research, electron mobility ranging from 10^{-4}-$10^{-3}$$cm^2$/Vs was achieved as exhibited in Figure 1-4. [12]

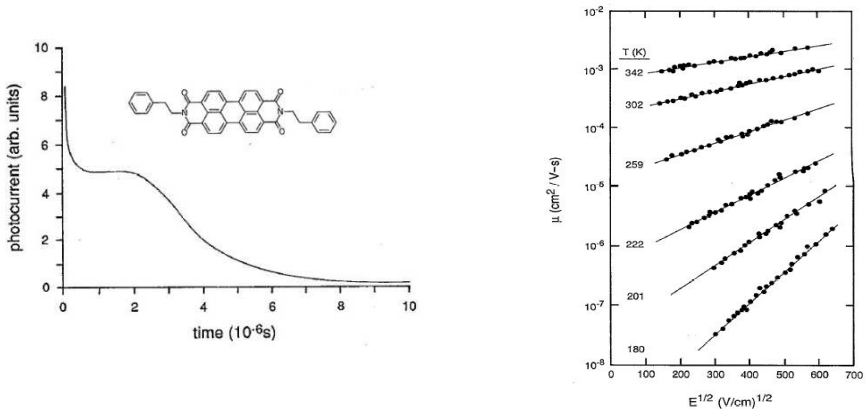

Figure 1-4 The molecular structure of N, N-bis(2-phenethyl)-perylene- 3,4:9, 10-bis(dicarboximide) (PECI), its transient photocurrent and Logarithm of the mobility vs $E^{1/2}$, parametric in T.

From the above discussion, it is obvious that charge carrier mobility in small molecules strongly relies on the order of molecular orientation. In single crystals, mobility is two or three orders of magnitude higher than that in polycrystals and

amorphous states.

On the other hand, oligomers also were studied widely for organic semiconductors, like oligothiophene, tetracene and pentacene. For an instance, tetracene exhibited high hole mobility by time of flight technique over 10^0 $cm^2V^{-1}s^{-1}$ in single crystal, 10^{-3} $cm^2V^{-1}s^{-1}$ in polycrystalline state and 10^{-4} $cm^2V^{-1}s^{-1}$ in amorphous state, which reveals that grain boundaries and molecular misorientation are detrimental to charge carrier transport.

Oligo polydithienopyrroles (DTP) as a new unit in conjugated materials have received attention because of its planar structure, extended π-conjugation across the fused rings and the N－H bond, which can be easily substituted by various functional groups as shown in Figure 1-5. [13]

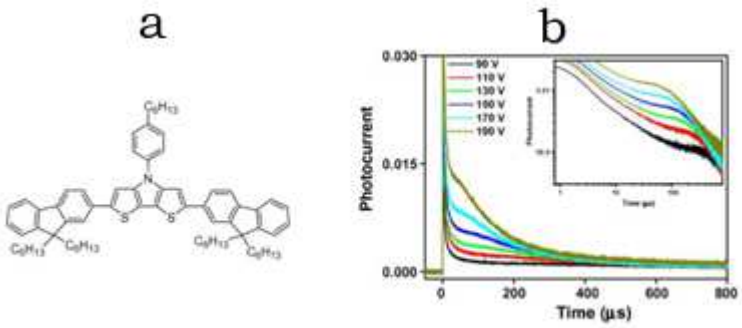

Figure 1-5 Molecular structure of oligomer (DTP-FLU) and its transient photocurrent

This material formed polycrystalline film, in which charge carrier transport was measured in time of flight (TOF), and the transit time t_T, for the arrival of carriers was readily obtained from the inflection point in the double logarithmic plot of photocurrent versus time. At 298 K, the hole mobility was found to be 7.7×10^{-6} cm^2V^{-1} s^{-1} at an applied electric field of 2.9×10^5 V/cm. The hole mobility was found to have positive temperature dependence, which illustrates the typical hopping mechanism of charge transport in DTP-FLU. Generally speaking, the transport of charge carriers in conjugated molecular compounds occurs via hopping between the localized sites on individual molecules.

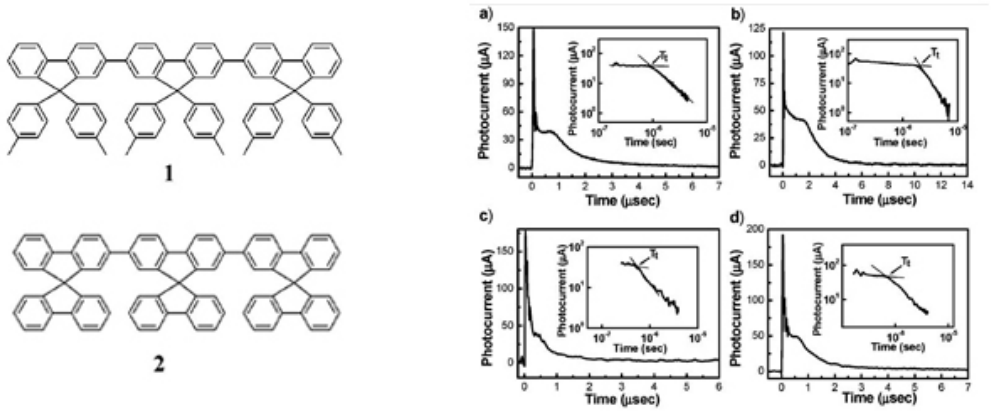

Figure 1-6 Chemical structures of ter(9,9-diarylfluorene)s: 1 and 2. Representative TOF transients for 1 and 2 samples (both 1.5um thick): (a) 1, electron, E) 3.3×10^5 V/cm, (b) 1, hole, E) 3.3×10^5V/cm, (c) 2, electron, E) 6.7×10^5 V/cm, (d) 2, hole, E) 8×10^4 V/cm. Insets of (a-d) are double logarithmic plots of (a-d).

Ter(9, 9-diarylfluorene)s 1 and 2 in Figure 1-6 were found to form amorphous films, which interestingly showed non-dispersive transient photocurrent in time of flight (TOF) measurement. The ambipolar mobility on glass/Ag (30 nm)/organic (1.5 ím)/Al (150 nm) samples was estimated to be 10^{-3}-10^{-2} cm^2/Vs. [14]

This is the first report of nondispersive electron and ambipolar transport in fluorene-based materials. Although thorough understanding still remained some questions and requires further studies, several difference can be extracted to distinguish the present ter(9,9- diarylfluorene)s from previous works.

In particular, the well-defined conjugation length of oligomeric systems may prevent formation of deep electron traps due to structural defects which easily occurs in polymeric systems.

1-1-2 Polymers

In the last two decades, molecularly doped polymers (MDPs) act as photoreceptors have been used in xerographic applications, in which the charge

carrier transport has been well investigated.

In particular, the charge carrier transport in poly (p-phenylenevinylene) (PPV) has been studied by the time-of-flight (TOF) technique. [15] Mobility of holes in PPV was determined and found to be quite dispersive character. The dispersion parameters were analyzed in the frame of a multiple trapping model. The drift mobility of the positive carriers was determined to be at the order of 10^{-5} $cm^2V^{-1}s^{-1}$ at room temperature under an electric field of 10^5 V/cm and has positive field and temperature dependence in Figure 1-7. The mobility exhibits thermally activated behavior, which shows an activation energy about 0.75 eV at zero field. This result clearly points out that the charge carrier transport in PPV can be understood through a polaron transport.

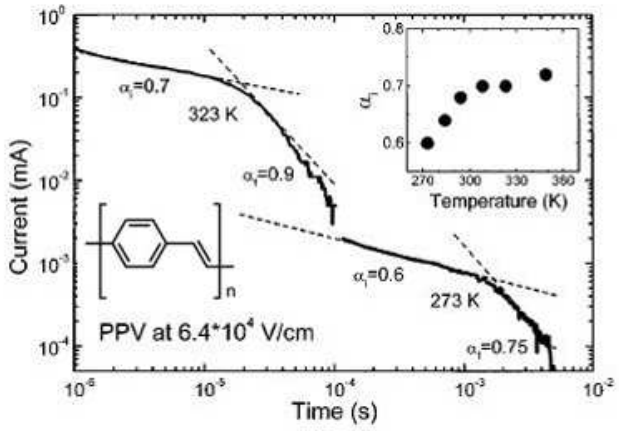

Figure 1-7 Molecular structure of PPV and transient photocurrent under the electric field of 6.4×10^4V/cm

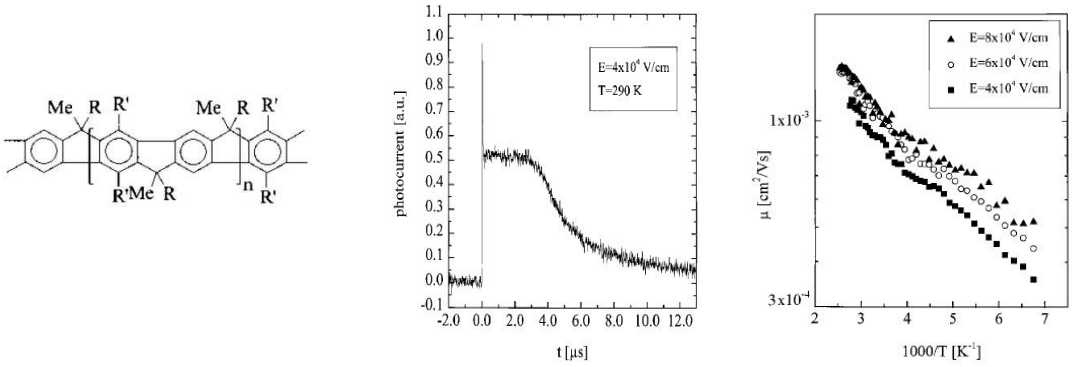

Figure 1-8 the chemical structure of the MeLPPP (R: 1,4-C_6H_4-n-$C_{10}H_{21}$; R': n-C_6H_{13}). Photocurrent transient of the ITO/MeLPPP/Al sample after excitation through the ITO

anode with light pulses of 450 nm at 290 K and an applied electric field of 4×10^4 Vcm^{-1}. The hole mobility is 8×10^{-4} cm^2V^{-1} s^{-1}. Arrhenius plot of the mobility of the MeLPPP at different applied electric fields.

The reduced influence of disorder in MeLPPP leads to non-dispersive charge carrier transport and unusually large hole mobilities exhibited in Figure 1-8 compared to PPV and its derivatives. [16] The greatly improved hole mobility of MeLPPP offers further hope that fast-response polymer light-emitting diodes and electrically driven polymer lasers can be developed, for which high mobilities and high injection rates are critical factors.

1-2 Self-organizing organic semiconductors based on liquid crystals

Through molecular self-organization properties organic materials can form ordered structures, thereby enhancing charge carrier transport. There are many intermolecular interactions involve in molecular self-organization, such as H-bond, [17] S-S interaction [18] and super-amphiphobic nature [19] and π - π interaction [20] as well.

Thermotropic liquid crystals, which mainly use π - π interaction to form long-range order structure have been known for one centuries. [21] However, charge carrier transport property was just reported 20 years ago. [22] In that time, charge mobility measured by time of flight in the typical discotic liquid crystalline triphenylene derivtaives was firstly reported in Haarer group. [22] And then three years later, in Hanna group, charge carrier mobility in calamitic liquid crystal, i.e., 2-(4′-heptyloxyphenyl)-6- dodecylthiobenzothiazole, was found. [23] Unlike discotic and calamitic liquid crystals, liquid crystalline polymers have been reported relatively fewer, due to difficulty of forming mesophase, as the consequence, charge carrier transport property was just report in very few of them. [24]

In recent years, researchers have tried to employ variety of methods for higher charge carrier mobility in liquid crystals, which actually points out the development

directions of liquid crystalline semiconductors.

1-2-1 Calamitic liquid crystals

Calamitic liquid crystals usually exhibit two types of mesophases, namely, nematic and smectic. In the nematic phase, the molecules are aligned uniaxially and don't have positional order, while in the smectic phase, molecules are aggregated in layers, which are called smectic layers, and have both translational and positional order. In SmA, SmB, SmB_{cryst}, and SmE phases, the molecules sit perpendicular to the smectic layer, on the other hand, in SmC, SmF, SmG, and SmH phases, the molecules sit tilted against the smectic layer.

In calamitic liquid crystals, charge carrier mobility strongly depends on the order of mesophases. For an instance, a liquid-crystalline photoconductor, 2-(4-octylphenyl) - 6-n- butoxynaphthalene, exhibited quite high ambipolar mobility in SmE phase up to $10^{-2}cm^2/Vs$, while in SmA phase, it just showed mobility around 10^{-4} cm^2/Vs. [25] This result, on the one hand, is consistent with the case that SmE phase has smaller intermolecular distance than SmA phase, and on the other hand reveal that high densely phase is beneficial for suppressing molecular motions, thus enhancing charge carrier transport.

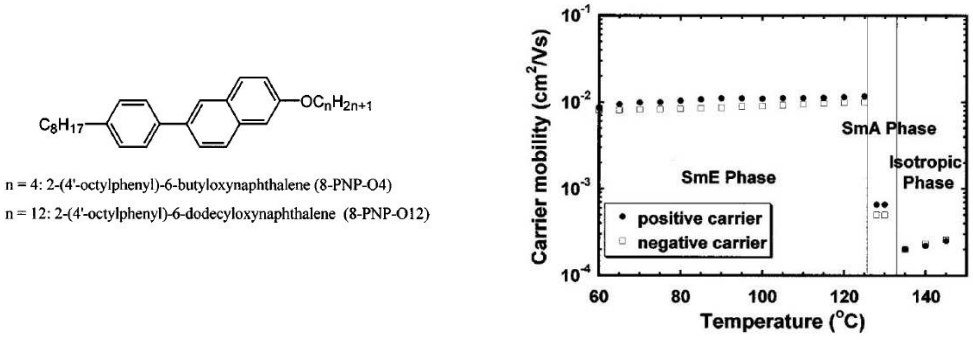

Figure 1-9 Molecular structure of 8-PNP-O4 and its mobility in each phase

Recent research in charge carrier mobility in thiophene-based calamitic liquid crystals made a big progress, in which quite high hole mobility up to $10^{-1}cm^2/Vs$ has

been achieved. [26] This result could be explained by two reason: one is the large π -conjugated core, and the other is the smaller intermolecular distance of 3.9Å. As reported, in other mesophases, the intermolecular distance is over 4.2Å.

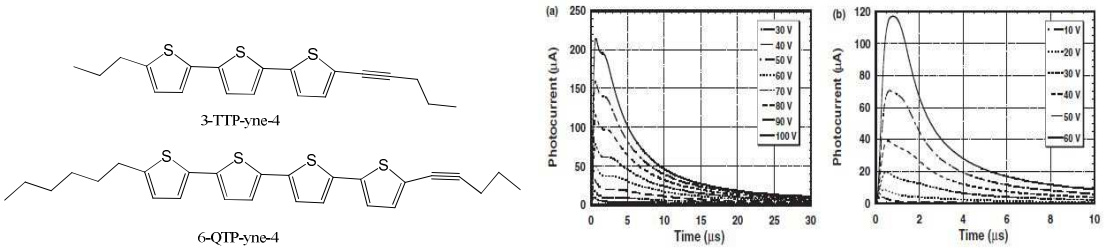

Figure 1-10 Thiophene-based calamitic liquid crystals and their transient photocurrents.

1-2 Liquid crystalline polymers

In liquid crystalline polymer [27], generally speaking, to enhance charge carrier transport also requires less defective structure and shorter π - π interaction distance.

The typical example is main-chain poly(9,9-dioctylfluorene), in which high hole mobility of 8.5×10^{-3} cm^2/Vs was obtained. [27a] When the same polymer is deposited as an isotropic film, the hole mobility was detected to be 4×10^{-4} cm^2/Vs [27b]. This result described the utility of mesophase alignment as a means to enhance carrier mobilities for conjugated main-chain liquid-crystalline polymers.

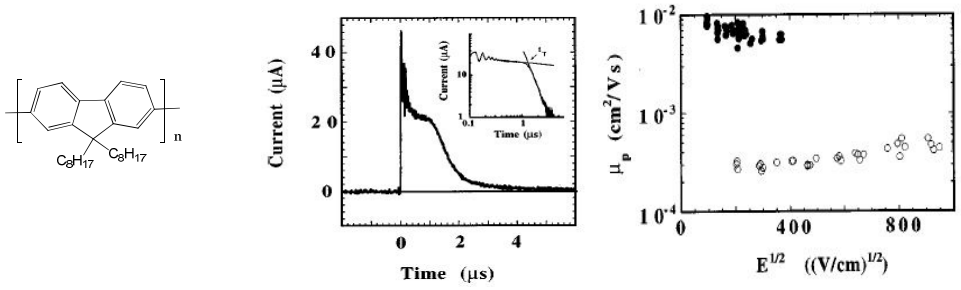

Figure 1-11 Molecular structures of poly (9, 9-dioctylfluorene) and its transient photocurrent and electric field dependence of mobility

It can be observed that mesophilic poly (9, 9-dioctylfluorene) shows one order of

magnitude higher mobility than non-mesophilic polyfluorene-based MeLPPP, which primarily indicates that ordered structure provides with less defective pathway for charge carriers, thereby enhancing conduction.

On the other hand, side-chain liquid crystalline polymer just exhibited lower charge carrier mobility than main-chain polymers. This probably can be explained that charge carrier can be fast transported along the chains in main chain polymer, while in side chain polymers charge carrier only is transported by hopping.

1-2-3 Discotic liquid crystals

1-2-3-1 Structure of discotic liquid crystals

Discotic (disc-like) molecules typically comprising a rigid aromatic core and flexible peripheral chains have been attracting growing interest because of their fundamental importance as model systems for the study of charge and energy transport and due to the possibilities of their application in organic electronic devices.

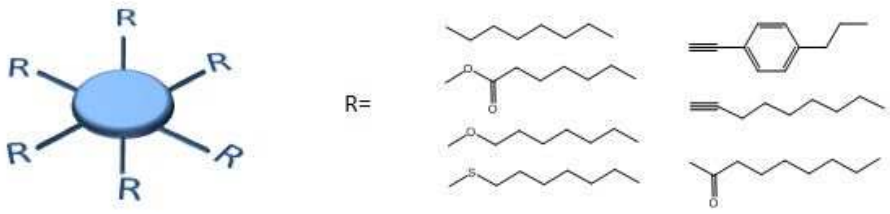

Figure 1-12 General structure for DLC molecular architecture

A majority of DLCs form columnar mesophases probably due to intense π – π interactions of polycyclic aromatic cores. The core – core (intracolumnar) separation in a columnar mesophase is usually of the order of 3.6Å, so that there is considerable overlap of π-orbitals. As flexible long aliphatic chains surround the core, the intercolumnar distance is usually 20 – 40Å, depending on the number of lateral chains and their lengths. [28]

1-2-3-2 Discotic columnar phases [29]

Discotic liquid crystals are able to exhibit typical discotic columnar phases. In the discotic columnar phase, molecules aggregate into columns. The discotic columnar phases are classified by the order of molecules in the intra-column, and the order of inter-columns in the two dimensions.

In the classification of the order of columns, there are two categories, i.e., the columnar hexagonal (Col_h) and columnar rectangular (Col_r) phases. In the Col_h, columns are aligned in a hexagonal pattern as shown in Fig. 1-3 (b). In this Col_h phase, the vertical alignment of the columns (homeotropic alignment in general) does not have retardation. Thus, it is easy to confirm the alignment by observation with a polarized optical microscope, in which we just can see dark in the whole visible region. In the Col_r, columns are aligned in a rectangular pattern, as shown in Fig. 1-3 (c). And also, in this Col_r phase, the columns are tilted in the most cases. Thus, the homeotropic alignment has retardation.

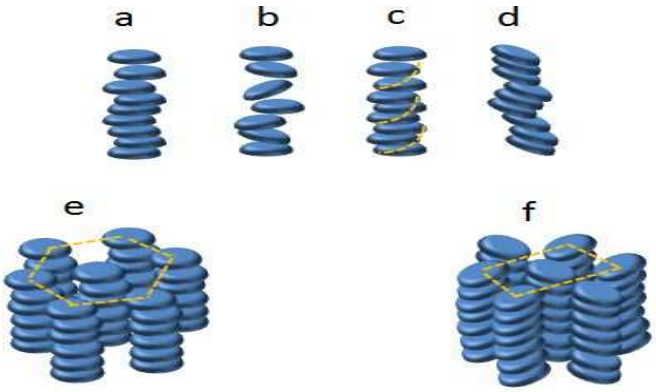

Figure1-13 Different kinds of columnar structures formed by discotic mesogens: (a) ordered column, (b) disordered columns, (c) helical column, and (d) tilted column. These self-assembled columns selforganize into different types of 2D columnar lattices (e: hexagonal columnar phase; f: rectangular columnar phase).

In the classification of the order intra-column, there are four categories, the columnar disordered (Col_d) phase, the columnar ordered (Col_o) phase, the columnar plastic (Col_p) phase, and the Helical (H) phase. In the Col_d phase, the position of

molecules in column is disordered, so the X-ray diffraction pattern does not have the peak in a wide angle. In the Col_o phase, the molecules in column have a long-range orientational order but the molecules can move a little, so the X-ray diffraction pattern has a broad peak in the wide angle. In the Col_p phase, the molecules in the column have a long range order and the molecules cannot move in a column, so the X-ray diffraction pattern has some sharp peaks at a wide angle. In the H phase, the molecules in column are aligned in hexagonal-like pattern, so this phase has a three dimensional structure like a crystal.

1-2-3-3 Conductivity in discotic liquid crystals [30]

DLCs, like any other organic molecule, are insulators in pure form due to the large energy gap and low intrinsic charge concentration. However, they can be made conducting by generating charges via chemical or photochemical doping. The columnar phase provides a facile path for the movement of generated charges. As the molecules are packed closely, charges can migrate easily via hopping from one molecule to another. Due to the 1D stacking of molecules in the columnar phase, charge migration in these materials is expected to be quasi-1D. Conductivity along the columns in columnar mesophases has been reported to be 3 orders of magnitude greater than in the perpendicular direction. [31]

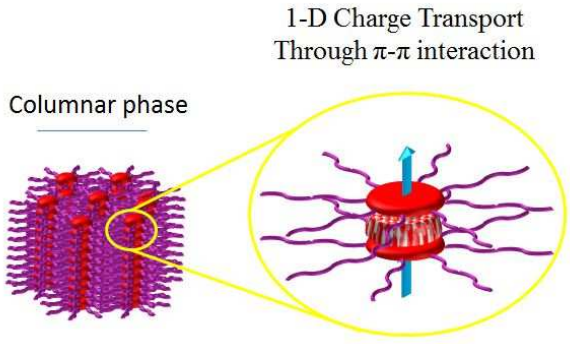

Figure 1-14 One-dimensional charge transport in a columnar phase.

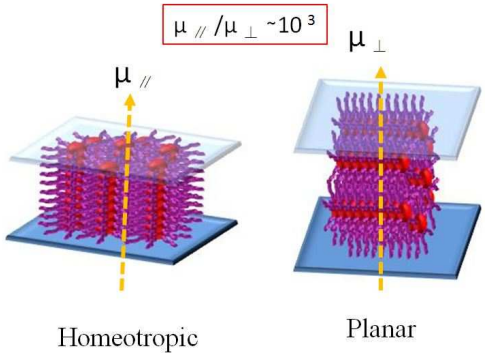

Figure 1-15 The conductivity difference in the direction of columnar axis and the vertical direction

1-2-3-4 charge carrier transport mobility

As discussed above, charge carrier transported in dicotic columnar phase has to go along the columnar axis direction, where the overlap of π - π occurs. In the case, the charge carrier mobility was expected to be quite high.

In fact, there are several techniques for measuring charge carrier mobility in discotic liquid crystals, namely, time of flight (TOF) technique, Pulse-Radiolysis Time-Resolved Microwave Conductivity Technique (PR-TRMC), space charge limited current (SCLC) method and field effect transistor method.

Consideration of measuring long-range intrinsic charge carrier transport in homeotropic columnar phase of discotic liquid crystals, the time of flight technique usually can meet well the requirement. [31]

The earliest report about charge carrier mobility of discotic liquid crystals by TOF was proposed in the 1990s in a DLC triphenylene derivative, hexapentyloxytriphenylene (H5T), which showed hole mobility of $10^{-3}cm^2/Vs$. [22] After that, another triphenylene derivative of hexahexyloxytriphenylene (H6T) with hole mobility of $3\times10^{-4}cm^2/Vs$ was reported. [32] When triphenylene with $OC_{11}H_{23}$ groups (H11T), the mobility is around $10^{-4}cm^2/Vs$, 20 times lower than H5T. [33] The decrease of hole mobility from H5T to H11T can be explained that longer side chains causes stronger molecular motions in discotic columnar phases.

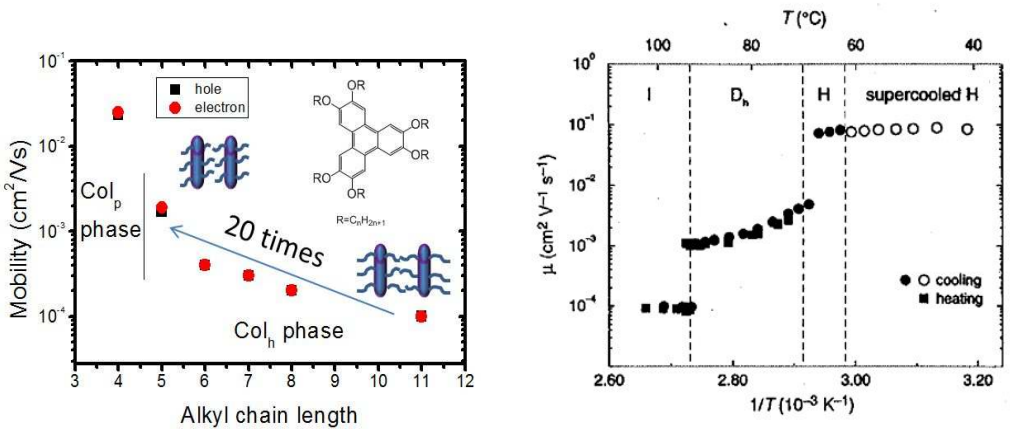

a) b)

Figure 1-16 Side chain length dependence of charge carrier mobility in triphenylene derivatives (a) and temperature dependence of charge carrier mobility in hexahexylthiotriphenylene (HHTT)

For further investigation of higher mobility in discotic columnar phases, various cores with kinds of side chains have been prepared and characterized in terms of charge carrier transport. One of the most effective strategies to achieve high mobility in discotic columnar phases is to suppress molecular motions, namely, translational and vertical, as well as rotational. [34] For examples, in highly ordered phase, the Col_{hp} phase of hexabutyloxytriphenylene (H4T), the hole mobility is 1×10^{-2} cm^2/Vs was determined. [35] And also, in the H phase of hexahexylthiotriphenylene (HHTT), the hole mobility came up to 0.1 cm^2/Vs, the highest in all triphenylene analogues. So, it is obvious that in discotic columnar phases the carrier mobility strongly depends on the order of phase.

However, in some literature, people thought that larger core will result in higher charge carrier mobility, due to stronger π - π interaction. But, the data from experiment told us that this conclusion is invalid. For instances, discotic liquid crystalline phthalocynine derivatives in columnar phase exhibited hole mobility to be 10^{-3}cm^2/Vs, [36] which almost at the same order with H5T, although phthalocyanine has much large core size than triphenylene. Another DLC hexabenzocoronene, in which 13 benzene rings are contained, couldn't exhibit any typical transient photocurrent in

TOF measurement, because it only forms columnar phase with edge-on alignment (columnar axis is parallel to the electrodes). [37]

Based on above discussion, the effect factors for charge carrier transport can be summarized and shown below:

(1) The local molecular arrangement should be optimal

Since charge transport in discotics is described by the hopping formalism according to Marcus theory, the charge transfer between neighboring molecules within a column strongly depends on their relative positions and orientations. The probability for charge hopping would be maximal when the intermolecular separation is minimal, with the polyaromatic cores being on top of each other (no lateral slide) and the mutual orientation being cofacial [34b].

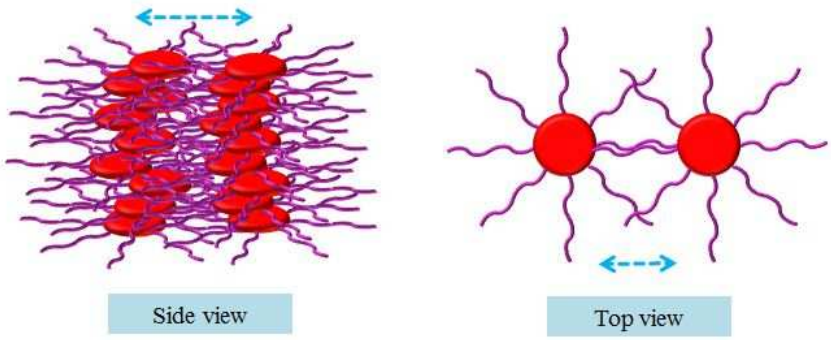

Figure 1-17 Schematic illustration of homeotropic discotic columnar alignment with molecular slipping.

(2) The number of chemical impurities and structural defects must be minimal on a large spatial scale

Since one dimensional charge transport is limited by the slowest transfer rates. Chemical impurities and structural defects will form deep traps for charge carrier, directly increasing the transient time.

(3) The thermal motion of the molecules perturbs the rather “soft” charge-transport system

Charge transfer between neighboring molecules, which is on the picosecond time scale, is hindered by the slow whole-body movements of the discs on similar and slower time scales [34b].

This study mainly focuses on finding a general molecular design strategy for discotic liquid crystals, which can be applied in kinds of discotic cores to form homeotropic columnar mesophases with high charge carrier transport mobility.

1-3 Enhancement of charge carrier transport in homeotropic discotic columnar mesophases

As discussed above, high charge carrier mobility in discotic columnar phases measured by TOF technique requires well-defined homeotropic alignment, less defective structure and stabilized molecular arrangement.

There have been lots of publications reporting how discotic liquid crystals can align homeotropically, mainly including two types: the one is to use modified substrate for induced homeotropic columnar alignment; [38] the other one is to exploit discotic liquid crystals by molecular engineering. [39] The former is based on the interaction between molecules and substrate, while the lateral relatively relay on the nature of molecules. So, the lateral usually requires unique molecular structures. In consideration of charge carrier transport measurement, the lateral exhibits much more advantages, like independence of electrodes (molecular orientation) and spontaneity in columnar alignment.

In the homeotropic columnar alignment, less defective structure and stabilized molecular orientation will bring out high speed charge carriers through the columns between two electrodes. Here, let's briefly introduce the recent progress regarding of how to stabilize columnar structure in hoemeotropic columnar mesophase for high charge carrier mobility through subtle interplay between molecules.

In homeotropic columnar phases, enhacement of chage carrier transport mainly has been made through suppress molecular thermal motions. In fact, two strategies can be done to achieve this goal: the one is to use intermolecular interaction within columns, while the other is to use intercolumnar factors.

1-3-1 Using intermolecular interaction to stabilize the columnar phase

Intermolecular interactions within columns have been considered as tools to suppress molecular motions in columnar mesophase, like H-bond, S-S interaction, and so on.

A. Demenev, et al., reported a discotic liquid crystalline H-Bonded Benzotristhiophene Derivative, whose columnar mesophases cover a temperature range from −50 to 280℃. Charge carrier mobility measured by TOF method is about 10^{-3} cm^2 V^{-1} s^{-1} for electron in both hexagonal columnar mesophases. [40]

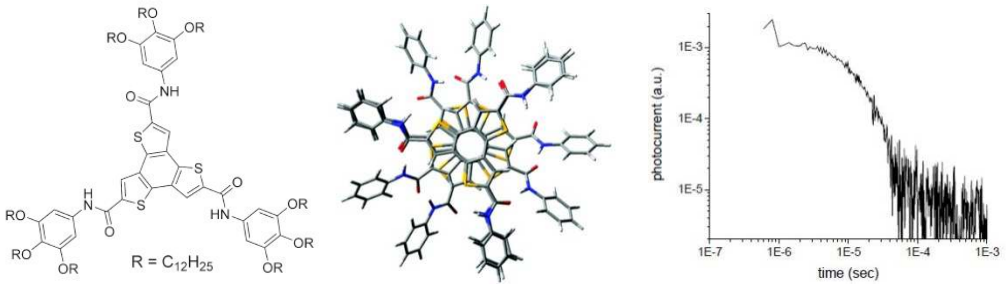

Figure 1-18 Molecular structure of H-Bonded Benzotristhiophene Derivative and its negative transient photocurrent in columnar phase

Recently, Q. Xiao, et al., prepared kinds of propeller-shaped regioisomers of fused oligothiophenes, which was said to form columnar phase with S-S interaction. And also, in each LC column, well-organized intermolecular S–S contacts are developed triple-helically along the columnar axis with a helical pitch of 4.04 nm. They measured charge carrier transport using TOF technique, and found in columnar phases ambipolar mobility to be 10^{-2} cm^2 V^{-1} s^{-1}. [41]

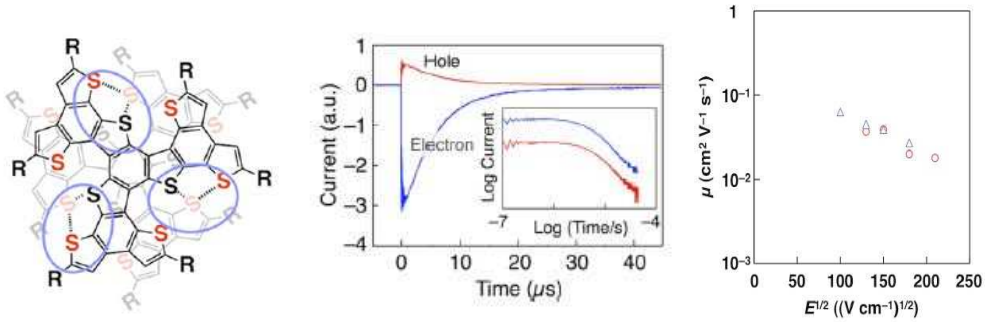

Figure 1-19 Molecular structure of a propeller-shaped regioisomer of fused oligothiophenes, its transient photocurrent and electric field dependence of mobility

From the two reports, it is clear that to some extent columnar structure can be stabilized by introduction of intermolecular interaction within columns, thereby enhancing charge carrier transport. Especially, the S-S interaction made a good molecular arrangement in columnar phase, which led a higher ambipolar mobility over $10^{-2}cm^2V^{-1}s^{-1}$, one order of magnitude higher than usual.

1-3-2 Using physical gels to stabilize columnar structure

Y. Hirai, et al., prepared discotic liquid-crystalline (LC) physical gels by combining the self-assembled fibers of a low-molecular-weight gelator and semiconducting LC triphenylene derivatives. [42]

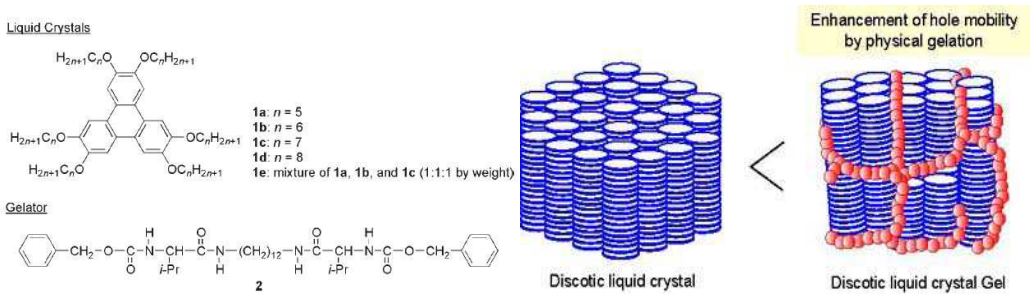

Figure 1-20 Molecular structures of discotic LC physical gels and schematic illustration of columnar structures

The hole mobilities of the discotic LC physical gels measured by a time-of-flight method become higher than those of LC triphenylenes alone. For example, when n=8, the mobility increased by 23 times. The introduction of the finely dispersed networks of the gelator in the hexagonal columnar phases was reported to strongly affect the molecular dynamics of the liquid crystals, thereby resulting in the enhancement of hole transporting behavior in the LC gel state.

1-3-3 Incorporation of side chains into bay positions to form densely packed columnar phase

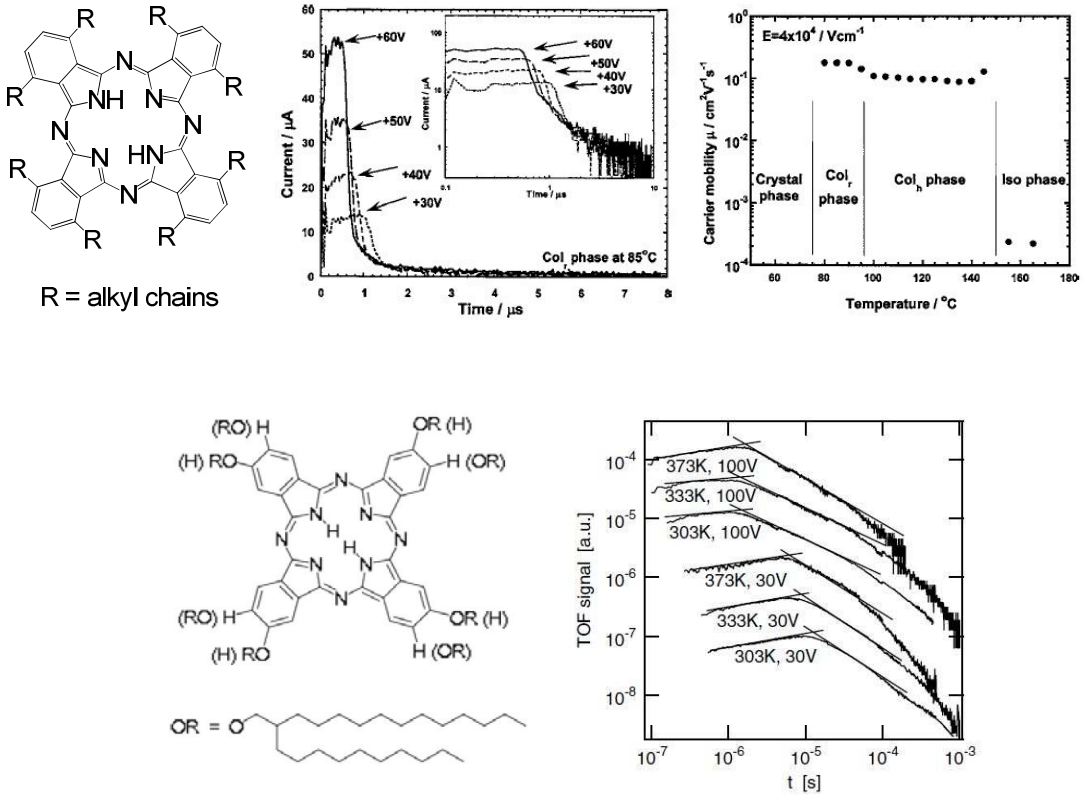

Figure 1-21 Molecular structure of bay-substituted phthalocyanine, its transient photocurrent and temperature-dependence of mobility; Molecular structure of peri-substituted phthalocyanine and its transient photocurrent

In Hanna Lab. previous researches revealed that very high charge carrier mobility over 0.1cm^2/Vs could be determined in bay-substituted phthalocyanine

derivatives even in disordered columnar phases. This mobility is almost 100 times high than that determined in peripheral-substituted DLC phthalocyanines which exhibited ordered columnar phases. [43]

Importantly, this is the first report that charge mobility in discotic liquid crystalline columnar mesophase over $10^{-1}cm^2/Vs$. Such high mobility could be obtained, probably originated from the below reasons:

1) Easy access to isotropic phase making thermal self-healing for homeotropic alignment possible

2) High pure sample by recrystallization

3) Densely packed columnar structure suppressing molecular motions

Interestingly, such high mobility was determined in “disordered columnar phases”. So, from this result, several research issues can be extracted:

a) Why such high mobility could take place in “disordered columnar phases”?

b) Is it possible that high mobility can be observed in other discotic liquid crystals with bay substituents?

1-4 Objective and approach of this study

This research progress on organic semiconductors including amorphous, crystalline, and liquid crystalline small molecules and polymers has been reviewed as a background of the present research. In particular, it is highlighted that liquid crystals as self-organizing organic semiconductors are promising for device application in the future, because of high mobility ranging from 10^{-4} $cm^2V^{-1}s^{-1}$ to $0.1cm^2V^{-1}s^{-1}$ and possible control of molecular alignment. Additionally, it is pointed out that what determines the charge transport properties has not been clarified in discotic liquid crystals yet, while the recent reported results on a bay-substituted phthalocyanine derivative exhibiting high mobility over $0.1cm^2/Vs$ in disordered columnar phase actually can be a key for understanding charge carrier transport properties in discotic columnar phases. Based on these results from historical studies, the motivation and

purpose of the present study are described:

1) To address why high mobility can be determined in disordered columnar phase, but can't in ordered columnar phase; to answer a question about why such high mobility can be achieved in disordered columnar phases of bay-substituted Phthalocyanines and whether high mobility can be observed in other discotic liquid crystals bay-substituted with long alkyl chains, which can give us some idea about how the bay-substituted discotic liquid crystals are available as an organic semiconductor.

2) Generalize this molecular design concept to other types of discotic liquid crystals. In order to obtain more information about the liquid crystallinity, charge carrier transport property and molecule structure as well as molecular orientation, we attempt to prepare various bay-substituted discogens, and study their phase transition and charge carrier transport, and investigate their general characteristics.

To make these questions clear will not only let us more deeply understand charge carrier transport in discotic columnar mesophases, but also give us some ideas about how the bay-substituted discotic liquid crystals can be exploited and further possess the availablity as an organic semiconductor.

1-4-1 Investigation of bay-substituted discotic liquid crystalline phthalocyanines and tetrabenzoporphyrins

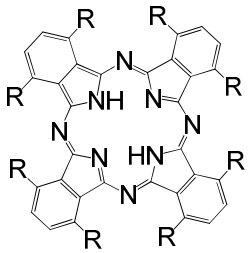

R = alkyl chains

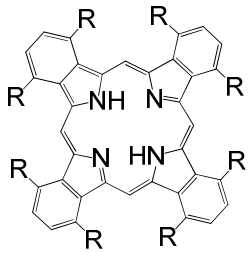

R = alkyl chains

Figure 1-22 Molecular structures of bay-substituted phthalocyanine and bay-substituted tetrabenzoporphyrin

As a reference, the analogue of phthalocyanine, i.e., tetrabenzoporphyrin, was

designed, due to their similar molecular shape. And also, both of them show quite similar chemical and physical properties, such as optical absorption and molecular arrangement in single crystal.

1-4-2 Generalization of the molecular design concept to various discotic liquid crystals

As typical example, triangular molecules usually exhibit quite perfect liquid crystal properties and behavior as good semiconducting natures. So, in the section of generalization, two types of triangular disclike cores were chosen for the generalization of this concept, namely, Hexaazatrinaphthylenes (HATNA) and truxene, which are representative and always act as model molecules for simulation of charge carrier transport. So, there have been abundant reference experimental results available for my study.

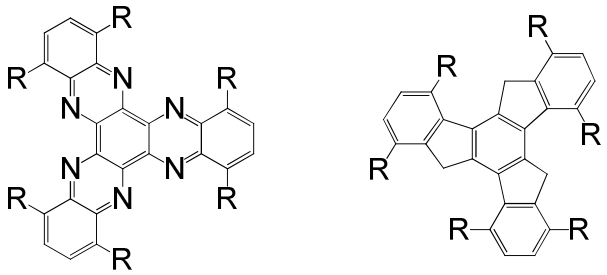

Figure 1-23 Molecular structures of typical triangular disoctic liquid crystals, Hexaazatrinaphthylenes (HATNA) and truxene with bay-located substituents

And also, it is necessarily mentioned that the planar core must be retained after introduction of bay substituents for maintaining the intrinsic electronic property. For some molecules, the incorporation of side chains into bay position probably destroys the planarity of the core, because of strong steric hindrance, like triphenylene derivative and perylene diimides.

References of Chapter 1

1. J. M. Shaw, P. F. Seidler, Organic electronics: introduction. *IBM Journal of Research and Development*, **45**, 3 (2001)

2. K. Nomura, H. Ohta, A. Takagi, T. Kamiya, M. Hirano, H. Hosono, Room-temperature fabrication of transparent flexible thin-film transistors using amorphous oxide semiconductors. *Nature*, 432, 488(2004)

3. J. Wen, G. L. Wilkes, *Chemistry of Materials*, **8**, 1667 (1996)

4. X. Duan, C. Niu, V. Sahi, J. Chen, J. W. Parce, S. Empedocles, J. L. Goldman, *Nature*, **425**, 274 (2003)

5. H. Sirringhaus, *Advanced Materials*, **17**, 2411 (2005)

6. S. Reineke, F. Lindner, G. Schwartz, N. Seidler, K. Walzer, B. Lüssem, K. Leo, *Nature*, **459**, 234 (2009)

7. L. Schmidt-Mende, A. Fechtenkötter, K. Müllen, E. Moons, R. H. Friend, J. D. MacKenzie, *Science*, **293**, 1119 (2001)

8. J. L. Brédas, J. P. Calbert, D. A. da Silva Filho, J. Cornil, *Proceedings of the National Academy of Sciences*, **99**, 5804 (2002)

9. S. R. Forrest, *Nature*, **428**, 911(2004)

10. B. Chen, S. Liu, *Synthetic metals*, **91**, 169(1997)

11. S. Naka, H. Okada, H. Onnagawa, Y. Yamaguchi, T. Tsutsui, *Synthetic metals*, **111**, 331(2000)

12. E. H. Magin, P. M. Borsenberger, *Journal of applied physics*, **73**, 787(1993).

13. M. Parameswaran, G. Balaji, T. M. Jin, C. Vijila, S. Vadukumpully, Z. Furong, S. Valiyaveettil, *Organic Electronics*, **10**, 1534 (2009)

14. C. C. Wu, T. L. Liu, W. Y. Hung, Y. T. Lin, K. T. Wong, R. T. Chen, Y. Y. Chien, *Journal of the American Chemical Society*, **125**, 3710(2003)

15. E. Lebedev, T. Dittrich, V. Petrova-Koch, S. Karg, W. Brütting, *Applied physics letters*, **71**, 2686(1997)

16. F. Laquai, G. Wegner, C. Im, H. Bässler, S. Heun, *Journal of applied physics*, **99**, 023712 (2006)

17. A. Demenev, S. H. Eichhorn, T. Taerum, D. F. Perepichka, S. Patwardhan, F. C.

Grozema, R. Klenkler, *Chemistry of Materials*, **22**,1420 (2010)

18. Q. Xiao, T. Sakurai, T. Fukino, K. Akaike, Y. Honsho, A. Saeki, T. Aida, *Journal of the American Chemical Society*, **135**, 18268 (2013)

19. J. P. Hill, W. Jin, A. Kosaka, T. Fukushima, H. Ichihara, T. Shimomura, T. Aida, *Science*, **304**, 1481 (2004).

20. T. Yasuda, T. Shimizu, F. G. Liu, Ungar, T. Kato, *Journal of the American Chemical Society*, **133**, 13437 (2011)

21. P. G. De Gennes, *Molecular Crystals and Liquid Crystals*, **7**, 325 (1969)

22. D. Adam, F. Closs, T. Frey, D. Funhoff, D. Haarer, P. Schuhmacher, K. Siemensmeyer,. Transient *Physical review letters*, **70**, 457 (1993)

23. M. Funahashi, J. I. Hanna, *Physical review letters*, **78**, 2184 (1997)

24. V. P. Shibaev, M. V. Kozlovsky, L. A. Beresnev, L. M. Blinov, N. A. Plate, *Polymer Bulletin*, *12*, 299 (1984)

25. M. Funahashi, J. I. Hanna, *Applied physics letters*, **73**, 3733 (1998)

26. M. Funahashi, J. I. Hanna, *Advanced Materials*, **17**, 594 (2005)

27. a) A. Babel, S. A. Jenekhe, *Macromolecules*, **36**, 7759 (2003); b) M. Redecker, D. D. C. Bradley, M. Inbasekaran, E. P. Woo, Applied Physics Letters, 73, 1565(1998).

28. S. Kumar, *Chemical Society Reviews*, **35**, 83 (2006)

29. S. Chandrasekhar, G. S. Ranganath, *Reports on Progress in Physics*, **53**, 57 (1990).

30. N. Boden, R. J. Bushby, J. Clements, M. V. Jesudason, P. F. Knowles, G. Williams,. *Chemical physics letters*, **152**, 94 (1988)

31. N. Boden, R. J. Bushby, J. Clements, *The Journal of chemical physics*, **98**, 5920 (1993)

32. A. Ochse, A. Kettner, J. Kopitzke, J. H. Wendorff, H. Bässler, *Physical Chemistry Chemical Physics*, **1**, 1757 (1999).

33. T. Kreouzis, K. J. Donovan, N. Boden, R. J. Bushby, O. R. Lozman, Q. Liu, *J. Chem. Phys*. **114**, 1797 (2001)

34. a) Y. Olivier, L. Muccioli, V. Lemaur, Y. H. Geerts, C. Zannoni, J. Cornil, *The Journal of Physical Chemistry B*, **113**, 14102 (2009) b) Kumar, S. Chemical Society Reviews, 35, 83(2006).

35. D. Adam, P. Schuhmacher, J. Simmerer, L. Häussling, K. Siemensmeyer, K. H. Etzbachi, D. Haarer, *Nature*, *371*, 141 (1994)

36. H. Fujikake, T. Murashige, M. Sugibayashi, K. Ohta, *Applied physics letters*, **85**, 3474 (2004)

37. A., Rybak, J. Pfleger, J. Jung, M. Pavlik, I. Glowacki, J. Ulanski, Y. Geerts, *Synthetic metals*, **156**, 302 (2006)

38. V. De Cupere, J. Tant, P. Viville, R. Lazzaroni, W. Osikowicz, W. R. Salaneck, Y. H. Geerts. *Langmuir*, ***22***, 7798 (2006); E. Pouzet, V. De Cupere, C. Heintz, J. W. Andreasen, D. W. Breiby, M. M. Nielsen, Y. H. Geerts, *Journal of Physical Chemistry Part C: Nanomaterials and Interfaces*, ***113***, 14398 (2009); T. Kajitani, Y. Suna, A. Kosaka, T. Osawa, S. Fujikawa, M. Takata, T. Aida, o-Phenylene octamers as surface modifiers for homeotropic columnar ordering of discotic liquid crystals. *Journal of the American Chemical Society*, **135**, 14564(2013).

39. N. Terasawa, H. Monobe, K. Kiyohara, Y. Shimizu, *Chemical Communications*, **14**, 1678(2003)

40. A. Demenev, S. H. Eichhorn, T. Taerum, D. F. Perepichka, S. Patwardhan, F. C. Grozema, R. Klenkler, *Chemistry of Materials*, **22**,1420(2010)

41. Q. Xiao, T. Sakurai, T. Fukino, K. Akaike, Y. Honsho, A. Saeki, T. Aida, *Journal of the American Chemical Society*, **135**, 18268(2013)

42. Y. Hirai, H. Monobe, N. Mizoshita, M. Moriyama, K. Hanabusa, Y. Shimizu, T. Kato, *Advanced Functional Materials*, **18**, 1668(2008)

43. H. Iino, J. I. Hanna, R. J. Bushby, B. Movaghar, B. J. Whitaker, M. J. Cook, *Applied Physics Letters*, **87**, 132102(2005).

Chapter 2

Experimental methods

2-1 General methods

2-1-1 Chemicals and solvents

Unless otherwise noted, all the reagents and solvents were used as received from Aldrich Chemical, Tokyo Chemical Industry, and Wako Pure Chemical Industries. Dry solvents, like dry THF, were dehydrated in a home-made equipment.

2-1-2 Purification of samples

2-1-2-1 Chromatography

Column chromatography was carried out with Wako gel silica (particle size: 200 μm). Compounds were detected by fluorescence quenching at 254 nm, self-fluorescence at 366 nm. For eluents, GC-level solvents were used without further treatment. The compositions of the eluents are given together with the retension value R_f.

2-1-2-2 Recrystallization

Through repeated recrystallization in ethanol and *n*-hexane, we are trying to remove the ionic and neutral impurities. In the last time, distilled *n*-hexane is required to remove the remained polar solvent and few impurities.

2-1-3 Inert atmosphere

Oxygen or moisture sensitive reactions were carried out in an argon atmosphere (Linde). If not mentioned specifically, reactions were degassed by bubbling a stream of argon though the reaction mixture.

2-2 Structure characterization of materials

2-2-1 Nuclear magnetic resonance spectroscopy (NMR)

NMR technique can be used to check chemical structure of organic materials. Usually, ^{1}HNMR and ^{13}CNMR are commonly used. According to the chemical synthesis, structures of all compounds in this research have been confirmed by ^{1}HNMR.

In this study, ^{1}H spectra were recorded at 25℃ on a JEOL model JNM-ECA500 spectrometer, where chemical shifts (δ in ppm) were determined with respect to tetramethylsilane as an internal reference.

2-2-2 Mass spectrometry (MS)

MS spectra are used to determine the elements of a sample, the masses of particles and of molecules, and to elucidate the chemical structures of molecules.

In this research, HRMS were obtained on a double-focusing magnetic sector mass spectrometer JEOL JMS-700.

2-3 Characterization of phase transitions

2-3-1 Differential Scanning Calorimetry (DSC)

Basically, phase transitions will result in the energy changing with exothermic and endothermic processes when the samples are heated or cooled. Differential scanning calorimetry can be utilized for quantitatively studying the thermal transitions in liquid crystalline materials, in which a liquid crystal sample and an inert reference are heated, usually in a nitrogen atmosphere, and thermal transitions in the sample are detected and measured. Most commonly, the sample holder used is a very small aluminum cup, and the reference is either an empty cup or a cup containing an inert material, such as anhydrous alumina. Sample weight varies from 0.5 to about 10 mg.

In this research, DSC 220C system, Seiko Elec., was used. The reference is an empty cup. Sample weight is around 5mg.

2-3-2 polarizing optical microscope (POM)

Polarizing optical microscope can be used to observe the formed textures by birefringence in liquid crystals upon heating or cooling. Through the observation, we can know preliminary what mesophases the liquid crystal exhibits. In particular, we can use POM texture to distinguish the columnar alignment in discotic liquid crystals. As for the homeotropic columnar alignment, the POM graphs are absolutely dark, while planar alignment will exhibit lots of birefringence.

In this study, the polarized light microscope of Nikon and the hot-stage of Mettler Toledo, FP900 thermo system were used.

2-3-3 X-ray diffraction (XRD)

Evaluation of molecular alignment and crystallinity of polycrystalline phase and liquid crystal phases of liquid crystal materials, powder X-ray diffraction is a powerful tool to be measured.

In the θ-2θ scan, the spacing is estimated from Braggs equation.

$$d = \frac{\lambda}{2\sin\theta}$$

λ is the wavelength of X-ray radiation source CuKα, 1.54 Å. θ can be extracted from the system automatically. And then, d will be calculated based on the equation.

In the measurement of discotic liquid crystals, typical powder XRD patterns are shown in the Figure 2-1. Discotic hexagonal columnar phases can be considered as a 2D order lattice. And there are two typical structures, the first one is called as ordered hexagonal columnar phase, in which adjacent molecules within columns align parallel to each other with a uniform intermolecular distance; the second is called disordered hexagonal columnar phase, in which the intermolecular distances are not uniform. The difference can be easily distinguished from XRD patterns, in which the peak appearing at large angle regions representatives the intermolecular distance.

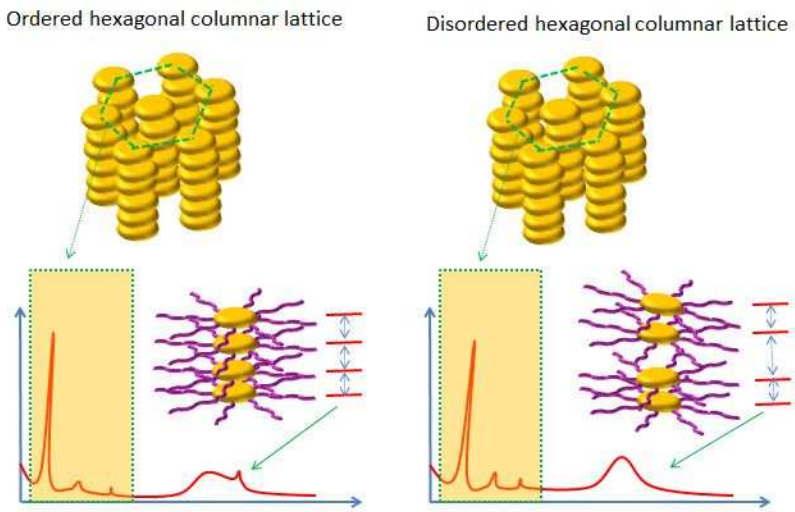

Figure 2-1 Schematic illustration of ordered and disordered hexagonal columnar lattice in discotic liquid crystals.

Through the characterization of powder XRD measurement, the phase structures, including lattice parameters shown in Figure 2-1, can be recognized.

In this study, x-ray diffraction equipment (Rigaku RAD-2B) was used.

2-4 Spectroscopy

2-4-1 Ultraviolet-visible spectrophotometer (UV)

The Ultraviolet-visible absorption spectroscopy is used for the detection and quantitative measurement of chromophores that undergo electronic transitions between different vibrational levels of the ground and excited states.

In our study, the spectrometer of Spectrophotometer 228, Hitachi was used. The range of wavelength is from190nm to 900nm. All of measurements were done in the atmosphere.

2-5 Cyclic voltammetry (CV)

Cyclic voltammetry, coupled with electronic spectrum, can be used to estimate the energy levels of materials. Here, each measurement was calibrated with the

ferrocene–ferrocenium couple (Fc/Fc^+) taking 4.8 eV as ferrocene's HOMO level. All solutions were purged with argon for 20 min before each experiment.

2-6 Preparation of liquid crystal cells

The liquid crystal cells for charactering electrical properties of liquid crystals, which are a sandwich type of cells, are made as shown in Figure 2-2 and 2-3. Electrodes materials are either indium tin oxide (ITO) or aluminum (Al). Spacers used are silica particles in a size of 5 to 15 μm.

A liquid crystalline material was capillary filled into the liquid crystal cells in the isotropic phase as Figure 2-2. The glue used for fixing the glass or quartz plates is an epoxy resin, which is available below 200℃. In Figure 2-3, thin film was fabricated by spin coating, and then electrode was deposited.

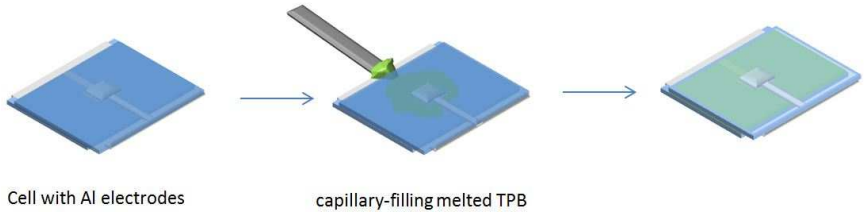

Figure 2-2 Fabrication and structure of liquid crystalline cells used for TOF measurement

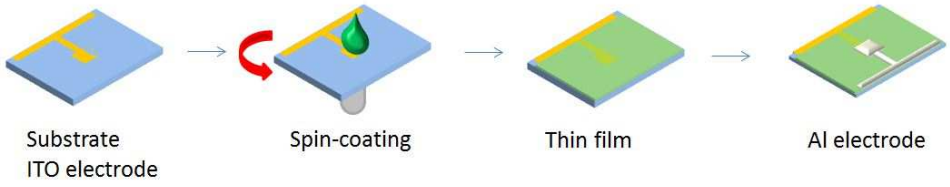

Figure 2-3 Devices fabricated for steady-state photocurrent measurement.

2-7 Evaluation of electric properties

2-7-1 Steady state dark current measurement

Steady state dark current measurement is able to characterize bulk (transport) and/or surface (injection) properties in sandwich-shaped cells, which is based IV measurement systems. [1]

In particular, when the energy levels, i.e., HOMO or LUMO, match the work function of metal electrodes to establish Ohmic contact, which leads to space charge limited current (SCLC). [2] On the one hand, by means of the method of SCLC, we can know some information about the energy levels, on the other hand, charge carrier mobility also can be estimated by SCLC methods. [3]

In this case of SCLC, high electric field or low mobility samples are used, thus leading to an excess amount of carriers injecting to the bulk from electrode. Such carriers stay near the injection electrode, resulting in very low electric field. I-V characteristics can be described as Child law in the following equation for trap free condition.

$$j = \frac{9}{8}\varepsilon_r \varepsilon_0 \mu \frac{V^2}{d^3}$$

Where d represents the thickness of thin film, $\varepsilon_r\varepsilon_0$ is dielectric constant of the organic material, μ is mobility. Based on this, the SCLC mobility is estimated from the above equation.

In this study, a source measurement unit, (Advantest R8340) was used and the steady-state dark current data collected using the home-made program on a personal computer through GPIB communication.

2-7-2 Steady state photocurrent measurement [4]

When Ohmic contact is established between a sample and an electrode, the photocurrent under steady-state illumination is described by the following equation,

$$I_p = n_P e \mu E = \alpha I_0 \Phi e \frac{\mu \tau E}{d}$$

Where α is the absorption coefficient of light, I_0 is the light intensity of unit time, Φ is the photo generation efficiency and τ is the life time of photo generated

carriers.

In this study, the measurement system for the steady-state dark and photocurrents is shown in Figure 2-4. The light source was a Xe lamp of 500 W, the UV wavelength of illuminating light was selected by the band pass filter (UVD-33S) and the on-off of light was controlled by the electromagnetic shutter.

The source measurement unit (Advantest R8340) is used and the steady state photocurrent data collected by the own-made program on a personal computer through GPIB communication.

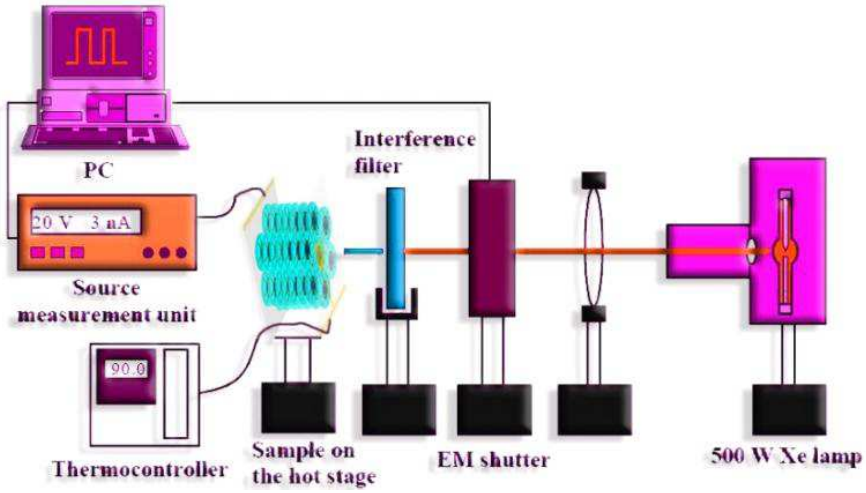

Figure 2-4 Setup for steady state photocurrent measurement, which consists of 500 W Xe lamp as an excitation light source, electromagnetic shutter, optical filters, lens, mirror, and sample hot stage.

2-7-3 Transient photocurrent measurement [4]

The transient photocurrent was measured by a conventional time-of-flight (TOF) setup, as shown in Figure 2-5. The sample is initially subject to a constant applied voltage *V* between two electrodes of the sandwich type cell in the dark; and at t = 0 a light pulse is illuminated onto the semitransparent electrode, i.e., one side of the sample, to produce a thin carrier sheet near the electrode surface of the sample. The resulting charge sheet drifts across the sample and reach to the opposite electrode along with an applied dc electric field. The transient current

flowing through the external circuit is amplified and recorded by a digital oscilloscope, which is called transient photocurrent. The duration of pulse illumination should be far shorter than a transit time, t_T of the carriers and penetration depth, d_p of illuminated light should be far smaller than a thickness of samples to meet one-carrier transport condition. The polarity of the applied field to the illuminated electrode determines the sign of the carriers that drift across the sample. The carrier mobility is described by the following equation,

$$\mu = \frac{d}{Et_T} = \frac{d^2}{Vt_T}$$

Where μ is the mobility, d is a sample thickness, E is the electric field, V is a given applied voltage and t_T is the transit time.

In general, carriers should be transported to counter electrode with a constant velocity in the TOF method, therefore electric field should be homogeneous across a sample. When an excess amount of charges, e.g., over 20% of the charges determined by a geometrical capacitance, are injected, the electric field becomes inhomogeneous. Therefore, the light intensity of pulse laser used for photo-excitation was set low enough to satisfy the amount of charges.

For evaluation of charge amount transported to the counter electrode, the transient photocurrent $I(t)$ was integrated as a function of transport time to give the collected charges Q.

$$Q = \int_0^\infty I(t)dt$$

The charge amount determined by the geometrical capacitance of a cell, Q_0 is the follow equation:

$$Q_0 = CV = \varepsilon_0 \varepsilon_r \frac{S}{d} V$$

In this study, photo intensity was controlled as $Q < 0.2Q_0$.

In this study, an N_2 laser (Photonics LN203C: λ = 337 nm, pulse duration = 600 ps) and a Nd:YAG laser with wavelength modulator (an optical parametrical oscillator (OPO): LOTIS TII LT-2215, a second harmonic generator (SHG):

LOTIS TII YHG-2, a third harmonic generator of LOTIS TII LS-2137UPM, λ = about 230 - 840 nm, pulse duration = 6-8 ns) was used as an excitation light. The energy of the laser pulse was measured by a pulse power meter. Bias voltage was applied by Kikusui PVA 250 or Keithley 237. The transient photocurrent was recorded by a digital oscilloscope (Nicolet, Pro92 or ACCURA 100 (12bit, 20MHz and 100MHz, respectively)).

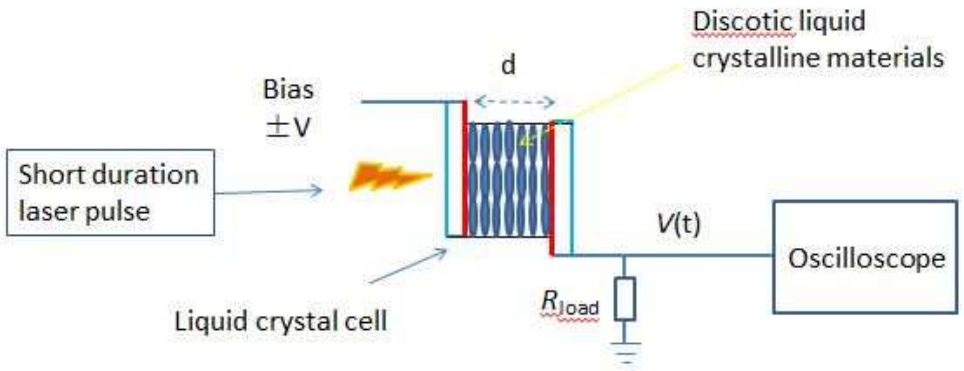

a)

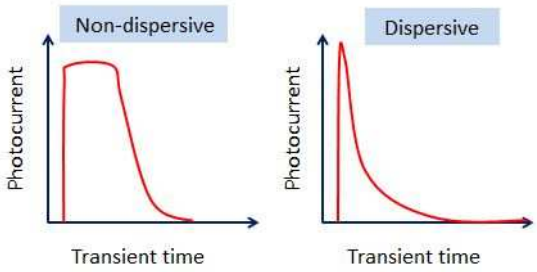

b) c)

Figure 2-5 TOF setup for this study (a), which consists of pulse laser, DC voltage source, resistors, digital oscilloscope, and hot stage, d is the thickness of the cell. b) and c) represent typical non-dispersive and dispersive transient photocurrent, respectively.

References of Chapter 2

1. P. Mark, W. Helfrich, *Journal of Applied Physics*, **33**, 205(2004).

2. A. J. Campbell, D. D. Bradley, H. Antoniadis, M. Inbasekaran, W. W. Wu, E. P. Woo, *Applied Physics Letters*, **76**, 1734(2000).

3. M. Abkowtz, D. M. Pai, *Philosophical Magazine B*, **53**, 193-216(1986).

4. H. Iino, PhD thesis, Tokyo Institute of Technology, 2005

Chapter 3

Bay-substituted discotic liquid crystalline benzoporphyrins

3-1 Introduction

In the former chapters, it was repeatedly emphasized that peripheral substituted discotic liquid crystals exhibited low charge carrier mobility ranging from 10^{-4} to 10^{-2}cm^2/Vs in ordered columnar phases, which could be enhanced through modification to some extent, but still below 10^{-1} cm^2/Vs. What' is surprising for us is that incorporation of side chains into bay positions of phthalocyanines shown in Figure 3-1 was capable of achieving high charge carrier mobility even over 0.1 cm^2/Vs in disordered columnar mesophases.

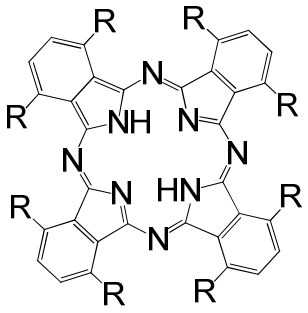

Figure 3-1 Molecular structure of bay-substituted phthalocyanine

To the best of our knowledge about liquid crystalline organic semiconductors, high charge transport mobility strongly depends on long-range ordered structures with less molecular displacement and motion.[1-3] However, bay-substituted phthalocyanines exceptionally showed such a high mobility in relatively low-ordered columnar phase,

i.e. disordered hexagonal columnar phase (Col_{hd}). One probably is wondering that why bay-substituted phthalocyanines show higher mobility than other discotic liquid crystals. Explicitly, this question has never been addressed in available literature reports.

Generally speaking, the electronic spectra of phthalocyanine derivatives must be closely relative to the configuration of their molecular stacking. [4]

As we observed, bay-substituted phthalocyanines actually exhibited quite different electronic spectra from those of peri-substituted ones. It is obvious that bay-substituted phthalocyanines always exhibited splitting Q-band in their temperature-dependent spectra, while peri-substituted phthalocyanines didn't do like that, shown in Figure 3-2.

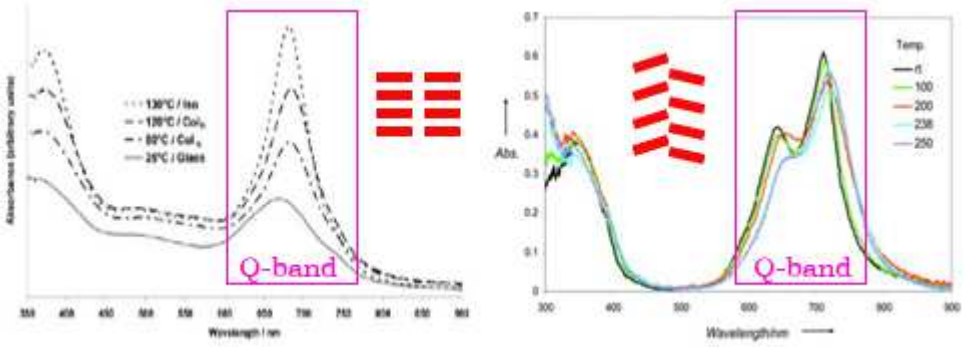

Figure 3-2 Temperature-dependent electronic spectra for peri-substituted phthalocyanine (left) and bay-substituted phthalocyanine (right), the former shows a face to face molecular orientation, while the lateral shows s herringbone configuration.

According to Kasha' report, only the oblique dimers show the split related band. So, in phthalocyanine derivatives, the split Q-band reveals that molecules aggregate together to form a unique oblique dimers shown in the below figure.

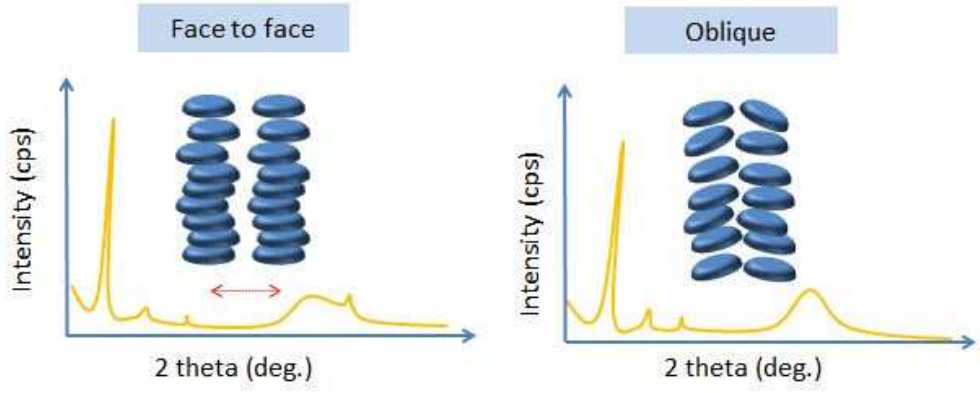

Figure 3-3 Face to face molecular orientation in peri-substituted phthalocyanines (left), in which molecules exhibit translational motion; oblique molecular orientation in bay-substituted phthalocyanines

Furthermore, bay-substituted phthalocyanines usually exhibited two separate mesophases, i.e., hexagonal columnar phase and rectangular columnar phase. From powder XRD patterns in Figure 3-3, it is clearly observable that in both mesophases XRD curves are quite similar. The only difference between them is the slight split peak at small angle region. In the hexagonal columnar phase, this peak can be assigned as (100), which split into (200) and (110) in rectangular columnar phase. And the intracolumnar distance is 4Å, which is little larger than usual (3.6Å). [5-7]

Although by this description, we can understand that why bay-substitued phthalocyanines exhibited disordered hexagonal columnar phase, this result couldn't be used to explain why bay-substituted phthalocyanines showed high mobility, while peri-substituted ones showed low mobility.

In chapter 1, the effect factors on charge transport in discotic columnar mesophase have been stated, which mainly include three aspects, namely, molecular orientation, defects and thermal motions. [8] When molecules of highly pure compounds form well-defined homeotropic alignment, molecular motions will dominate the charge carrier transport in columnar mesophases. [9-11] Obviously, both of bay-substituted and peri-substituted phthalocyanines meet the first two requirements,

which can form homeotropic molecular alignment and can be purified through repeated recrystallization. Only the last factor, thermal molecular motions probably play a distinguished role on their charge carrier transport.

As for the peri-substituted phthalocyanines, due to peripheral located side chains acting as natural spacer between molecular columns, molecules in mesophases can move freely in the translational direction, which is mainly caused by electrostatic repulsion and the fluctuation of flexible side chains.

In the case of bay-substituted phthalocyanines, side chains are located in the non-peripheral positions, which strongly confine the fluctuation of side chains, due to steric hindrance. Moreover, the phenyl rings are exposed, which makes the intermolecular distance between adjacent columns narrower than peri-substituted ones.

Based on the above discussion, we speculated that in columnar mesophase of bay-substituted discotic liquid crystals narrow intermolecular space originated from the incorporation of side chains at bay positions suppresses the molecular motions.

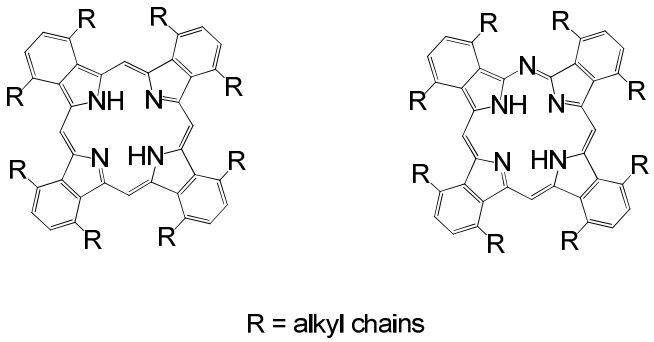

Figure 3-4 Molecular structures of bay-substituted benzoporphyrin analogues, which have similar shapes with bay-substituted phthalocyanines

This study aimed to extend this molecular design to a similar molecule system, namely, tetrabenzoporphyrin in Figure 3-4. They show similar molecular shapes and similar electronic spectra, which makes the generalization more controllable. Actually, analogous to phthalocyanines, benzoporphyrin derivatives are also considered to possess excellent optical and electrical properties, and also, can be substituted at bay

positions.[12] However, because of the difficulty in chemical synthesis, to introduce flexible chains into bay positions of benzoporphyrins just was reported in few early literatures.[13] Only the parent benzoporphyrin derivative, tetrabenzoporphyrin, was widely studied, which was reported to have a HOMO level of 5.1 eV and a narrow bandgap about 2eV and show relatively high intrinsic positive charge concentration.[14,15] Moreover, high optical absorption in the visible region qualifies it for photovoltaic application. [15]

Until recently, discotic liquid crystalline benzoporphyrin derivatives, i.e., 1,4,8,11, 15,18,22,25- hexyltetrabenzoporphyrin (TBP:compound 2) and compound 3, 1,4,8,11, 15, 18, 22, 25- hexyl tetrabenzomonoazaporphyrin (TBMAP: compound 3), substituted by long side chains at bay positions, were synthesized starting from thiophene shown in Schem 1. [16] However, the attempt to prepare high-purity 2 and 3 for electronic application was never reported, probably due to quite low yields in the whole synthetic route.

3-2 Synthesis

3-2-1 Previous synthetic route

Until recently, discotic liquid crystalline benzoporphyrin derivatives, 1,4,8,11,15,18,22,25- hexyltetrabenzoporphyrin (TBP: compound 2) and 1,4,8,11, 15, 18, 22, 25- hexyl tetrabenzomonoazaporphyrin (TBMAP: compound 3), substituted by long side chains at bay positions, were synthesized starting from thiophene shown in Schem 3-1. [16] However, their phase transition, optical and electronic properties are still unclear, which possibly resulted from very low yields in whole synthetic route.

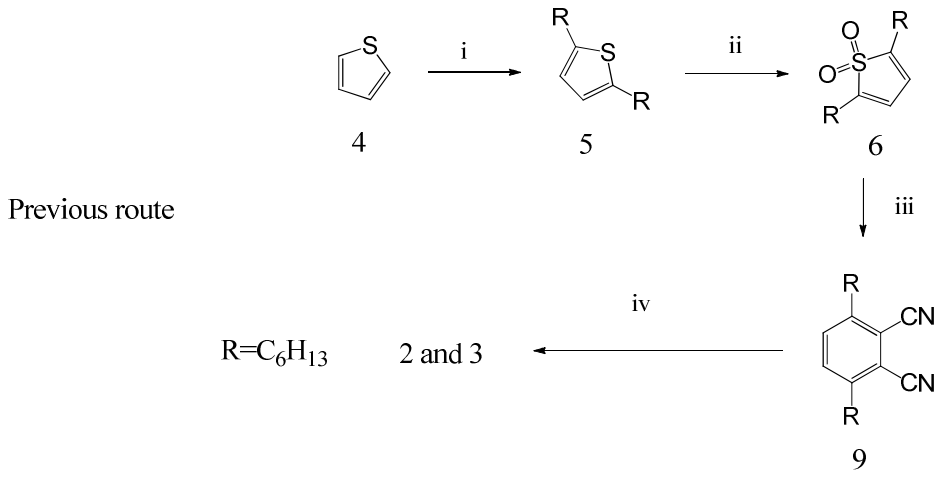

i: BrC_6H_{13}, n-BuLi, THF; ii: m-CPBA, CH_2Cl_2; iii: $CHCl_3$, 150℃, in sealed tube; iv: a) BrMgMe, THF, reflux,30min; b) Quinoline, 200℃, 12h; c) AcOH, reflux

Scheme 3-1 Previous synthetic route for benzoporphyrin derivatives

3-2-2 Novel synthetic route in this work

In this paper, we designed a versatile route for synthesis of benzoporphyrin derivatives, as shown in Scheme 3-2. In this new route, the commercial starting material, 2, 3-dicyanohydroquinone 7, was firstly triflated to prepare 8 in a yield of 90%. And then through Suzuki coupling, the precursor 9 was synthesized from compound 8 in a high efficiency and mild condition.

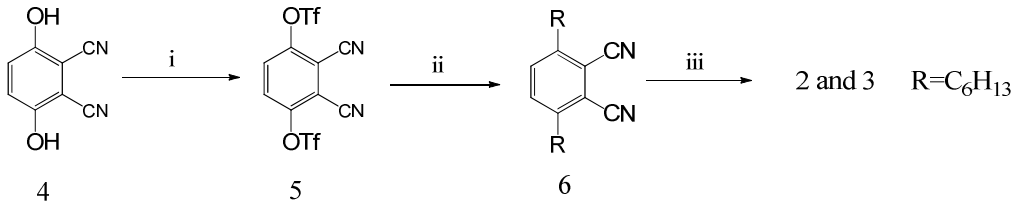

i: trifluoromethanesulfonic anhydride, pyridine, dry DCM; ii: $C_6H_{13}B(OH)_2$, $Pd(dppf)Cl_2$, AgO, K_2CO_3, THF, 80℃; iii: a) BrMgMe, THF, reflux,30min; b) Quinoline, 200℃, 12h; c) AcOH, reflux

Scheme 3-2 Novel synthetic route for benzoporphyrin derivatives

Finally, the cyclization reaction was carried out as reported in reference [16] to

prepare TBP and TBMAP with slight modification by using a 1 : 4 ratio of MeMgBr to precursor 6. Crude products were carefully isolated and extensively purified by column chromatography followed by repetitive recrystallization from a mixed solvent of THF and methanol, in order to further characterization of thermal and physical properties. Comparing with the previous one, our route showed quite high efficiency, mild conditions and functional group tolerance.

i: Synthesis of 3,6- bis(trifluoromethanesulfonyloxy)phthalonitrile

2,3-dicyanohydroquinone (5.2 g, 0.033 mol) was dissolved in a mixture of dry DCM (30 mL) and triethylamine (5 mL) and the resulting yellow solution was cooled to -20 °C. A solution of trifluoromethanesulfonic anhydride (22.1 g, 0.079 mol) in dry DCM (8 mL) was added dropwise over 30 min. The resulting mixture was allowed to warm to rt and stirred for 14 h under argon. The resulting brown solution was left in the fridge for 24 h to help the formation of crystals which were filtered off, washed with cold methanol and recrystallised from DCM/petrol to afford 3,6-bis(trifluoromethanesulfonyloxy)phthalonitrile (yield 90%). ^{1}H NMR ($CDCl_3$, 500 MHz, ppm): 7.87(s, 2H).

ii: Synthesis of 3,6- dihexylphthalonitrile

A suspension of compound 1(1.5g), Alkyl boronic acid (3 equiv.), Pd(dppf)Cl_2 (10%), powdered K_2CO_3 (3 equiv.),and Ag_2O (2.5 equiv.) in THF (75ml) was stirred under argon at 80°C in a sealed tube. After 48 h, the mixture was cooled to room temperature. The dark solid was filtered, and water was added into the solution. The solution was extracted using $CHCl_3$. After evaporation, chromatography column was carried out to purify the crude product to provide 0.85g white crystal, yield 60.9%. ^{1}H NMR ($CDCl_3$, 500 MHz, ppm): 7.47 (s, 2H), 2.86 (t, J=7.0Hz, 4H,), 1.67(m, 4H), 1.34 (m, 12H), 0.90 (t, 6H).

iii. Synthesis of benzoporphyrin derivatives (refer to reference 1)

Cyclization for bay substituted benzoporphyrin was operated as the reference, 3 (200

mg) A solution of MeMgBr in Et_2O (0.93ml, 2.9M in Et_2O, 4 equiv), dry quinoline (3 mL), Acetic acid (3 mL), green super-pure crystals after repetitive recrystallization in EL-level solvent were obtained (TBP: yield 2.4%; TBMAP: yield3.5%).

TBP: Transition temperature: 149℃ (K–D), 178℃ (D–I);

^{1}H NMR (300 MHz, [D8]THF): d=11.56 (s, 4 H), 7.92 (s, 8H), 4.41 (t, J=7.2 Hz, 16H), 2.25–2.44 (m, 16H), 1.5–1.8 (m, 16 H), 1.2–1.5 (m, 32H),0.75–0.95 (m, 24 H), –2.10 ppm (s, 2H);

TBMAP: Transition temperature: 149℃ (K–D), 177℃ (D–I);

^{1}H NMR (300 MHz, [D_8]THF): d=10.95 (s, 2H), 10.88 (s, 1 H), 7.96(d, J=7.6 Hz, 2 H), 7.84 (d, J=7.6 Hz, 2 H), 7.54 (m, 4H), 5.05 (t, J=7.2 Hz, 4H), 4.08 (t, J=7.2 Hz, 4H), 3.97(t, J=7.2 Hz, 4H), 3.85 (t, J=7.2 Hz, 4H), 2.35–2.42 (m, 4 H), 2.23–2.30(m, 4 H), 2.1–2.23 (m, 8H), 1.75–1.83 (m, 4H), 1.56–1.65 (m, 12 H), 1.26–1.45 (m, 32H), 0.80–0.91 (m, 24H), –1.36 ppm (s, 2H);

3-3 Phase transition

3-3-1 polarizing optical microscope (POM)

Their phase transition has been characterized, in which two mesophases were observed for both TBP and TBMAP. On heating, their clear points appeared at 178℃ and 177℃, respectively. And then, as temperature decreased from isotropic phase, their phase transition from first mesophase to the second one took place at 162℃and 161℃, and entered into crystal states at the same temperature of 149℃. These results are consistent with the previous report. [16]

POM textures of TBP and TBMAP are shown in Figure 3-5. It can be seen that both compounds exhibited quite characteristic textures in their separate mesophases. At 175℃ upon cooling, fan-like textures appeared (a and c in Figure 3-5), which are typical for hexagonal columnar phase,[3b] while, the black region can be considered as the existence of homeotropic columns.[9] At 155℃, their textures turned to be

broken fan type (b and d in Figure 3-5), which are commonly observable in the rectangular columnar phase.[12]

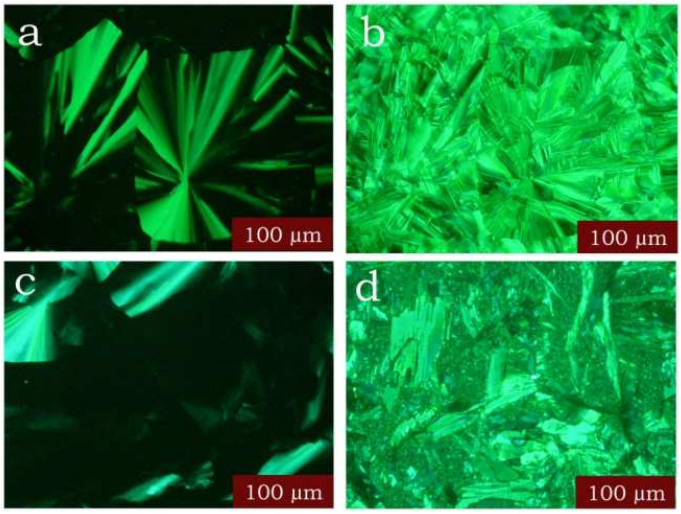

Figure 3-5 Polarized optical micrographs of TBP (a: 175℃; b: 155℃) and TBMAP(c: 175℃; d: 155℃)

3-3-2 X-ray diffraction (XRD)

In addition, we can see that XRD patterns of TBP and TBMAP in rectangular columnar phase did not show rather clear splitting peaks (200) and (110) (results by the splitting of the (100) reflection of the hexagonal columnar phase lattice, b and d in Figure 3-6) as usual [8b], which has been reported for some phthalocyanines with a very unique molecular alignment.[17] The uncommon results actually led to the difficulty in distinguishing the two separate columnar phases. So, the authors of the reference 16 defined the second phase as the other hexagonal columnar phase.

XRD data were summarized in Tab 3-1. Both TBP and TBMAP showed disordered hexagonal columnar phases judging from the absence of π-stacking reflection within a column at wide angle region. Interestingly, intracolumnar distances for both of TBP and TBMAP are arranged to be 20 to 22 Å, which seemed significantly small compared with those of peri-substituted compounds. [18] And even though both TBP and TBMAP exhibited disordered hexagonal columnar phases, their mean intracolumnar distances around 3.5 Å probably can be estimated from alkyl

chains reflection (3.8 Å), indicative of relatively stronger π-π electronic interaction than usual. [4b, 18] In the rectangular columnar phase, molecules tilted to form herringbone configuration.[17] This type of arrangement is very common in the field of organic crystallography, which is the lowest free energy possible arrangements for rigid molecules, leading to the closest stacks.[19]

As we can see in Figure 3-6, XRD patterns exhibited quite characteristic peaks for both TBP and TBMAP self-organizing into hexagonal and rectangular columnar phases, which agree with results of POM textures. As temperature decreases, the

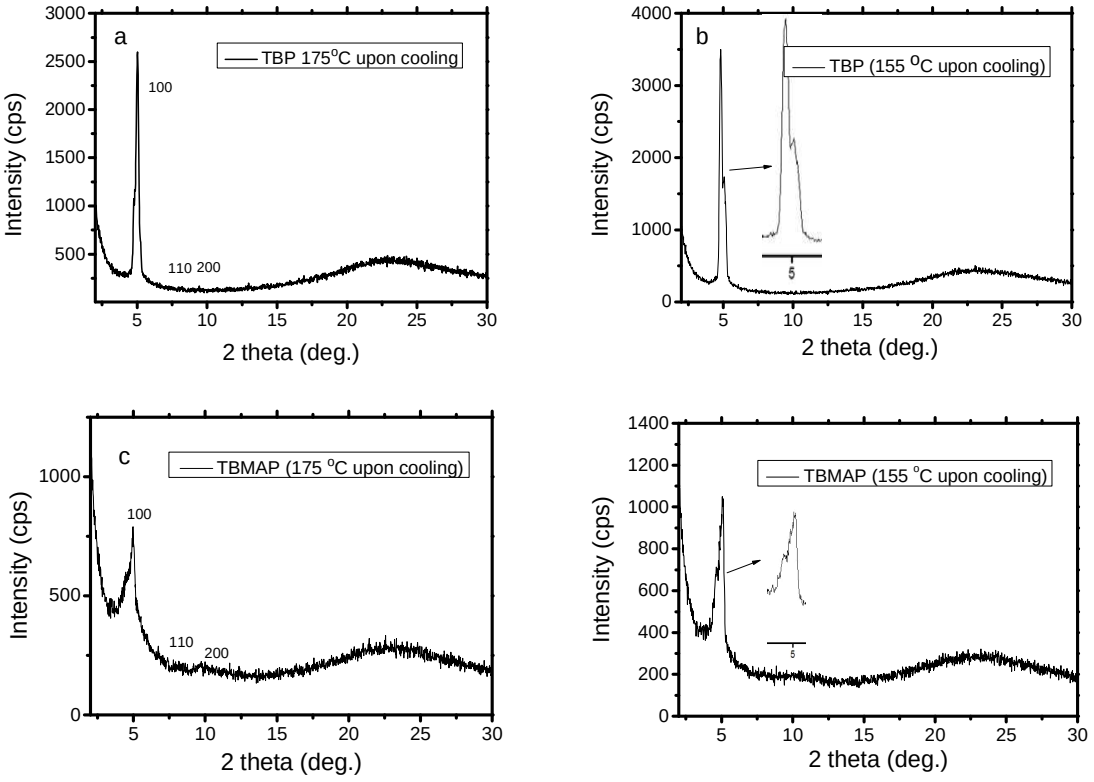

Figure 3-6 XRD patterns of TBP (a: 175℃; b: 155℃) and TBMAP (c: 175℃; d: 155℃)

hexagonal columnar phase quickly transformed to the rectangular one, which can be observable in some DLC materials, and the lateral shows higher order than the former. [12]

Table 3-1 Summary of X-ray diffraction data for TBP and TBMAP

T (℃)	d-spacin	Miller	Phase

		g (Å)	index (hlk)	(lattice parameter)
TBP	175	17.5	(100)	Col_{hd}
		10.8	(110)	a=21.6 Å
		9.3	(200)	
		3.8	alkyl	
	155	18.3	(200)	Col_r
		17.5	(110)	a= 36.6 Å
		3.9	alkyl	b= 19.9 Å
TBMAP	175	17.9	(100)	Col_{hd}
		10.8	(110)	a=21.6 Å
		9.2	(200)	
		3.9	alkyl	
	155	18.8	(200)	Col_r
		17.4	(110)	a=37.6 Å
		3.8	alkyl	b=19.6 Å

3-4 Electronic spectra in film states

Temperature-dependent electronic spectra of thin films of the representative derivative TBP were recorded in Figure 4-7. According to Kasha' report, [20] they theoretically illustrated that interaction between two neighbouring molecules in dimers affects their electronic spectra. And only the oblique dimers show the split related band. As can be seen from Figure 4-7, TBP gave split Q bands at isotropic phase, hexagonal columnar phase and rectangular columnar phase. The split Q bands in these phases correspond to oblique (roof-top-shaped) dimers, even in liquid state. In amorphous state, the intensity of Q-band decreased, but still split as well.

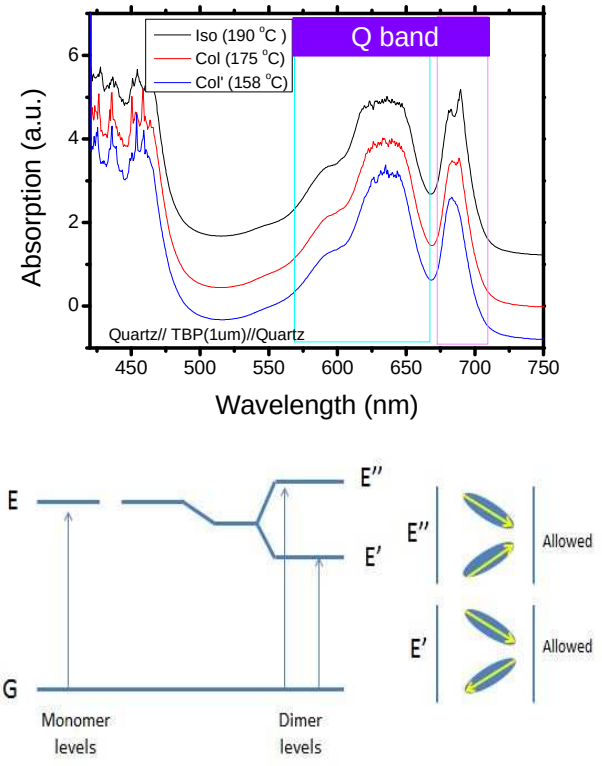

Figure 3-7 Temperature-dependent electronic spectra of visible region of the film of the representative derivative TBP and illustration of exciton energy diagrams for dimers

3-5 Steady- state photoconductivity measurement

Steady-state photocurrent measurement of TBP was carried out by using two type of devices: Al/TBP(9.1μm)/Al and Al/TBP(50nm)/ITO. The measured photocurrent spectra of TBP thin films are shown in Figure 4-8, in which photocurrent spectra were normalized to the number of absorbed photons. We can see that TBP showed relative low photocurrent in the long wavelength region comparing with that in the short wavelength region, mainly because photons in the long wavelength region have low excitation energy less than 2eV (bandgap of TBP) [14]. Interestingly, comparing with electronic spectra in Figure 3-8, the photocurrent spectra show minimums at the maximal absorption but maximums at the minimal absorption when large positive

bias was applied to the thick sample. On the other hand, the thin one's current response almost resembles the shape of the whole absorption spectrum. The striking relationship between the photocurrent and absorption spectra can be classified as antibatic for the former and symbatic for the latter. [22]

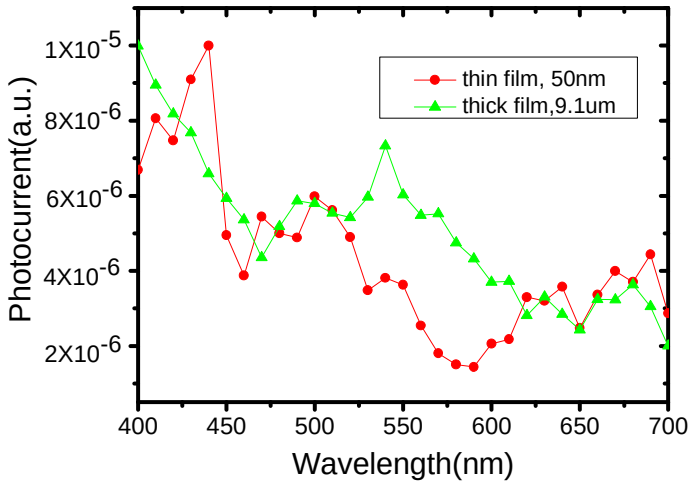

Figure 3-8 Normalized photocurrent spectra of TBP. The photocurrents were measured at 20V and 175℃for the thick and 5V at room temperature for the thin. The voltage was applied on the same side of Al as the incident light.

Similar results have been reported by other researchers on tetrabenzoporphyrin derivatives. [23] This effect usually is called as photocurrent rectification, which was interpreted as resulting from the interaction between the bulk photoconductivity and the injection current.[23b] For thick cells, the weakly absorbed light will penetrate into the sample deeply, leading to a relative small resistance and a relative large current at these wavelengths, while its resistivity and current at strongly absorbed wavelengths are still practically at its dark level. However, for the thin cell, the strongly absorbed light will penetrate a substantial portion of the sample, while only a fraction of the weakly absorbed light will be absorbed by the cell. At this point the spectral characteristics of the bulk and injected currents should be similar.

3-6 Transient photocurrent measurement

In order to investigate charge carrier transport and photo-carrier generation property in benzoporphyrins in detail, the transient photocurrent measurement was performed by a conventional time-of-flight (TOF) experiment, using a nitrogen gas laser (λ= 337 nm, pulse duration time =600ps, power per pulse=13.6μJ) for photo-excitation. Liquid crystal cells with Al and ITO electrodes for the TOF experiments were prepared, and TBP and TBMAP were capillary-filled into the cells at their isotropic temperatures. The resulting transient photocurrents were recorded by digital oscilloscope and were analysed in linear and double logarithmic plots. Carrier mobility μ was obtained through an equation of $\mu=d^2/V\tau_T$, where d is the sample thickness, and V the applied Voltage, and τ_T the transit time of photo-generated carriers traversing the sample layer. The τ_T is determined from an inflection point in a double logarithmic plot of transient photocurrent as a function of time.

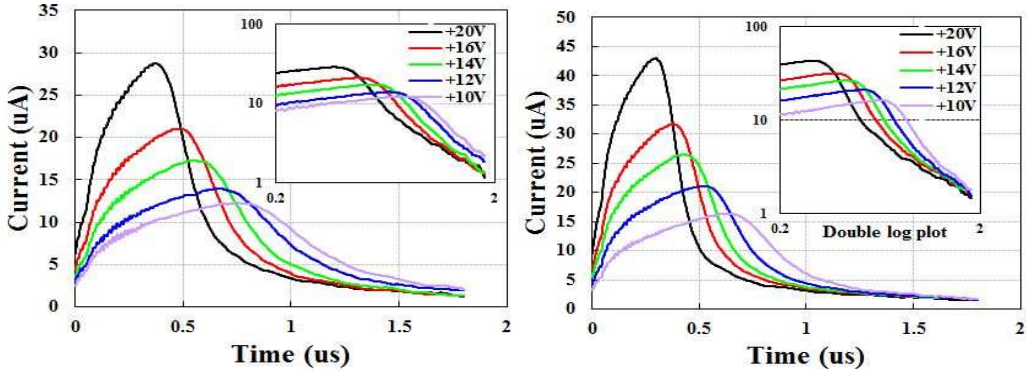

Figure 3-9 Transient photocurrents of TBP in columnar mesophases, the left was measured at 175℃ in the hexagonal columnar phase, while the right at 155℃ in rectangular columnar phase.

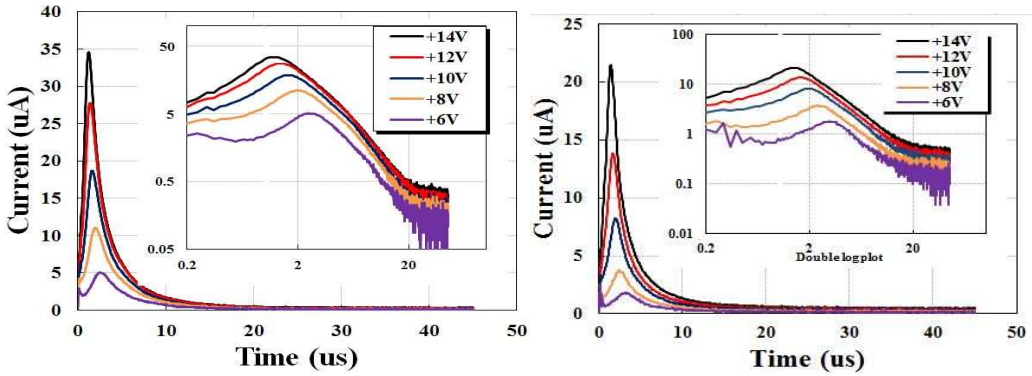

Figure 3-10 Transient photocurrents of TBMAP in columnar mesophases, the left was measured at 175℃ in the hexagonal columnar phase, while the right at 155℃ in rectangular columnar phase.

Figure 3-9 and 3-10 show well-defined non-dispersive hole transient photocurrent of both materials in the hexagonal columnar phase at 175℃ and rectangular columnar phase at 155℃. Each photocurrent exhibits a slow rise of the photocurrent, which is probably due to thermally activated detrapping of the photo-generated charges at the electrode interface,[24] so that a peak instead of a shoulder was shown followed by a slow decay of the current. The mobility exceeded 0.1 cm^2/Vs in the Col phases, which is high enough to attribute it to be the hole conduction. [15 24] This value is comparable to those of bay-substituted phthalocyanine derivatives [12] and about one order of magnitude higher than that of polycrystalline non-mesomorphic tetrabenzoporphyrin determined by field effect transistor (FET) technique [14(b), 25] and two order of magnitude higher than that using the space charge limited current (SCLC) technique [26].

The positive carrier mobility for both TBP and TBMAP, as shown in Fig 3-11 (a), is almost same and increases in a stepwise manner from 10^{-3} $cm^2V^{-1}s^{-1}$ in isotropic phase to 10^{-1} $cm^2V^{-1}s^{-1}$ in both disordered hexagonal and rectangular columnar phases, when the phase transition took place. Judging from such high mobility over $10^{-3}cm^2/Vs$, the conductivity was surely confirmed to be electronic but not ionic, [2b] which indicated high purity in both compounds. [27] However, after samples entered into crystal states, due to lot of grain boundaries, the signals of their photocurrent

became quite dispersive so that charge transport mobility couldn't be obtained.

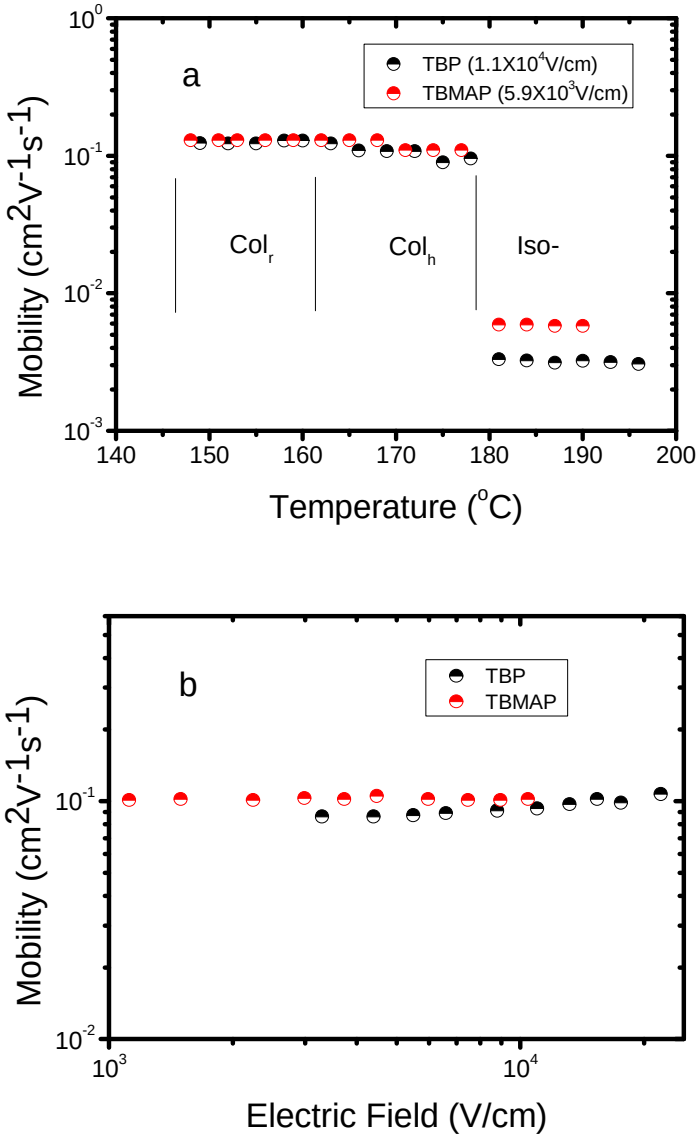

Figure 3-11 Mobility of TBP and TBMAP as a function of temperature at a fixed electric field (a) and as a function of electric field at 175℃in Col_{hd} phase (b)

This fact of high mobility indicates that bay-substituted benzoporphyrin derivatives are surely beneficial for enhancement of charge transport in columnar phases. It implies that molecular motions in the packed columns probably can be suppressed through introducing side chains into bay positions, which allows the special herringbone configuration to construct in disordered hexagonal columnar phase and rectangular columnar phase. Coincidentally, bay-substituted

phthalocyanines having high mobility also showed the split Q-band in their electronic spectra,[28] but those peripheral substituted phthalocyanines with low mobility didn't show the split Q-band even though they exhibited highly ordered hexagonal columnar phase. [9, 29] Furthermore, the relationship between high mobility and herringbone configuration has been explored in single crystals, like pentacene [30], and calamitic liquid crystalline smectic E phase [31].

The hole mobility hardly depends on the temperature in both mesophase irrespective of the compounds, which was often reported in other discotic[6] and smectic liquid crystals [32]. These features have been well explained by a narrow distribution of density ranging from 40 to 60 meV comparable to *kT,* and T is the temperature for TOF experiments [33]. And also, the hole mobility of TBP and TBMAP as a function of electric field is illustrated in Fig 3-11 (b). It is very clear that the hole mobility in two samples doesn't have dependence of electric field which is also quite common behaviour in the electronic conduction of liquid crystals, which is attributed to a small intermolecular distance of around 3.5Å in the liquid crystalline phases (as mentioned above) and small dipole moment of the molecules

3-7 Summary of Chapter 3

In conclusion, a facile synthetic route was proposed to prepare high-purity bay-substituted benzoporphyrin derivatives of TBP and TBMAP having alkyl groups at bay positions for characterization of phase transition, optical and photoconductive properties. Results from characterization by POM and XRD confirmed that both compounds showed disorder hexagonal and rectangular columnar phases. Temperature-dependent electronic spectra illustrated that these bay-substituted DLCs exhibited split Q-band, which has been theoretically explained for resulting from herringbone configuration.

And also, we investigated charge carrier transport and photoconductive behaviours in two discotic liquid crystalline benzoporphyrin derivatives. Interestingly, through time of flight technique, these materials exhibited very high hole mobility over 0.1cm^2/Vs in Col_{hd} and Col_r, which originated from herringbone configuration within long range columns. Moreover, very high photo-generation efficiency up to 2% in the columnar phase has been achieved.

According to the present results, TBP is very promising as a p-type of organic semiconductor for photovoltaic applications. Furthermore, TBMAP as a good derivative, its availability and potentials also will be worthy of attention. Nowadays, we are focusing on how we can develop more efficient synthetic methods as well as application in high performance photovoltaic devices.

Through this study, we found that bay-substituted benzoporphyrins exhibited similar molecular orientation in mesophases and same order of mobility of $10^{-1}cm^2$/Vs. The results from bay-substituted benzoporphyrin confirmed our speculation originated from bay-substituted phthalocyanines, which reveals that bay-substituted discotic liquid crystals with tetragonal symmetry can exhibited high charge carrier mobility.

References of Chapter 3

1 (a) S. Sergey, W. Pisula, and Y. H. Geerts, Chem. Soc. Rev., 36, 1902 (2007); (b) V.Percec, M. Glodde, T. K. Bera, Y. Miura, I. Shiyanovskaya, K. D. Singer, H. Duan, Nature, 419 384 (2002).

2. (a) S. Kumar, Liq. Cryst., 1089 (2005); (b) D. Adam, P. Schuhmacher, J. Simmerer, L. Haussling, K. Siemensmeyer,K. H. Etzbach, H. Ringsdorf, and D. Haarer, Nature (London), 1994, 371, 141

3. (a) J. Wu, M. D. Watson, L. Zhang, Z. Wang, K. Müllen, J. Am. Chem. Soc., 126, 177 (2004); (b) P. Herwig, C. W. Kayser, K. Müllen, H. W. Spiess, Adv. Mater., 8, 510 (1996).

4. (a) M. J. Cook, M. F. Daniel, K. J. Harrison, N. B. McKeown, A. J. Thomson, Journal of the Chemical Society, Chem. Comm., 14, 1086 (1987); (b) Y. Shimizu, Y. Miyakea, H. Yoshid, H. Monobe, M. J. Cook, A. Fujii M. Ozaki, Mol. Cryst. Liq. Cryst. 549, 127 (2011).

5. Y. Kikuzawa, T. Mori, H. Takeuchi, Org. Lett., 9, 4817 (2007).

6. M. Ghedini, D. Pucci, A. Crispini, A. Bellusci, M. L. Deda, I. Aiello, T. Pugliese, Inorg. Chem. Comm., 10, 243 (2007).

7. (a) L. Schmidt-Mende, A. Fechtenkötter, K. Müllen, E. Moons, R. H. Friend, J. D. MacKenzie, Science, 293, 1119 (2001); (b) T. Hori, Y. Miyake, N. Yamasaki, H. Yoshida, A. Fujii, Y. Shimizu, M. Ozaki, Appl. Phy. Express, 3, 1602 (2010).

8. (a)V. Lemaur, D. A. Silva Filho, V. Coropceanu, M. Lehmann, Y. Geerts, J. Piris, J. Cornil, J. Am. Chem. Soc., 126, 3271 (2004); (b) E. Fontes, P. A. Heiney, M. Ohba, J. N. Haseltine, A. B. Smith, Phy. Rev. A., 37, 1329 (1988); (c) W. Pisula, M Kastler, D Wasserfallen, M Mondeshki, J Piris, I. Schnell, K. Mullen, Chem. Mater. 18, 3634-3640 (2006);

9. H. Fujikake, T. Murashige, M. Sugibayashi, K. Ohta, Appl. Phy. Lett., 85, 3474 (2004).

10. C. Deibel, D. Janssen, P. Heremans, V. De Cupere, Y. Geerts, M. L. Benkhedir, G.

J. Adriaenssens, Org. Electronics, 7, 495 (2006).

11. H. Iino, J. I. Hanna, D. Haarer, Phy. Rev. B., 193203 (2005).

12 (a) H. Iino, J. I. Hanna, R. J. Bushby, B. Movaghar, B. J. Whitaker, M. J. Cook, Appl. Phy. Lett., 87, 132102 (2005); (b) Y. Miyake, Y. Shiraiwa, K. Okada, H. Monobe, T. Hori, N. Yamasaki, H. Yoshida, M.J. Cook, A. Fujii, M. Ozaki, Y. Shimizu, Appl. Phys. Express, 4, 021604 (2011); (c) I. Chambrier, M. J. Cook, M. Helliwell and A. K. Powell, J. Chem. Soc., Chem. Commun., 19, 444 (1992).

13 Y. Matsuzawa, K. Ichimura, K Kudo, Chim. Acta. 277, 151 (1998).

14. (a)S. Aramaki, Y. Sakai, N. Ono, Appl. Phys. Lett. 84, 2085 (2004); (b) P. B. Shea, J. Kanicki, N. Ono, J. Appl. Phys. 98, 014503 (2005);

15. M. Guide, X. Dang, T. Nguyen, Adv. Mater., 23, 2313 (2011)

16. A. N. Cammidge, I. Chambrier, M. J. Cook, D. L. Hughes, M. Rahman, and L. Sosa-Vargas, Chem. Eur. J. 17, 3136 (2011)

17. (a) G. Schweicher, G. Gbabode, F. Quist, O. Debever, N. Dumont, S. Sergeyev, Y. H. Geerts, Chem. Mater., 21, 5867 (2009); (b) P. Weber, D. Guillon, A. Skoulios, Liq. Cry. 9, 369 (1991).

18. M. K. Engel, P. Bassoul, L. Bosio, H. Lehmanns, M. Hanacks, J. Simon. Liquid Crystals, 15, 709 (1993)

19. Y. Kitaigorodske, Molecular Crystals and Molecules, 1973, (Academic Press).

20. M. Kasha, H. R. Rawls, M. A. El-Bayoumi, Pure. Appl. Chem., 1965, 11, 371.

21. P. Weber, D. Guillon, A. Skoulios, Liq. Cry., 9, 369 (1991).

22 (a) K. J. Donovan, K. Scott, S. Spagnoli, J. Berrehar, Chemical Physics. 250, 61 (1999); (b) M. G. Harrison, J. Gruner, and G. C. W. Spencer, Phys. Rev. B. 55, 7831 (1997).

23. (a) H. Gerischer, M. Liibke, B. J. Bressel, Electrochem. SOC. 130, 2112 (1983); (b)B. A. Gregg, M. A. Fox, and A. J. Bard, J. Phys. Chem., 94, 1586 (1990); (c) Y. Shimizu, A. Ishikawa, S. Kusabayashi, M. Miya and A. Nagata, J. Chem. Soc., Chem. Commun., 7 656 (1993).

24. a) H. Zhang and J. Hanna, J. Phys. Chem. B, 103, 7429 (1999); b) D. Adam, F. Closs, T. Frey, D. Funhoff, D. Haarer, H. Ringsdorf, P. Schuhmacher, K.

Siemensmeier; Phys. Rev. Lett., 70, 457 (1993).

25 (a) S. Aramaki, Y. Sakai, N. Ono, Appl. Phys. Lett., 84, 2085 (2004);

26 M. Guide, X. Dang, T. Nguyen, Adv. Mater., 2011, 23, 2313 (2011).

27. (a) H. Ahn, A. Ohno, J. Hanna, Jpn. J. Appl. Phys., 44, 3764 (2005); (b) M. Funahashi, F. Zhang, N. Tamaoki, and J. Hanna, Chem. Phys. Chem. 9, 1465 (2008).

28. N. B. Pal, C. Chaure, S. Barard, T. Kreouzis, A. K. Ray, A. N. Cammidge, M. G. Cain, J. Mater. Chem., 22, 19179 (2012).

29. F. Nekelson, H. Monobe,M. Shiroc, Y. Shimizu, J. Mater. Chem., 17, 2607 (2007).

30. D. H. Kim, D. Y. Lee, H. S. Lee, W. H. Lee, Y. H. Kim, J. I. Han, K. Cho, Adv. Mater., 19, 678 (2007).

31. (a) H. Iino, J. I. Hanna, Adv. Mater., 23, 1748 (2011); (b) M. A. Stokes, R. Kortan, S. R. Amy, H. E. Katz, Y. J. Chabal, C. Kloc, T. Siegrist, J. Mater. Chem., 17, 3427 (2007).

32. (a) M. Funahashi, J. Hanna, Appl. Phys. Lett., 2000, 76, 2574; (b) M. Funahashi, J. Hanna, Appl. Phys. Lett., 71, 602 (1997).

33. A. Ohno, J. Hanna, D. Dunlap, Jpn. J. Appl. Phys., 47, 1079 (2008).

34. M. K. Engel, P. Bassoul, L. Bosio, H. Lehmanns, M. Hanacks and J. Simon, Liq. Cry., 15, 709 (1993)

35. (a) M. Funahashi, J. Hanna, Appl. Phys. Lett. 73, 3733 (1998); (b)T. Kreouzis, K. J. Donovan, N. Boden, R. J. Bushby, O. R. Lozman, and Q. Liu, J. Chem. Phys., 114, 1797 (2001); (c) K. Zhao, C. Chen, H. Monobe, P. Hu, B. Wang and Y. Shimizu, Chem. Commun., 47, 6290 (2011).

36. H. Zhang, J. Hanna, J. Appl. Phys., 88, 270 (2000).

Chapter 4

Bay-substituted discotic liquid crystalline hexaazatrinaphthylene (HATNA) derivatives

4-1 Introduction

Semiconducting molecular columns, living in discotic liquid crystalline (DLC) columnar phases, are capable of forming one dimensional channel for charge transport and natively behavior as superior models for study of charge-transfer process.[1] Furthermore, their homeotropic molecular alignment within "out of plane" columns, in which the molecules adopt face-on orientation on the substrate, allows long-range fast charge carrier transport between the top and bottom electrodes favoring high photovoltaic and light-emitting performance.[2] In order to make further advancement in such electronic devices, it is of fundamental importance to investigate how to make DLC molecules spontaneously grow "out of plane" between the electrodes, thus generating long-range charge carrier transport with fast mobility.

Over the past couple of years, abundant researches have addressed that "out of plane" molecular columns can be organized by p-type semiconducting DLCs themselves through thermal annealing process, in which hole can be transported with mobility ranging from $10^{-4}cm^2V^{-1}s^{-1}$ to $10^{-1}cm^2V^{-1}s^{-1}$.[3] However, only few reports aimed at discussing the self-directed n-type DLCs to organize "out of plane" molecular columns for high electron transport,[4] which actually subject to not only the low chemical stability and high reactivity of their radical anions with H_2O and O_2,[5] but also the strong trend to "in plane" grow with their axis parallel to substrates (planar alignment). To form stable n-type organic semiconductors, primarily two molecular design strategies are accessible: i) to introduce electron-withdrawing groups (-CN, -COR or $–NO_2$); ii) to incorporate N-containing heterocycles (pyridine

or diazine). The former can preferentially lower the energy of the LUMO and have a smaller impact on the HOMO, making both electron and hole injection possible, while the lateral tends to decrease both the occupied and unoccupied orbitals, thus favoring electron injection but blocking hole injection. [6] So, the lateral should be considered as the ideal n-type active materials for bulk heterojunction devices.

As shown in Figure 4-1, hexaazatrinaphthylene (HATNA) is a C_3 symmetric heterocyclic aromatic core, in which there are six embedded nitrogen atoms so that the first reduction potential can be significantly increased, thus beneficial for electron injection. [7]

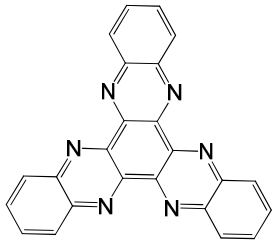

Figure 4-1 Structure of 5, 6, 11, 12, 17, 18-Hexaazatrinaphthylene (HATNA)

Up to date, very few HATNA compounds have been explored as discotic liquid crystalline materials, [8] in spite of various derivatives studied as model compounds to determine the crystal structure, [9] ionization potential, [10] and electron affinity. [11]

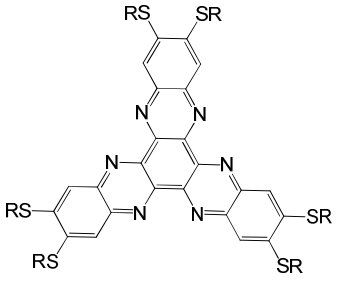

R= C_nH_{2n+1} n=6, 8, 10, 12

HATNA-SR	Phase transition temperature
R=C_6H_{13}	Cr 205 Col_h > 250 dec
R=C_8H_{17}	Cr 175 Col_h > 250 dec
R=$C_{10}H_{21}$	Cr 113 Col_{r1} 134 Col_{r2} 181 Col_{r3} 222 Col_h > 250 dec
R=$C_{12}H_{25}$	Cr 90 Col_r 149 Col_h > 250 dec

Figure 4-2 Structure of peripheral-substituted HATNA with alkylthio groups and their phase transition temperature

The first discotic columnar HATNA derivatives shown in Figure 4-2 were prepared about ten years ago by Geerts, et al [8a, 8d]. They have already prepared a series of HATNAs with hexathioethers and characterized their thermal properties. Moreover, the thermotropic behavior was found to strongly rely on the length of side chains. However, before the observation of their decomposition clearing temperatures wasn't obtained, so that further studies on their physical and electronic properties were hampered. Although incorporation of swallow-tailed type of hexathioethers chains HATNA derivative had its isotropic temperature and exhibited multiple crystalline phases prior to decomposition, these compounds failed to show any columnar mesophase.

On the other hand, HATNAs with alkoxyl groups was found to exhibit columnar mesomorphism shown in Figure 4-3 [8c]. The synthesis of these compounds involves the condensation of freshly prepared cyclohexane-1,2,3,4,5,6- hexaone with 1,2-dialkoxy-4,5-diaminobenzene under the condition of acid. The transition temperatures of these compounds are summarized in Figure 4-3. Unlike their thioether counterparts, hexaethers showed obvious transition from mesophase to isotropic transitions, which was confirmed by POM and DSC. These compounds exhibited very wide columnar mesophase temperature ranges, in which rectangular and/or hexagonal symmetry were checked.

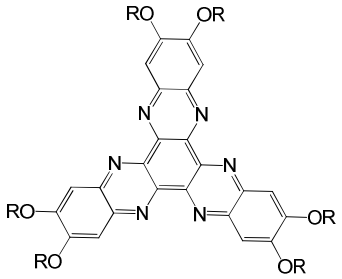

R= C_nH_{2n+1} n=6, 8, 10, 12

HATNA-OR	Phase transition temperature
R=C_6H_{13}	Cr 187.1 Col_r 230.3 I
R=C_8H_{17}	Cr 114.5 Col_r 176 Col_h 224.4 I
R=$C_{10}H_{21}$	Cr 86 Col_h 214.6 I
R=$C_{12}H_{25}$	Cr 94.2 Col_h 206.1

Figure 4-3 Structure of peripheral-substituted HATNA with alkoxyl groups and their phase transition temperature

Importantly, from the above HATNA derivatives, we conclude that the introduction of six electron-donating side chains, such as hexathioethers or hexaethers could not override the electron-deficiency of the core, which has been confirmed by measuring the reduction potential of these compounds by cyclic voltametry studies.

With a view to charge carrier transport, electron mobility through time of flight (TOF) technique still wasn't accessible because of the absent long-range "out of plane" molecular columns. As a consequence, only ambiguous mobility of 10^{-3}-10^{-1} $cm^2V^{-1}s^{-1}$ detected using the pulse-radiolysis time-resolved microwave conductivity (PR-TRMC) [8] or the steady-state space-charge limited current (SCLC) [7d, 7e] techniques is always referred to highlight the good electron transport property of HATNA.

This section will describe that how HATNAs with bay-located thioether groups form mesophases, and the charge carrier transport in their columnar mesophase.

4-2 Alkyl-substituted HATNAs

4-2-1 synthesis

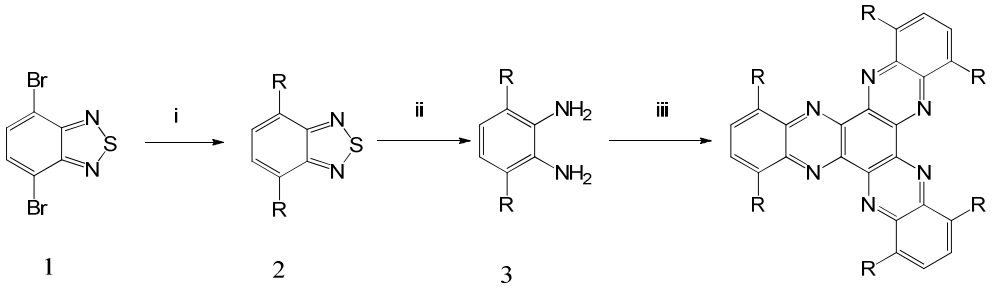

i) R-$B(OH)_2$, $Pd(dppf)_2Cl_2$, Ag_2O, K_2CO_3, THF; ii) Zn, AcOH, reflux, 15min;

iii) Hexaketocyclohexane, R= C_4H_9 and C_6H_{13}, AcOH : $CHCl_3$ (1:1) reflux 1h; R=$C_{10}H_{21}$ and $C_{14}H_{29}$, AcOH:$CHCl_3$ (2:1) reflux 1h

Scheme 4-1 Synthetic route for alkyl-substituted HATNA derivatives

To introduce alkyl chains to bay positions of HATNA is outlined in Scheme 4-1

and showed good yield at each step even if these side chains are in variety of lengths. Dialkylbenzothiadiazole was synthesized through Kumada coupling, and here is the first report about it. Afterward, excessive Znic powder in AcOH was used in reduction system to obtain diamine. Finally, cyclization was carried out in two different volum ratio solvents in terms of side chain' steric hindrance. Four final compounds can be easily recrystallized in hexane, even butyl side chain.

Synthesis of 2:

A suspension of compound 1 (298mg, 1mmol), decyl boronic acid (3 equiv.), Pd(dppf)Cl_2 (10%), powdered K_2CO_3 (3 equiv.),and Ag_2O (2.5 equiv.) in THF (75ml) was stirred under argon at 80°C in a sealed tube. After 48 h, the mixture was cooled to room temperature. The dark solid was filtered, and water was added into the solution. The solution was extracted using $CHCl_3$. After evaporation, chromatography column was carried out to purify the crude product.

R_1=C_4H_9: yield 73.3%. ^{1}HNMR (300MHz, D/chloroform): δ = 7.26 (s, ArH, 2H), 3.08(t, *J=7.5Hz*, 4H), 1.75-1.80 (m, -CH_2-, 4H), 1.20-1.51(t, -CH_2-, 4H), 0.86(t, Me, 6H)

R_1=C_6H_{13}: yield 66.2%. ^{1}HNMR (300MHz, D/chloroform): δ = 7.23 (s, ArH, 2H), 3.05(t, *J=7.5Hz*, 4H), 1.72-1.81 (m, -CH_2-, 4H), 1.21-1.52(t, -CH_2-, 12H), 0.86(t, Me, 6H)

R_1=$C_{10}H_{21}$: yield 74.6%. ^{1}HNMR (300MHz, D/chloroform): δ = 7.24 (s, ArH, 2H), 3.06(t, *J=7.5Hz*, 4H), 1.75-1.80 (m, -CH_2-, 4H), 1.20-1.50(t, -CH_2-, 28H), 0.86(t, Me, 6H)

R_1=$C_{14}H_{29}$: yield 69.5%. ^{1}HNMR (500MHz, D/chloroform): δ = 7.25 (s, ArH, 2H), 3.07(t, *J=7.5Hz*, 4H), 1.75-1.80 (m, -CH_2-, 4H), 1.25-1.53(t, -CH_2-, 44H), 0.86(t, Me, 6H)

Synthesis of 3:

A mixture of 2 (5.2 mmol) zinc dust (26 mmol) and AcOH (20 mL) was refluxed with stirring over 15 min. The reaction mixture was stirred for 1 h, and then was allowed to

cool to room temperature. The mixture was diluted with MeOH and filtered through Celite, rinsing well with MeOH, and filtrate was concentrated. The residue was partitioned between saturated aqueous $NaHCO_3$ (150 mL) and EtOAc (100 mL), and the organic phase was collected. The aqueous phase was extracted with two additional volumes of EtOAc (100 mL). The combined organic phases were dried with Na_2SO_4 and concentrated to give colorless oil.

R_1=C_4H_9: yield 72.5% ^{1}HNMR (300MHz, D/chloroform): δ = 6.58 (s, ArH, 2H), 3.78(s, NH2, 4H), 2.50(t, *J=7.5Hz*, 4H), 1.56-1.61 (m, -CH_2-, 4H), 1.36-1.44(t, -CH_2-, 4H), 0.95(t, Me, 6H)

R_1=C_6H_{13}: yield 70.4% ^{1}HNMR (500MHz, D/chloroform): δ = 6.95 (s, ArH, 2H), 3.93(s, NH2, 4H), 2.85(t, *J=7.5Hz*, 4H), 1.67-1.73 (m, -CH_2-, 4H), 1.25-1.41(t, -CH_2-, 12H), 0.88(t, Me, 6H)

R_1=$C_{10}H_{21}$: 66.5%. ^{1}HNMR (300MHz, D/chloroform): δ = 6.58 (s, ArH, 2H), 3.78(s, NH2, 4H), 2.49(t, *J=7.5Hz*, 4H), 1.55-1.60 (m, -CH_2-, 4H), 1.20-1.51(t, -CH_2-, 28H), 0.88(t, Me, 6H)

R_1=$C_{14}H_{29}$: yield 23.6% ^{1}HNMR (300MHz, D/chloroform): δ = 6.58 (s, ArH, 2H), 3.77(s, NH2, 4H), 2.49(t, *J=7.5Hz*, 4H), 1.56-1.60 (m, -CH_2-, 4H), 1.20-1.51(t, -CH_2-, 44H), 0.88(t, Me, 6H)

Synthesis of bay-substituted HATNAs with alkyl chains:

Mixture of hexaketocyclohexane octahydrate (1 mmol) and appropriate o-phenylene diamines (0.33mmol) was added to deoxygenated acetic acid (20 mL). The mixture was refluxed for 3 h under nitrogen. After the mixture was cooled to room temperature, the resulting solid was collected by filtration and was washed with acetic acid. All compounds were further purified by chromatography using chloroform and cyclohexene as eluent. Finally, repeated recrystallization was carried out to get high purity sample.

HATNA-4: a yellow solid, yield: 45.6%. Melting point: 205.6℃.

^{1}HNMR (300MHz, D/chloroform): δ = 7.74 (s, ArH, 6H), 3.61 (t, *J=7.5Hz*, 12H), 1.96-2.06(m, - CH_2-, 12H), 1.52-1.62(m, -CH_2-, 12H), 1.04(t, Me, 18H);

HRMS (m/z): $[M]^+$ calcd. for $C_{48}H_{60}N_6$: 720.4933; found: 720.4930.

HATNA-6: a yellow solid, yield: 44.2%. Melting point: 151.1℃.

^{1}HNMR (300MHz, D/chloroform): δ = 7.72 (s, ArH, 6H), 3.58 (t, *J=7.5Hz*, 12H), 1.95-2.05(m, - CH_2-, 12H), 1.27-1.53(m, -CH_2-, 36H), 0.86(t, Me, 18H);

HRMS (m/z): $[M]^+$ calcd. for $C_{60}H_{84}N_6$: 888.6757; found: 888.6739.

HATNA-10: a yellow solid, yield: 55.6%. Melting point: 101.9℃.

^{1}HNMR (300MHz, D/chloroform): δ = 7.73 (s, ArH, 6H), 3.59 (t, *J=7.5Hz*, 12H), 1.98-2.06(m, - CH_2-, 12H), 1.23-1.56(m, -CH_2-, 84H), 0.84(t, Me, 18H) ;

HRMS (m/z): $[M]^+$ calcd. calcd for $C_{84}H_{133}N_6$: 1226.0592; found: 1226.0590.

HATNA-14: a yellow solid, yield: 69.8%. Melting point: 85.3℃.

^{1}HNMR (300MHz, D/chloroform): δ = 7.76 (s, ArH, 6H), 3.62 (t, *J=7.5Hz*, 12H), 1.99-2.07(m, - CH_2-, 12H), 1.25-1.57(m, -CH_2-, 132H), 0.89(t, Me, 18H);

HRMS (m/z): $[M]^+$ calcd. calcd for $C_{108}H_{180}N_6$: 1562.6358; found: 1562.6355.

4-2-2 phase transition

4-2-2-1 DSC

From DSC curves in Figure 4-4, four compounds didn't exhibit mesophase. **HATNA-4** showed a wide exothermic peak around 80℃ upon first cooling, which might be caused by crystal transition, because there wasn't presence of any mesophase in XRD (figure 4-6). As increase of side chain' s length, decline of clear points looked rapid from **HATNA-4** to **HATNA-6** and **HATNA-6** to **HATNA-10**, but slowed down from **HATNA-10** to **HATNA-14**. The reason is that clear point can be strongly influenced by both of side chain's length and molecular weight.

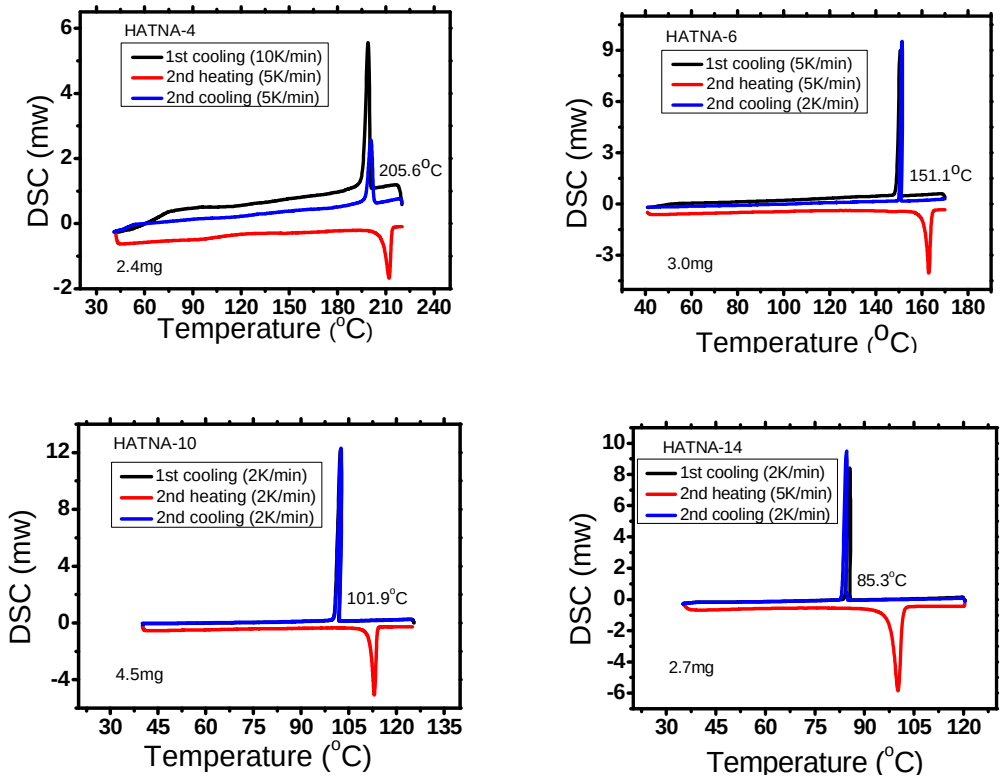

Figure 4-4 DSC curves of **HATNA-4**, **HATNA-6**, **HATNA-10** and **HATNA-14**

4-2-2-2 POM

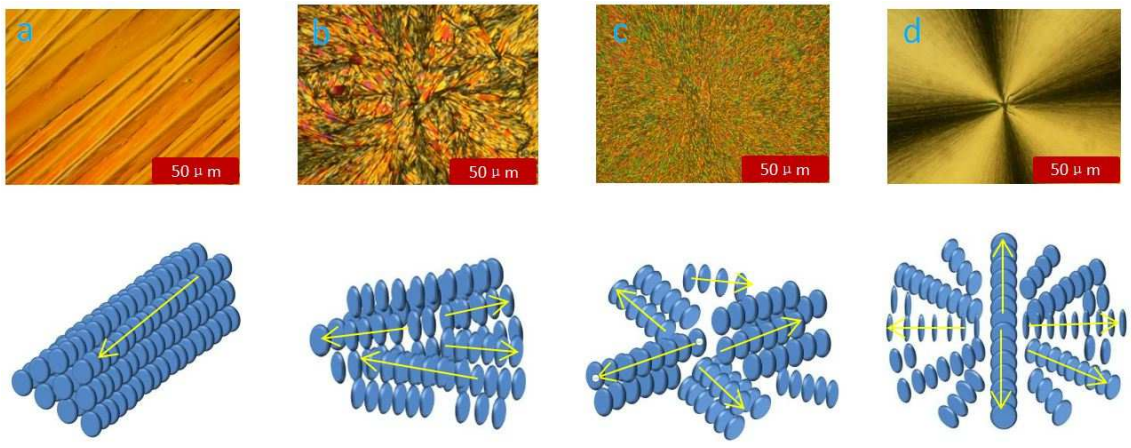

Figure 4-5 POM of **HATNA-4**(a), **HATNA**(b), **HATNA-10**(c) and **HATNA-14**(d) and their organization structure. The arrows in the drawings represent the assembly directions of the columns during solidification. The samples were prepared between

two glass slides.

As shown in Figure 4-5, **HATNA-4** formed long and highly birefringent fibres with lengths exceeding several millimetres during slow cooling, in which the columns were oriented uniaxially along the fibre axis. In contrast, well-ordered spherulites nucleated over the whole sample area of **HATNA-14**, suggesting a radial alignment of the columnar structures from the centre and an edge-on arrangement of the molecules. However, both of **HATNA-6** and **HATNA-10** didn't present typical textures, and just prefered random growth directions.

4-2-2-3 XRD

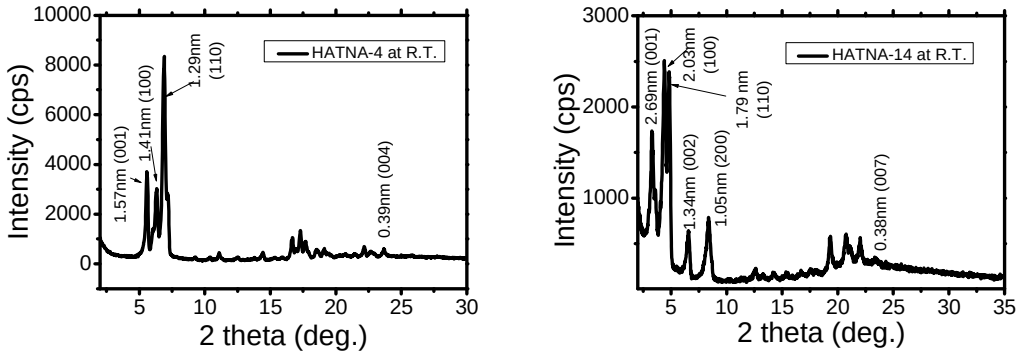

Figure 4-6 XRD curves of **HATNA-4** and **HATNA-14** in polycrystalline phase at room temperature

Powder XRD curves are shown in Figure 4-6. The 2D lateral hexagonal unit cells were found for both of **HATNA-4** and **HATNA-14** from the the XRD curves, which were fitted to the characteristic correlation of 2: $3^{1/2}$: 1, describing the intercolumnar organization. 3.9Å and 3.8Å at wide angle correspond to face-to-face distances between the disc-shaped molecules. **HATNA-14** might form titled columns, so the face to face distance is smaller than that of **HATNA-4**. 15.71Å and 26.9 Å at small angle region suggested additional intracolumnar correlations between every 5^{th} disc for **HATNA-4** and 8^{th} disc for **HATNA-14** (one pitch), which can be proved

further through the obtained rotation angles.

4-2-3 Summary

In this study, HATNA with bay-located alkyl chains have been synthesized through a three-step reaction. After optimizing these reaction, the yields came up to a mediate level, which made milligram-scale sample available for further investigation, including DSC and POM and also XRD.

By DSC and POM measurement, all of these compounds were found to be non-mesophilic. The observation of strong birefringence from the thin films revealed that all of them form molecular columns with their columnar axis parallel to the substrates. XRD patterns of **HATNA-4** and **HATNA-14** gave the detailed information that how the molecule oriented in the thin films: the introduction of short side chains produced parallel columns, while to introduce longer side chains will lead to radial molecular growth. HATNA with mediate length side chains exhibited random growth columns.

Although these compounds didn’t exhibit any mesophase, they provided very basic thermal behavior of bay-substituted HATNA, which told us that HATNA with mediate length side chains will probably be induced to show homeotropic columnar alignment.

4-3 Alkylethynyl-substituted HATNA

4-3-1 synthesis

Bay-alkylated HATNA derivatives have been reported to show crystalline phase only in whole temperature ranges below their clear points even bearing various length side chains, i.e. butyl, hexyl, decyl and myristyl. This result probably derived from strong intermolecular π-π stacking, which is widespread in large conjugated systems. To obtain liquid crystalline properties from these materials, the key issue is to suppress the ability of crystallization, but not to destroy their planar structures absolutely. So, heteroatoms (like O, S and N) and space-required groups (like phenyl, alkynyl and swallow-tailed chains) usually are needed. Here, alkynyl groups were inserted between rigid HATNA core and surrounding flexible aliphatic chains shown in Figure 5-2. In this case, side chains might be out of core's plane with small line-face angle. As a result, intermolecular affinity leading to crystallization becomes weaker than usual.

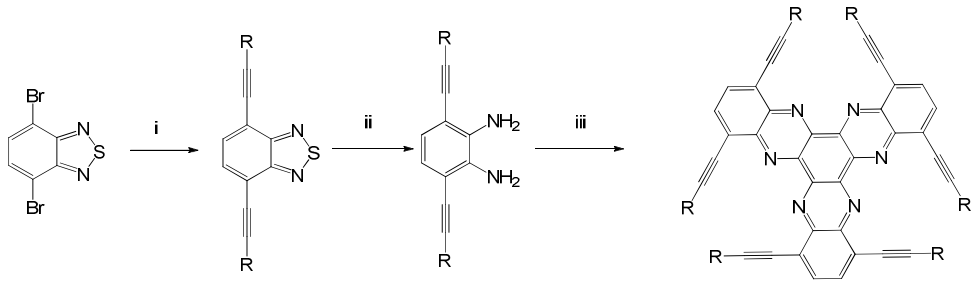

i) , $Pd(dppf)_2Cl_2$, CuI, Et_3N, 1,4-Dioxane; ii) $R_{1,a}$: Zn, AcOH, reflux, 15min; $R_{2,a}$: LiAlH4, THF, 0℃-room temperature; iii) Hexaketocyclohexane, AcOH:$CHCl_3$ (1:1) reflux 1h;

Scheme 4-2 Synthetic routes for variety of HATNA derivatives with

The reaction yields optimized are shown below, which are enough high comparing with synthesis of alkylated HATNA. It is worth mentioning, to purify the final product used to be difficult. Because lots of green by-products accompanied designed compound whenever carrying out chromatography or recrystallization. We speculated that such HATNA with bay-located acetylene bonds exhibited low stability at high temperature, which decomposed slowly during the final reaction.

All compounds appeared bright yellow color. Their optical absorption will be reported in below section.

Synthesis of 2

To an oven-dried Schlenk flask was added dry 1,4-dioxane (20 mL) and triethylamine (3.5mL), which was then vacuum degassed three times. 4,7-dibromobenzo[c][1,2,5]thiadiazole 2 (4mmol), 1-decyne (12.0 mmol), copper(I) iodide (0.48 mmol), and bis(triphenylphosphine)palladium(II) chloride (0.4 mmol) were all added at room temperature. The Schlenk flask was sealed and heated to 60°C, whereupon the solution was stirred for 12 h. After the reaction was cooled to room temperature, water (200 mL) was added to the mixture and the aqueous solution was extracted with dichloromethane (2 x 100mL). The combined organic layers were washed with water (3 x 200mL), dried with magnesium sulfate, filtered, and dried in vacuo. The residue was purified by column chromatography on silica gel using pure hexane.

R_2=octynl: 90.1% yellow crystals. ^{1}HNMR (300MHz, D/chloroform): δ = 7.59 (s, ArH, 2H), 2.58(t, *J=7.5Hz*, 4H), 1.67-1.72 (m, -CH_2-, 4H), 1.31-1.49(t, -CH_2-, 8H), 0.90(t, Me, 6H)

R_2=decynl: 88.2% yellow crystals. ^{1}HNMR (300MHz, D/chloroform): δ = 7.59 (s, ArH, 2H), 2.58(t, *J=7.5Hz*, 4H), 1.67-1.72 (m, -CH_2-, 4H), 1.25-1.4(t, -CH_2-, 28H), 0.88(t, Me, 6H)

Synthesis of 3

Dry THF (50 mL) was added to a flame-dried 100-mL Schlenk flask charged with 5 or 7 (1mmol), then $LiAlH_4$ (14 equiv) was added to the mixture under a stream of

nitrogen over a period of 30 min, and stirring was continued for 4 h.

R_2=octynl: with yield of 73.1%. ^{1}HNMR (500MHz, D/chloroform): δ = 6.73 (s, ArH, 2H), 3.86(s, -NH_2, 4H), 2.46(t, *J=7.5Hz*, 4H), 1.57-1.67 (m, -CH_2-, 4H), 1.25-1.45(t, -CH_2-, 8H), 0.90(t, Me, 6H)

R_2=decynl: with yield of 74.7%. ^{1}HNMR (500MHz, D/chloroform): δ = 6.57 (s, ArH, 2H), 3.87(s, -NH_2, 4H), 2.46(t, *J=7.5Hz*, 4H), 1.57-1.67 (m, -CH_2-, 4H), 1.25-1.45(t, -CH_2-, 28H), 0.88(t, Me, 6H)

Synthesis of 4

Mixture of hexaketocyclohexane octahydrate (1 mmol) and appropriate o-phenylene diamines (0.33mmol) was added to deoxygenated acetic acid (20 mL). The mixture was refluxed for 3 h under nitrogen. After the mixture was cooled to room temperature, the resulting solid was collected by filtration and was washed with acetic acid. All compounds were further purified by chromatography using chloroform and cyclohexene as eluent. Finally, repeated recrystallization was carried out to get high purity sample.

I-d: a yellow solid, yield: 69.8%. Melting point: 85.3℃.

^{1}HNMR (300MHz, D/chloroform): δ = 7.76 (s, ArH, 6H), 3.62 (t, *J=7.5Hz*, 12H), 1.99-2.07(m, - CH_2-, 12H), 1.25-1.57(m, -CH_2-, 132H), 0.89(t, Me, 18H);

HRMS (m/z): $[M]^+$ calcd. calcd for $C_{108}H_{180}N_6$: 1562.6358; found: 1562.6355.

II-a: a yellow solid, yield: 46.5%. Melting point: over 180℃.

^{1}HNMR (500MHz, D/chloroform): δ = 8.05 (s, ArH, 6H), 2.72(t, *J=7.5Hz*, 12H), 1.77-1.81(m, -CH_2-, 12H), 1.52-1.58(m, -CH_2-, 12H), 1.35-1.38(m, -CH_2-, 24H), 0.91(t, Me, 18H);

HRMS (m/z): $[M]^+$ calcd. for $C_{72}H_{85}N_6$: 1033.6836; found: 1033.6801.

4-3-2 phase transition

4-3-2-1 DSC

In Figure 4-7, compound **HATNA-yne-6** was heated to isotropic temperature over

170℃ at the heating rate or 5K/min. It was found that this compound started to decompose from 165℃, which probably resulted from its twist molecular structure. Usually twist molecules show low thermal instability.

Before the isotropic phase transition, one high peak appeared at 98℃, which could be assigned as the transition from crystal phase to columnar mesophase. As observed, this material began to decompose after melting, which made further cooling cycle of DSC measurement impossible. So, only first heating process was exhibited.

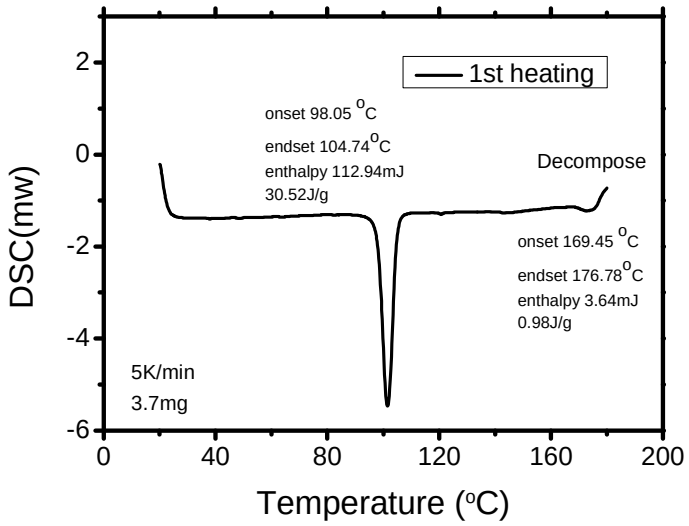

Figure 4-7 DSC traces of HATNA-octyne showing only first heating process

As for **HATNA-yne-8**, although it gave a low isotropic temperature blow 150℃, it still exhibited an instability property upon heating to high temperature (Figure 4-8). In the first heating process, we can see that a small peak appearing at 37 ℃ can be assigned as a transition from a crystal phase to another one, while the peak at 84℃ should be phase transition for crystal phase to mesophase.

Upon cooling, this compound didn't exhibit any clear peak from isotropic phase to crystal phase at 3.7℃. This result usually was reported to be a liquid crystalline glass. And also, it is observable that the peak of crystal transition shifted to 3.7℃ from 84 ℃, which is another evidence for forming a glassy phase. We have to use other technique to confirm this conclusion.

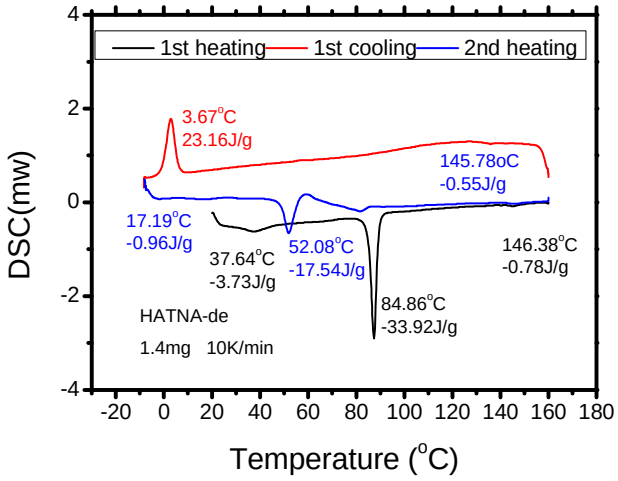

Figure 4-8 DSC curves for HATNA-yne-8

4-3-2-2 POM

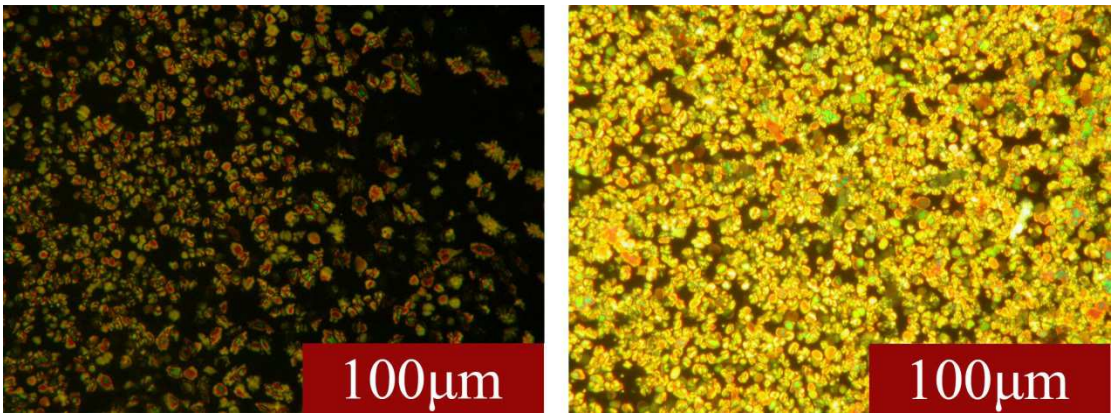

Figure 4-9 POM graphs for HATNA-yne-6

Through characterization of DSC, **HATNA-yne-6** was found to be thermal instability when heating to isotropic phase for a while. So, in the characterization of POM textures, **HATNA-yne-6** was quickly cooled to liquid crystalline phases after melting in isotropic phase. The POM images are shown in Figure 4-9. It is obvious that compound **HATNA-yne-6** exhibited typical mosaic textures in mesophase, which is characteristic for hexagonal columnar phase with edge-on molecular alignment. And also, it was found that this compound formed a glass phase, which could be

observed in room temperature.

HATNA-yne-8 exhibited more stable property in DSC measurement, even if it also turned green color when staying at isotropic phase for a while. So, in POM measurement, we quickly cooled down the temperature after **HATNA-yne-8** was melted. The POM images exhibit typical dendritic texture in the whole visible region shown in Figure 4-10, which can be assigned as homeotropic hexagonal columnar phase with columnar axis perpendicular to the substrates. In the texture, we also can find some bright birefringence, meaning very few defects in the thin films.

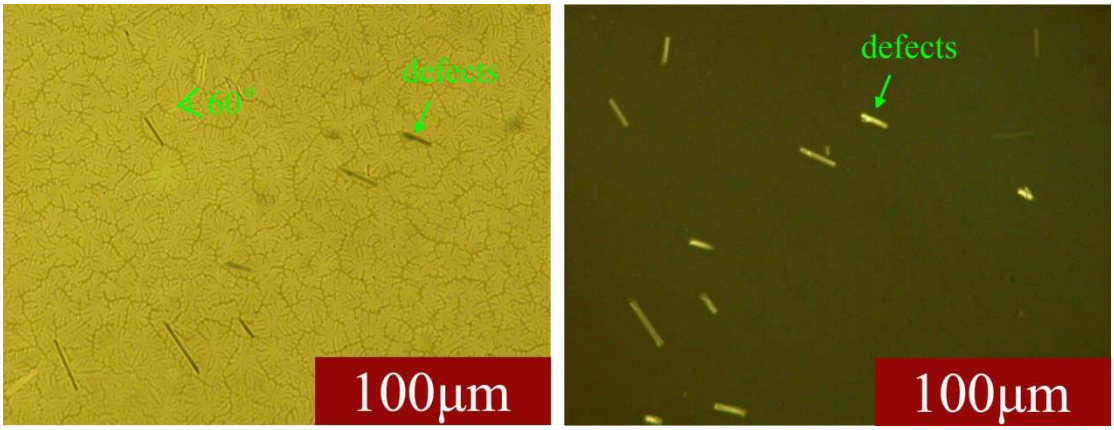

Figure 4-10 POM graphs for **HATNA-yne-8** in hexagonal columnar phase, the left was taken without crossed polarizers, while the right was taken under crossed polarizers.

In the figure, the black region usually is seen as well-defined homeotropic columnar alignment, which always was observed in discotic liquid crystalline hexagonal columnar mesophases, like in triohenylenes and phthalocyanines.

4-3-2-3 XRD

The sample of **HATNA-yne-6** was carefully placed on the glass substrate and then melted with a cover film made by polyimide. Immediately, the sample was cooled down to mesophase, avoiding the sample to decompose in the isotropic phase. The

cooling rate was 10K/min.

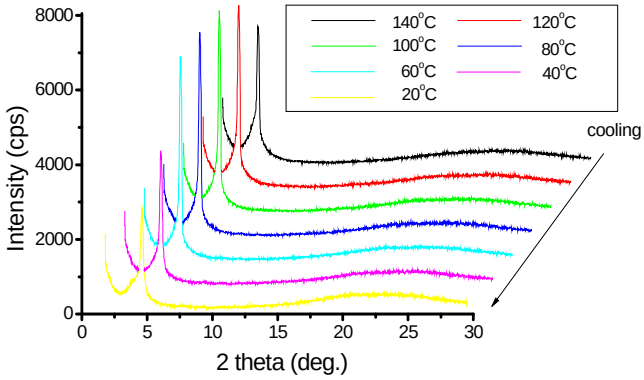

Figure 4-11 XRD patterns for HATNA-yne-6

From the temperature-dependence of XRD patterns shown in Figure 4-11, it can be seen that **HATNA-yne-6** showed a hexagonal columnar, which usually exhibits a clear sharp peak at the small angle region of XRD pattern and wide diffraction in wide angle region by alkyl chains. The lattice parameter in columnar phase of **HATNA-yne-6** can be estimated to be 21.3 Å. Due to the absence of the peak regarding of π - π interaction, **HATNA-yne-6** was considered to form a disordered hexagonal columnar phase.

X-ray diffraction (XRD) pattern of the LC mesophase of **HATNA-yne-8** was given in Figure 5-12. As illustrated from this cure, four peaks with d spacings of 19.6, 11.8, 9.8 and 4.2 Å (Figure 2) which was indexed as diffractions from the d_{10}, d_{11} and d_{20} planes, respectively, coincide clearly with hexagonal columnar structure. This Col_h structure of 1b with a lattice parameter (a) of 23.6 Å can be calculated, which is little larger than **HATNA-yne-6**. However, the diffraction peak at wide angle region which usually can be assigned to the face-to-face distance of the π-πstacked along the columnar axis is absent here, suggesting random intracolumnar distances, i.e. disordered columnar phase.

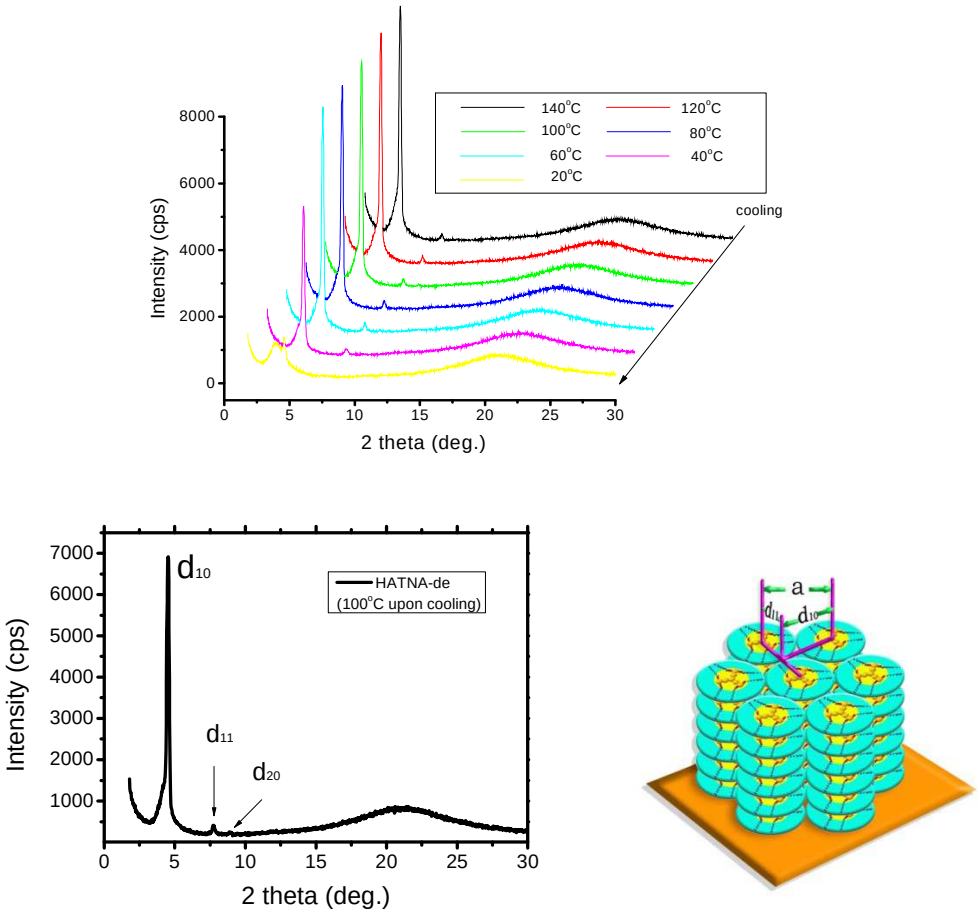

Figure 4-12 XRD pattern of R2,2. The left for temperature dependence; The right for 100℃on cooling (insert: Schematic illustration of the homeotropically aligned Col_h structure)

The disordered hexagonal columnar phase in **HATNA-yne-6** and HATNA-yne-8 probably is influenced by the strong steric hindrance for bay-located side chains, which arrange in narrow space leading a twist molecular configuration.

4-3-3 UV absorption and photoluminescence

Furthermore, comparing with absorption of **HATNA-14**, that of **HATNA-yne-8** exhibited clear red shift about 50nm, which could be explained by much larger conjugation system due to the introduction of triple bonds. The absolute

photoluminescence quantum yield of **HATNA-yne-8** in neat thin film was measured in an integrated sphere at room temperature under air atmosphere. The wavelength of the excitation source used is 254 nm laser line. This result shows that 1b is an excellent semiconducting material for LEDs with good photoluminescence efficiencies (the maximum 10.2%) and an emission maximum around 700 nm.

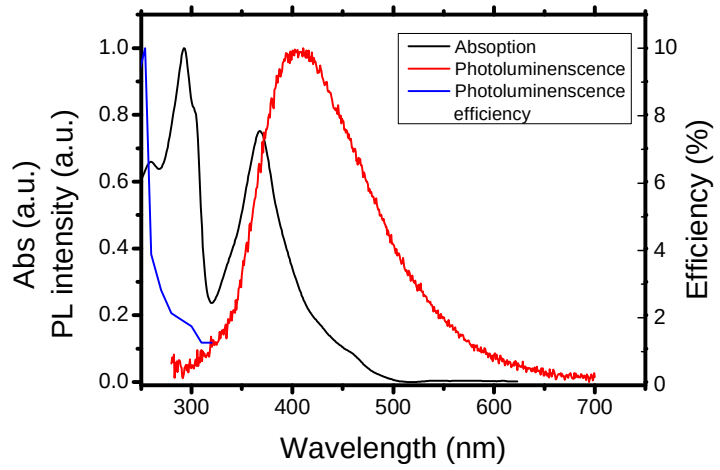

Figure 4-13 Optical absorption, photoluminescence (PL) and PL efficiency of **HATNA-yne-8**

4-3-4 IV measurement

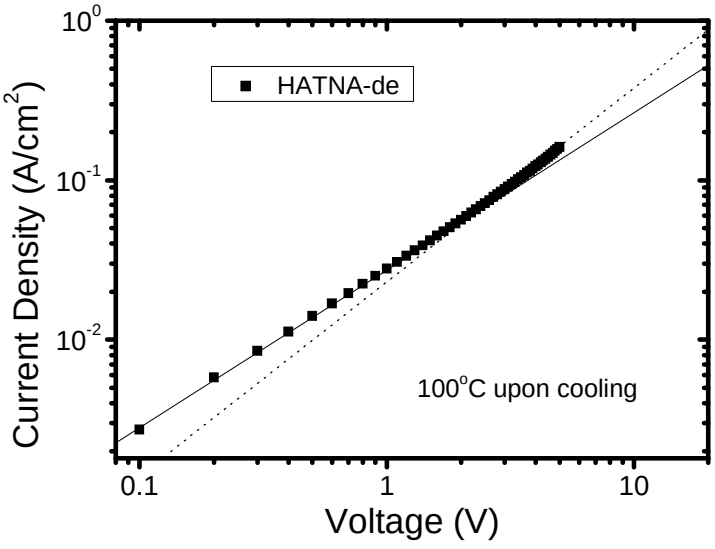

Figure 4-14 IV curve for **HATNA-yne-8**, the cell thickness is 9um

When charge carrier transport was measured in TOF measurement, **HATNA-yne-8** compound always showed high dark current, so that mobility was not accessible. So, IV measurement in Figure 4-14 was carried out to check the dark current directly. We found that the current increased to 0.2A under the voltage of 5V.

We speculated that such high dark current probably was caused by the decomposed **HATNA-yne-8**, but not by itself. In the below section, we will discuss the energy levels of HATNA-yne-8 by CV measurement and optical band gap.

4-3-5 CV measurement

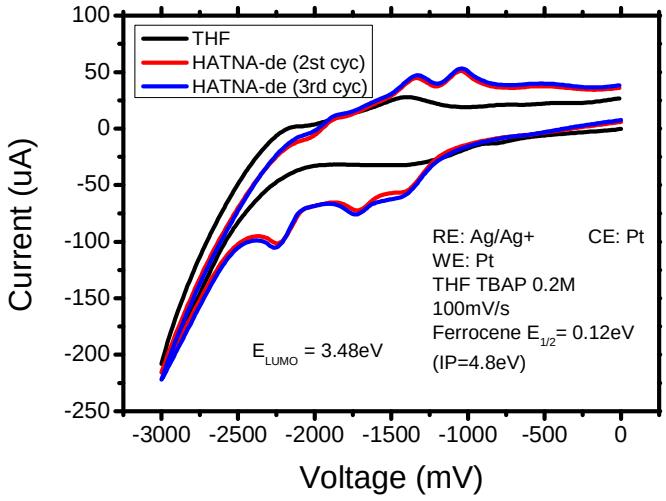

Figure 4-15 Cyclic voltammograms of **HATNA-yne-6** and **HATNA-yne-8** recorded in THF solution of $[(C_4H_9)_4N]ClO_4$ (0.20m). Here, the second scanning is presented for 1b and 1c. Scanning rate=100mVs^{-1}

Cyclic voltammetry was employed to study electrochemical stability of HATNA-yne-8, and to estimate HOMO/ LUMO levels combined with their electronic spectra. To determine LUMO energy values, each measurement was calibrated with the ferrocene–ferrocenium couple (Fc/Fc +) taking 4.8 eV as ferrocene's HOMO level. The cyclic voltammograms show three reversible reduction peaks for both HATNA-yne-8, but no oxidation waves were observed in accessible window

highlighting their dominantly reducible feature. The first reduction peaks for HATNA-yne-8 occurring at –1.1 mV result in their LUMO energy levels of –3.5 eV, respectively. Up to three cycles were recorded and no changes in the redox peaks were observed, which indicates **HATNA-yne-6** and **HATNA-yne-8** have electrochemical stability and reversibility.

The optical band-gap, obtained from the absorption edges of absorption spectra in thin film, was found to be 2.5 eV for **HATNA-yne-8**. So HOMO values can be calculated to be 6.0eV for **HATNA-yne-8** from the optical band-gap and the LUMO levels. Moreover, the results also confirmed that the introduction of six electron-donating side chains could not override the electron-deficiency of the HATNA core.

4-3-6 Summary

In this study, two HATNA derivatives with alkylethynyl groups have been synthesized, whose molecular structure were characterized by HNMR and MS spectrum. Through DSC, POM and XRD measurement, two HATNA derivatives were found to show disordered hexagonal columnar phase. However, probably due to strong steric hindrance of side chains at bay positions, the planarity of HATNA core was destroyed to become a twist structure, which may be the reason for instability when heating to isotropic phase.

Furthermore, their energy levels could be estimated by CV measurement and optical band gap. This result also confirmed that HATNA actually acts as good n-type semiconductor, because of low LOMO level around 3.5eV.

4-4 Alkylthio-substituted HATNA

Based on the last study, the introduction of acetylene bond destroy the planarity of HANTA core, which let us consider that flexible groups will probably be better for HATNA to sustain its original electronic structure and appear liquid crystalline. So, sulfur atoms were inserted between HATNA core and flexible side chains.

4-4-1 synthesis

The synthesis of HATNA with alkylthio groups were synthesized from reaction between the appropriate o-phenylene diamines and hexaketocyclohexane octahydrate with moderate yield in the presence of acetic acid. Prior to the condensation reaction, the preparation of these corresponding diamines commenced with the reduction, which were obtained through the related Pd-catalyzed coupling reactions staring from the same precursor, 4,7-Dibromo-2,1,3-benzothiadiazole (1).

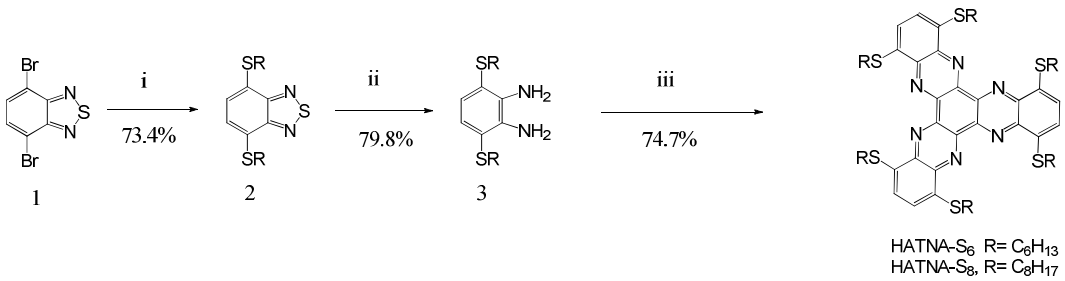

i, HS-C_6H_{13}, $Pd_2(dba)_3$, DPPF, $^iPr_2NEt$, reflux; ii, $LiAlH_4$, THF, 0°C–R.T.; iii, $CHCl_3$, AcOH, 60°C.

Scheme 4-3 Synthetic route for HATNAs with alkylthio groups (**HATNA-S6** and **HATNA-S8**)

In fact, to synthesize compound 2, several methods have been tried. However, the results from such synthetic methods just yielded a mixture of 2, monosubstituted and disubstituted. What' the most difficulty is the separation of the mixture using column chromatography, which exhibited same R_f value in TLC plates observed under 254 nm UV light, making purification impossible.

2 (588mg, 2mmol), $Pd_2(dba)_3$ (1 mol%), DPPF (2 mol%) and DIPEA (1.1 equiv) were dissolved in a flame-dried 50-mL Schlenk flask with 250ml toluene under a stream of nitrogen. After 10min, $C_8H_{17}SH$ (1.0 equiv) was added using a syringe. The temperature of oil bath was increased to 120℃. And stirring was continued 2 days. This reaction was stopped by pouring it into ice-water. Then, the solution was extracted using $CHCl_3$. After evaporation, chromatography column was carried out to purify the crude product.

R_3=SC_6H_{13}: yield of 73.4%. ^{1}HNMR (300MHz, D/chloroform): δ = 7.32 (s, ArH, 2H), 3.11(t, *J=7.5Hz*, 4H), 1.70-1.80 (m, -CH_2-, 4H), 1.30-1.50(t, -CH_2-, 12H), 0.89(t, Me, 6H)

R_3=SC_8H_{17}: yield of 75.2%. ^{1}HNMR (300MHz, D/chloroform): δ = 7.32 (s, ArH, 2H), 3.11(t, *J=7.5Hz*, 4H), 1.69-1.75 (m, -CH_2-, 4H), 1.43-1.55(t, -CH_2-, 20H), 0.88(t, Me, 6H)

Dry THF (50 mL) was added to a flame-dried 100-mL Schlenk flask charged with 5 or 7 (1mmol), then $LiAlH_4$ (14 equiv) was added to the mixture under a stream of nitrogen over a period of 30 min, and stirring was continued for 4 h.

R_3=SC_6H_{13}: with yield of 79.8%. ^{1}HNMR (500MHz, D/chloroform): δ = 6.88 (s, ArH, 2H), 4.10 (s, -NH_2, 4H), 2.74 (t, *J=7.5Hz*, 4H), 1.50-1.60 (m, -CH_2-, 4H), 1.20-1.42(t, -CH_2-, 12H), 0.87(t, Me, 6H)

R_3=SC_8H_{17}: with yield of 82.5%. ^{1}HNMR (500MHz, D/chloroform): δ = 6.87 (s, ArH, 2H), 4.10 (s, -NH_2, 4H), 2.73 (t, *J=7.5Hz*, 4H), 1.52-1.58 (m, -CH_2-, 4H), 1.24-1.43(t, -CH_2-, 20H), 0.87(t, Me, 6H)

Mixture of hexaketocyclohexane octahydrate (1 mmol) and appropriate o-phenylene diamines (0.33mmol) was added to deoxygenated acetic acid (20 mL). The mixture was refluxed for 3 h under nitrogen. After the mixture was cooled to room temperature, the resulting solid was collected by filtration and was washed with acetic acid. All compounds were further purified by chromatography using chloroform and cyclohexene as eluent. Finally, repeated recrystallization was carried out to get high

purity sample.

III-a: a dark red solid, yield: 74.7%. Melting point: 148.5℃.

^{1}HNMR (500MHz, D/chloroform): δ = 7.67(s, ArH, 12H), 3.36(t, *J=7.5Hz*, 12H), 1.84-1.90 (m, -CH_2-, 12H)1.53-1.61(m, -CH_2-, 12H), 1.29-1.39(m, -CH_2-, 60H), 0.89(t, Me, 18H);

HRMS (m/z): $[M]^+$ calcd. for $C_{60}H_{85}N_6S_6$: 1081.5160; found: 1081.5136.

III-b: a dark red solid, yield: 69.3%. Melting point: 125.7℃.

^{1}HNMR (500MHz, D/chloroform): δ = 7.68(s, ArH, 12H), 3.37(t, *J=7.5Hz*, 12H), 1.83-1.89(m, -CH_2-, 12H), 1.39-1.60(m, -CH_2-, 60H), 0.87(t, Me, 18H);

HRMS (m/z): $[M]^+$ calcd. for $C_{72}H_{108}N_6S_6$: 1248.4096; found: 1248.4091.

4-4-2 phase transition

4-4-2-1 DSC

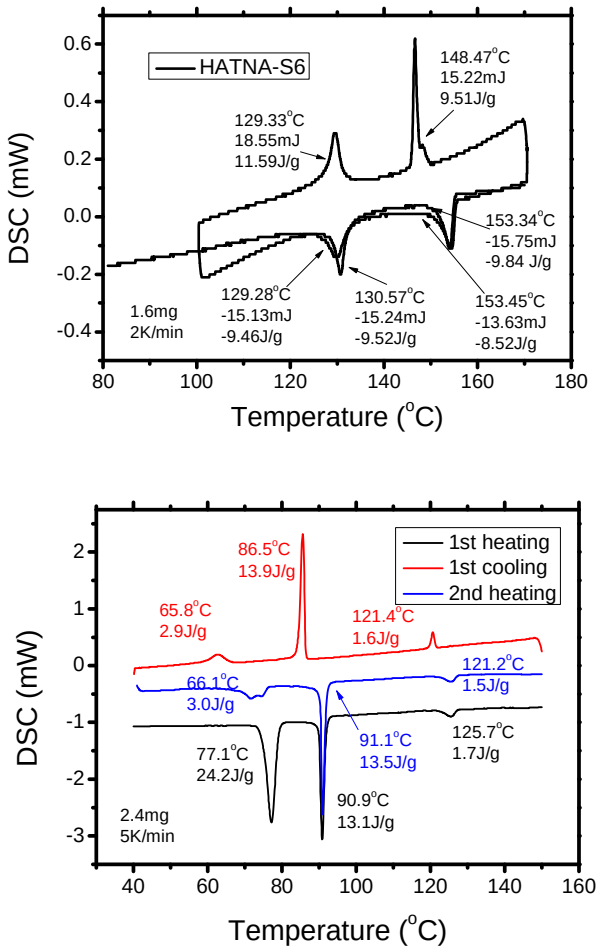

Figure 4-16 DSC curve for HATNA-S6 and HATNA-S8

HATNA-S6 displayed an LC mesophase between 130 and 153℃ (on heating) and between 148 and 129℃(on cooling). But, very small peak appears close to 148℃ upon cooling, which may another LC phase. If longer side chains are used, the two peaks might be separated completely. And, between them, this phase usually is hexagonal columnar phase, which tends to morph into rectangular phase.

According to DSC curves of **HATNA-S6**, it can be observable that upon cooling one shoulder peak appeared at 148℃. To extend the phase usually needs to introduce longer side chains into the corresponding core. So, here, we find that clear phase separation appears when C6 was insteaded by C8 in Fig 7. And **HATNA-S8** shows two reversible mesophases upon heating and cooling. The second mesophase probably is higher ordered than the first one, because the exothermic peak at 86.5℃ is quite larger than others.

4-4-2-2 POM

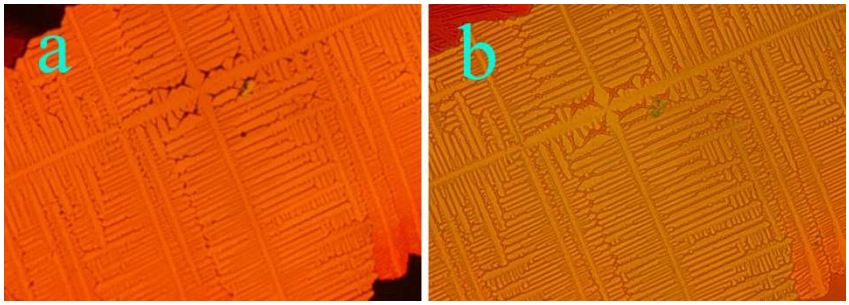

Figure 4-17 POM of **HATNA-S6** at 140℃ upon slow cooling (2K/min). a: crossed polarizers; b: no polarizers

POM textures of **HATNA-yne-6** and HATNA-yne-8 have been discussed in the previous section. In particular, **HATNA-yne-8** presented typical dendritic textures with 60° angle, which is characteristic for the homeotropic phase, in which the columnar axes are perpendicular to the substrates. And also, on slow cooling from the isotropic liquid, **HATNA-S6** sandwiched between a clean glass slide and a coverslip exhibit birefringent dendritic textural pattern emanating from the dark background of isotropic liquid. This pattern is well-known to be an important signature and

conclusive evidence for the occurrence of Col phase. As observed in Figure 4-17, these textures are arranged with 90° angle, which are significantly distinguished from others, like hexagonal columnar textures.

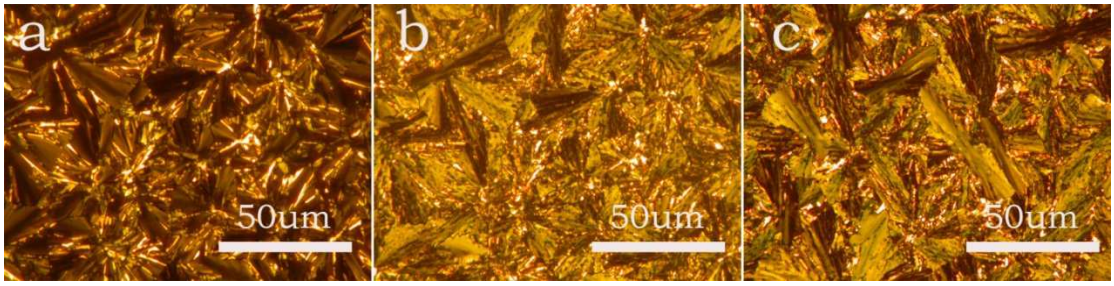

Figure 4-18 POM graphs of HATNA-S8 (a: 115℃; b: 80℃; c: 30℃)

As observed in POM graphs in Figure 4-18, at 115 ℃, **HATNA-S8** showed fan-like textures, which usually can be assigned as signature for tilted columnar phase. When cooling to 80℃, it gave broken fan-like textures, showing that a highly ordered columnar phase appears. Until to room temperature, the material entered into polycrystalline phase.

4-4-2-3 XRD

Upon cooling, **HATNA-S6** exhibited two liquid crystalline phases between 148 and 129℃ upon cooling. XRD patterns in Figure 4-19 are consistent with DSC results. At 148℃, the compound just entered the first mesophase. A peak appeared at small angle region suggesting the intercolumnar distance, while the wide peak around 25°usually was considered as the reflection of alkyl chains. As the decrease of temperature, the compound immediately accessed the second mesophase. XRD curve measured at 135℃ demonstrated this phase likely consists of columns of molecules in a rectangular two dimensional lattice. The lattice parameters are: a = 37.6Å, b = 16.8Å.

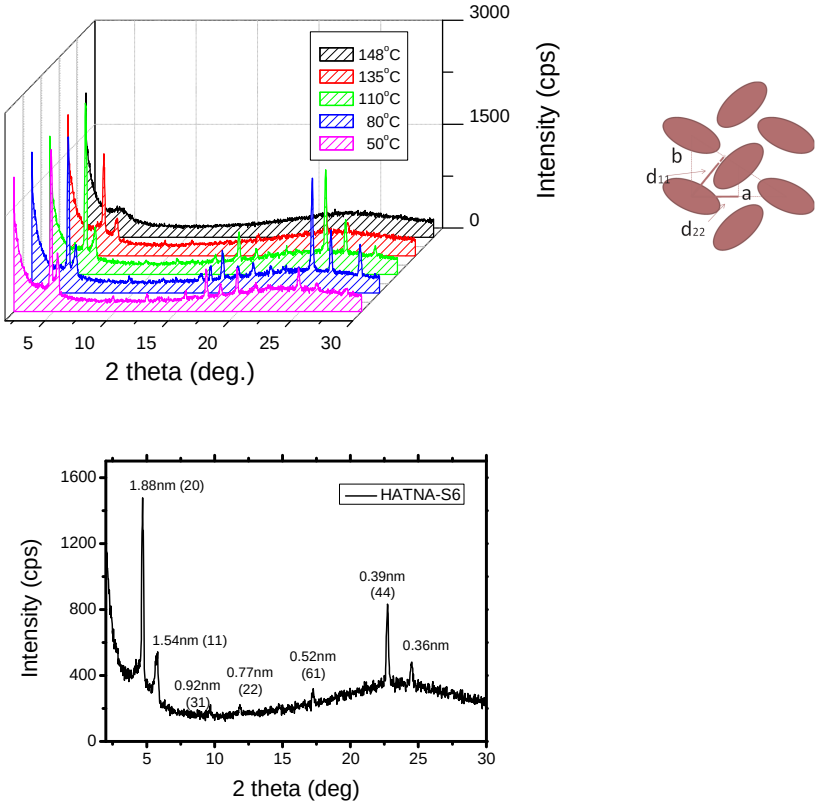

Figure 4-19 XRD pattern of **HATNA-S6**, the left for temperature dependence; The right for 135℃on cooling

As discussed above, upon cooling, HATNA-S6 exhibited two liquid crystalline phases between 148 and 129℃ upon cooling. XRD patterns are consistent with DSC results. At 148℃, the compound just entered the first mesophase. A peak appeared at small angle region suggesting the intercolumnar distance, while the wide peak around 25°usually was considered as the reflection of alkyl chains. As the decrease of temperature, the compound immediately accessed the second mesophase. XRD curve measured at 135℃ demonstrated this phase likely consists of columns of molecules in a rectangular two dimensional lattice. The lattice parameters are: a = 37.6Å, b = 16.8Å.

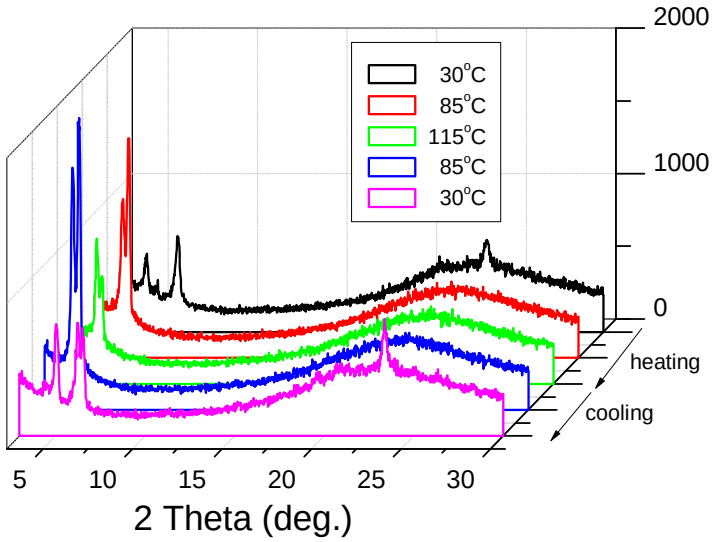

Figure 4-20 Temperature-dependence XRD patterns of **HATNA-S8**

In Figure 4-20, XRD measurement of **HATNA-S8** was carried out in each phase during heating and cooling, whose results are consistent with the judgment from POM textures. Both two mesophases can be assigned to rectangular columnar phase. Specularly, the tensity of the peaks (20) and (11) in second are quite higher than in first one, which is indictive of higher ordered structure. On the other hand, we also calculate the lattice parameters, a and b, to be 19.2 and 17.5 Å. For **HATNA-S6**, its lattice parameters are: a = 37.6Å, b = 16.8Å. Because the peaks of (20) and (11) in rectangular lattice are separated from the peak of (10) in hexagonal lattice. So, it is worth pointing out that longer side chains prefer to assist moleculars to form hexagonal phase in disctic liquid crystals. That to say, if HATNA is introduced with longer side chains, like C_{10} or C_{12}, it will probably exhibit hexagonal phase.

4-4-3 UV absorption

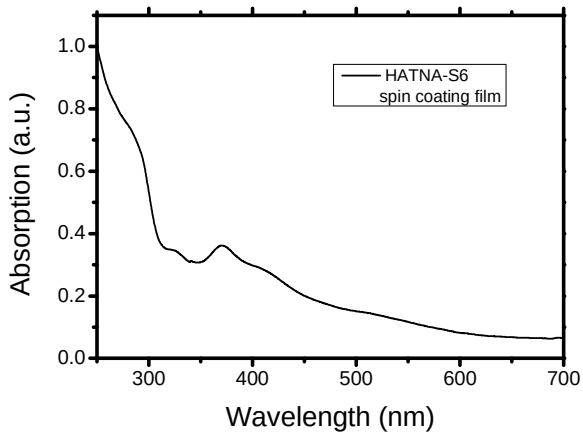

Figure 4-21 Optical absorption of HATNA-S6

HATNA-S6 presents dark red color and no photoluminescence, and its absorption spectrum almost covers the whole optical region below 700nm, which is quite different from the peri-substituted-thioether HATNA in literature. It is surprising to point out that the change of substitutes' positions has so strong influence on absorption. And the optical band gap can be calculated to be 1.91eV.

4-4-4 CV measurement

The cyclic voltammograms show three reversible reduction peaks for **HATNA-S6** (Figure 4-22). But no oxidation waves were observed in accessible window highlighting the dominantly reducible feature. The first reduction peaks occurring at –1.1 V result in almost identical LUMO energy levels of –3.48 eV. Up to three cycles were recorded and no changes in the redox peaks were observed, which indicates electrochemical stability and reversibility. The optical band-gap, obtained from the absorption edges of absorption spectra in thin film (see Figure 4-21), was found to be 2.43 eV for 1b. So HOMO values can be calculated to be 5.91eV from the optical band-gap and the LUMO levels. The energy levels of **HATNA-S6** were estimated to be 3.40eV for LUMO and 5.31eV, respectively.

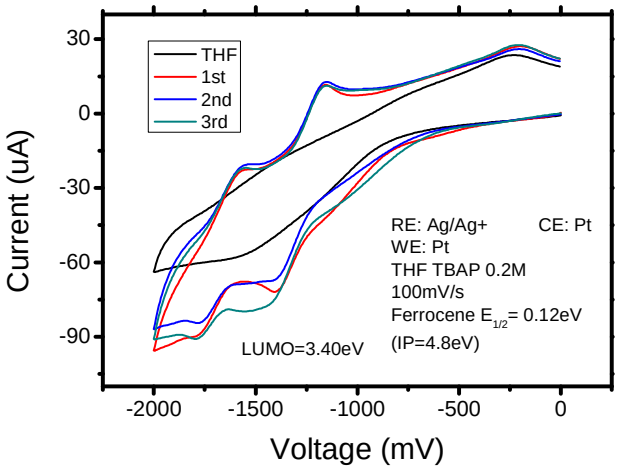

Figure 4-22 CV measurement of **HATNA-S6**

4-4-5 Transient state photoconductivity measurement

The transient photocurrent of **HATNA-S6** was discussed to be so dispersive (Figure 4-23) that the kink points couldn't be picked up, which can be explained through its edge on alignment.

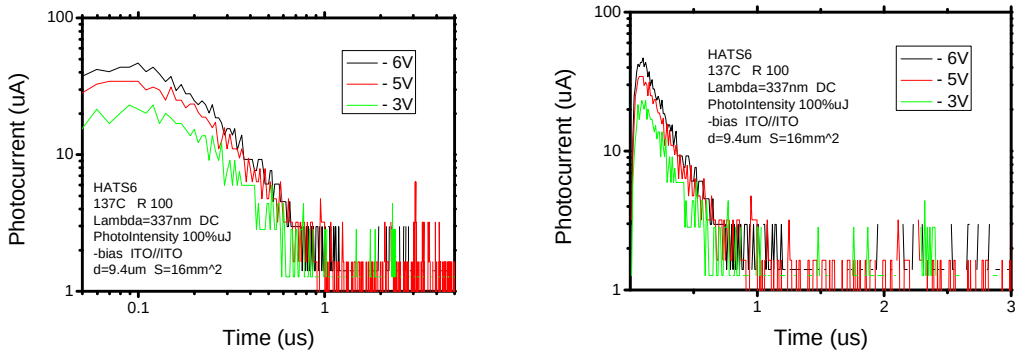

Figure 4-23 Transient photocurrent of **HATNA-S6** at 137℃(left: log-log; right: liner-log)

After recrystallization for several times, this material was injected into liquid crystal cell (9.4um) with ITO electrodes. Negative current could be observed at very low electric field shown in Figure 4-23. However, no positive current appeared even if high electric field was applied. This result is consistent with CV results (only showing

reductive peaks), probably meaning this compound has stable reduction state but unstable oxidation state. So, its molecules hardly transport hole through their overlaps.

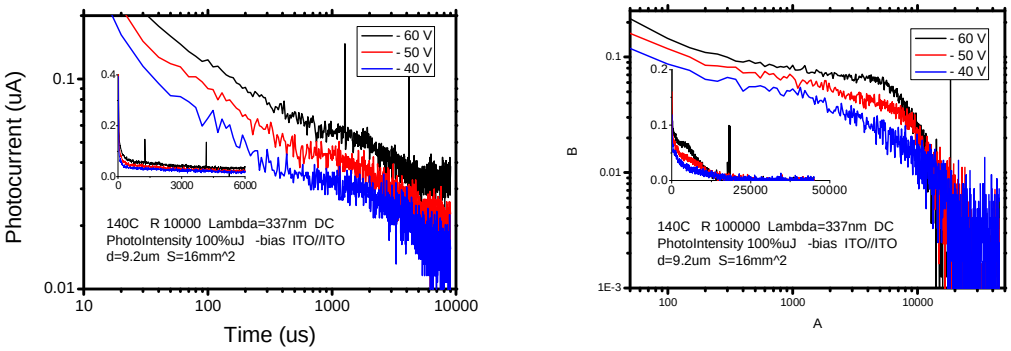

Figure 4-24 transient photocurrent of **HATNA-S8** in the isotropic (left: electron; right: ionic)

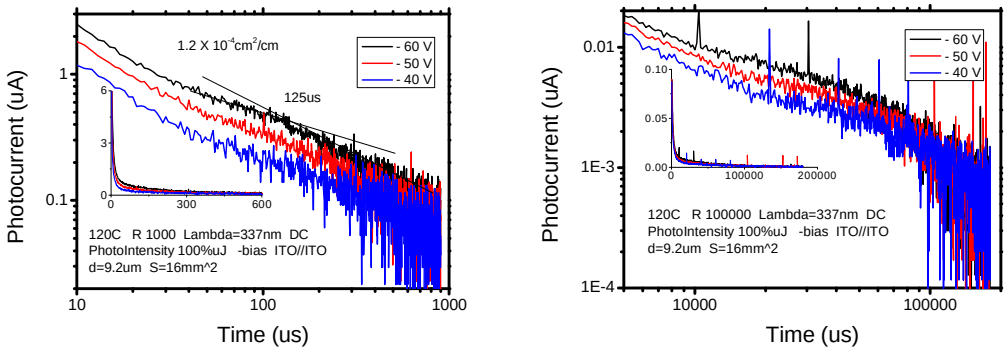

Figure 4-25 transient photocurrent of **HATNA-S8** in the Colr mesophase (left: electron; right: ionic)

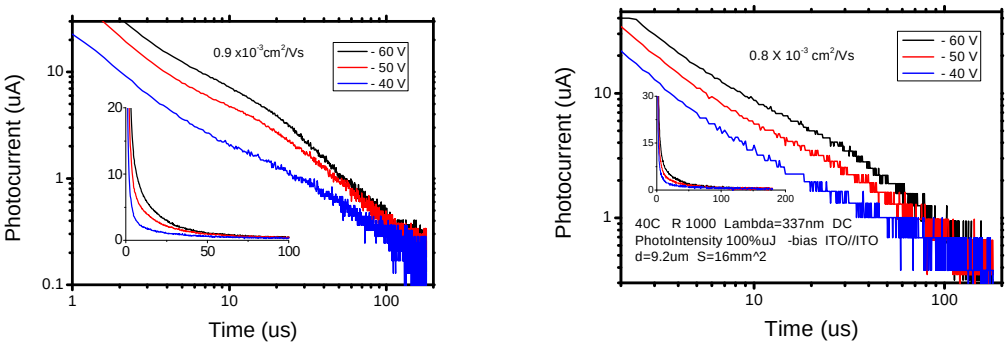

Figure 4-26 a) Typical transient photocurrent. The left is in colr' phase at 80℃, and the right in polycrystalline phase at 40℃. The thickness of liquid crystal cell used here is 9.3um, into which HATNA-S8 was injected at 150℃.

HATNA-S8 produced typical distinctly dispersive transient photocurrent for negative charge, which output clear kink points in double-log plots (shown in Figure 4-24, 4-25 and 4-26). Most notably, the electron mobility can be obtained to be 10^{-5} $cm^2V^{-1}s^{-1}$ in isotropic phase, and then increased to 10^{-4} $cm^2V^{-1}s^{-1}$ in the Col_r phase with obvious temperature dependence. In the Col_r' phase and polycrystalline phase, the electron mobility incrementally reaches to 10^{-3} $cm^2V^{-1}s^{-1}$, which is almost independent on temperature and weak dependent on electric field (in figure 4-27). In order to confirm that they are electroic transport, the ionic transport in each phase also was showed in Figure 4-24 and 4-25. In the colr' and polycrystalline phase, due to high viscosity, the ionic transport was hardly observed.

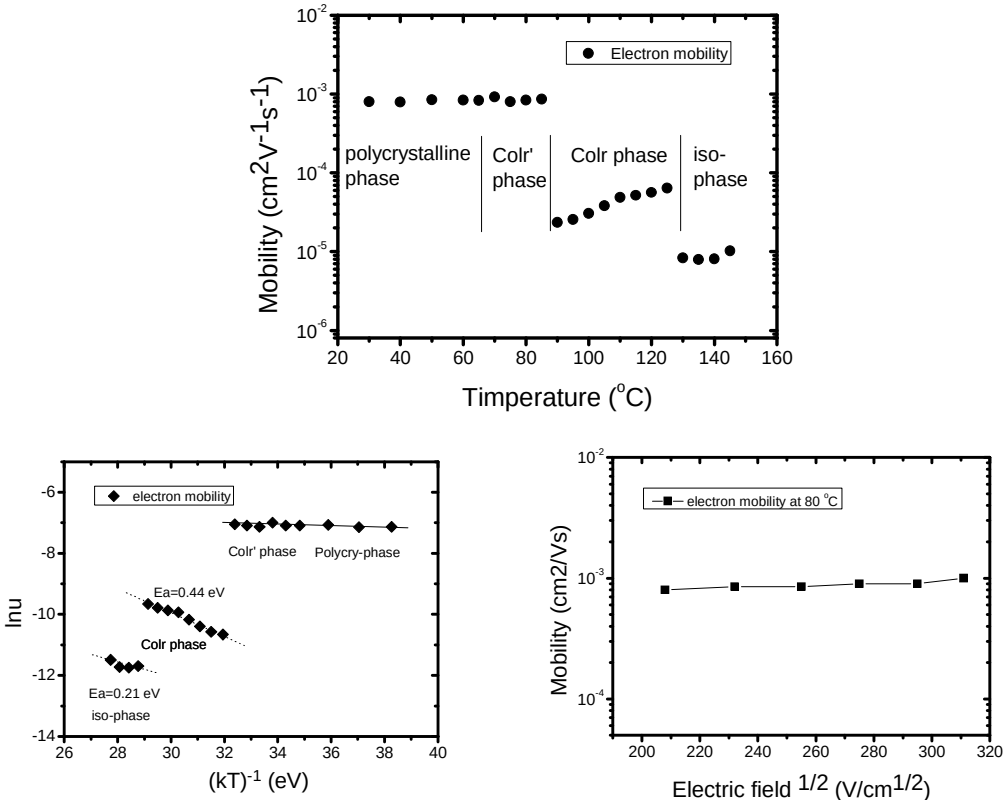

Figure 4-27 a) and b)Temperature dependence of electron mobility of HATNA-S8. E=6.5×$10^4$$Vcm^{-1}$ c) Electric field dependence of electron mobility in Colr' phase at 80℃.

In the Figure 4-27, arrhenius plot illustrates the temperature-dependent electron

mobility. We can observe that in the isotropic phase and Colr phase, probably due to the molecular dipole moment and disordered structure, the electron mobility has temperature dependence with activity energy of 0.21eV and 0.44eV, respectively, which are comparable with calamitic liquid crystalline 8-PNP-O12. In such disordered phases, transport generally proceeds via hopping and is thermally activated. Higher temperatures improve transport by providing the energy required to overcome the barriers created by energetic disorder. In the Colr' phase, a slight increase in mobility can be observed at high fields. Here, the applied voltage was not too high to yield a yield a Poole-Frenkel behavior.

4-4-6 Summary

In this section, two HATNAs with alkylthio groups were synthesized through a facile synthetic route. Their molecular structures have been confirmed by HNMR and MS spectra. Phase transition was characterized by DSC and POM. Using temperature-dependence XRD characterize their phase structures.

The HATNA with sulfur atom spacers surprisingly showed molecular columns with rectangular lattices, whose molecular alignment also varied sensitively depending on the alkyl chain length. Furthermore, CV measurements demonstrated that the introduction of various side chains could not override the electron-deficiency of the HATNA core. More importantly, we also found that the HATNA bay-substituted with octylthio groups showed high electron mobility in the bulk of Col_r' phase and even in polycrystalline phase up to 10^{-3} $cm^2V^{-1}s^{-1}$.

4-5 Summary of Chapter 4

In conclusion, series of bay-substituted HATNA derivatives have been synthesized through facile synthetic strategies. We found that all compounds can form long-range molecular columns with self-directed growth direction. Interestingly, the HATNA substituted with bay alkyl groups (Type I) presented typical “edge-on” molecular alignment to form in-plane-oriented molecular columns on the substrate. On the other hands, the HATNAs with acetylene spacers (type II) exhibited perfect hexagonal lattice patterns: II-a with short side chains showed in-plane molecular columns, while II-b with longer chains obviously resulted in out-of-plane-oriented columns with “face-on” molecular alignment.

In the case of III, the HATNA with sulfur atom spacers surprisingly showed molecular columns with rectangular lattices, whose molecular alignment also varied sensitively depending on the alkyl chain length. Furthermore, CV measurements demonstrated that the introduction of various side chains could not override the electron-deficiency of the HATNA core. More importantly, we also found that the HATNA bay-substituted with octylthio groups showed high electron mobility in the bulk of Col_r’ phase and even in polycrystalline phase up to 10^{-3} $cm^2V^{-1}s^{-1}$. The present molecular design strategy of introducing side chains at bay positions is an effective method to achieve long range molecular columns for fast charge transport, and also the out-of-plane–oriented molecular columns, which enables us to apply discotic liquid crystals to devices application in vertical electrode configuration.

References of Chapter 4

[1] a) D. Adam, P. Schuhmacher, J. Simmerer, L. Häussling, K. Siemensmeyer, K. H. Etzbachi, D. Haarer, *Nature*, *371*, 141 (1994). b) D. Adam, F. Closs, T. Frey, D. Funhoff, D. Haarer, P. Schuhmacher, K. Siemensmeyer, *Phys. Rev. lett. 70*, 457 (1993). c) N. Boden, R. J. Bushby, J. Clements, B. Movaghar, K. J. Donovan, T. Kreouzis, *Phys. Rev. B 52*, 13274 (1995). d) H. Iino, J. Hanna, R. J. Bushby, B. Movaghar, B. J. Whitaker, M. J. Cook, *Appl. Phys. Lett. 87*, 132102 (2000). e) D. Markovitsi, *Mol. Cryst. Liq. Cryst. 397*, 389 (2003); f) K. Ohta, K. Hatsusaka, M. Sugibayashi, M. Ariyoshi, K. Ban, F. Maeda, R. Naito, K. Nishizawa, A. M. van de Craats, J. M. Warman, *Mol. Cryst. Liq. Cryst. 397*, 325 (2003)

[2] a) H. Fujikake, T. Murashige, M. Sugibayashi, K. Ohta, *Appl. Phys. Lett. 85*, 3474 (2004). b) K. Ban, K. Nishizawa, K. Ohta, A. M. van de Craats, J. M. Warman, I. Yamamoto, H. Shirai, *J. Mater. Chem. 11*, 321 (2001). c) T. Komatsu, K. Ohta, T. Watanabe, H. Ikemoto, T. Fujimoto, I. Yamamoto, *J. Mater. Chem. 4*, 537 (1994).

[3] a) A. M. Van de Craats, J. M. Warman, A. Fechtenkötter, J. D. Brand, M. A. Harbison, K. Müllen, *Adv. Mater. 11*, 1469 (1999). b) L. Schmidt-Mende, A. FechtenkRtter, K. Mullen, E. Moons, R. H. Friend, J. D. Mackenzie, *Science 293*, 1119 (2001)

[4] a) K. Q. Zhao, C. Chen, H. Monobe, P. Hu, B. Q. Wang, Y. Shimizu, *Chem. Comm. 47*, 6290 (2011). b) X. Liu, J. Hanna, Prepared.

[5] a) S. Tatemichi, M. Ichikawa, T. Koyama, Y. Taniguchi, *Appl. Phys. Lett. 89*, 112108 (2006). b) Z. An, J. Yu, S. C. Jones, S. Barlow, S. Yoo, B. Domercq, S. R. Marder, *Adv. Mater. 17*, 2580 (2005).

[6] a) I. O. Shklyarevskiy, P. Jonkheijm, N. Stutzmann, D. Wasserberg, H. J. Wondergem, P. C. Christianen, J. C. Maan, *J.Am. Chem. Soc. 127*, 16233 (2005).

b) C. Deibel, D. Janssen, P. Heremans, V. De Cupere, Y. Geerts, M. L. Benkhedir, G. J. Adriaenssens, *Org. Electron*. *7*, 495 (2006).

[7] B. A. Jones, M. J. Ahrens, M. H. Yoon, A. Facchetti, T. J. Marks, M. R. Wasielewski, *Angew. Chem. Int. Ed*. *116*, 6523 (2004).

[8] a) M. Lehmann, G. Kestemont, R. Gómez Aspe, C. Buess‐Herman, M. H. Koch, M. G. Debije, D. A. Ivanov, Chem. Eur. J. 11, 3349 (2005). b) H. Bock, A. Babeau, I. Seguy, P. Jolinat, P. Destruel, ChemPhysChem, 3, 532 (2002). c) C. W. Ong, S. C. Liao, T. H. Chang, H. F. Hsu, J. Org. Chem. 69, 3181(2004) d) G. Kestemont, V. De Halleux, M. Lehmann, D. A. Ivanov, M. Watson, Y. H. Geerts, 20, 2074(2001).

[9] a) B. R. Kaafarani, T. Kondo, J. Yu, Q. Zhang, D. Dattilo, C. Risko, S. R. Marder, *J. Am. Chem. Soc*. *127*, 16358 (2005). b) T. Ishi-i, K. Yaguma, R. Kuwahara, Y. Taguri, Mataka, S. *Org. lett*. *8*, 585 (2006). c) H. L. Yip, J. Zou, H. Ma, Y. Tian, N. M. Tucker, A. K. Y. Jen. *J. Am. Chem. Soc*. *128*, 13042 (2006). d) B. R. Kaafarani,, T. Kondo, J. Yu, Q. Zhang, D. Dattilo, C. Risko, S. R. Marder, *J. Am. Chem. Soc*. *127*, 16358 (2005). e) B. Domercq, J. Yu, B. R. Kaafarani, T. Kondo, S. Yoo, J. N. Haddock, B. Kippelen, *Mol. Cryst. Liq. Cryst*. *481*, 80 (2008).

[10] M. Lehmann, G. Kestemont, R. Gómez Aspe, C. Buess‐Herman, M. H. Koch, M. G. Debije, D. A. Ivanov, *Chem. Eur. J*. *11*, 3349 (2005).

[11] S. Furukawa, T. Okubo, S. Masaoka, D. Tanaka, H. C. Chang, S. Kitagawa, *Angew. Chem. Int. Ed*. *44*, 2700 (2005).

[12] S. Barlow, Q. Zhang, B. R. Kaafarani, C. Risko, F. Amy, C. K. Chan, S. R. Marder, *Chem. Eur. J*. *13*, 3537 (2007).

[13] S. D. Ha, B. R. Kaafarani, S. Barlow, S. R. Marder, A. Kahn, *J. Phys. Chem. C 111*, 10493 (2007).

[14] O. Thiebaut, H. Bock, E. Grelet, *J. Am. Chem. Soc*. *132*, 6886 (2010). b) W. Pisula, M. Zorn, J. Y. Chang, K. Müllen, R. Zentel, *Macro. Rap. Comm*. *30*, 1179 (2009).

[15] a) H. Iino, Y. Takayashiki, J. I. Hanna, R. J. Bushby, *J. J Appl. Phys*. *44*, 1307 (2005). b) Y. Miyake, Y. Shiraiwa, K. Okada, H. Monobe, T. Hori, N. Yamasaki, Y. Shimizu, *Appl. Phys. Exp*. *4*, 1604 (2011). c) X. Y. Liu, T. Usui, H. Iino, J. I. Hanna, derivatives. *J. Mater. Chem. C 1*, 8186 (2013).

[16] E. Treossi, A. Liscio, X. Feng, V. Palermo, K. Müllen, P. Samorì, *Small*, *5*, 112 (2009).

[17] W. Pisula, F. Dierschke, K. Müllen, *J. Mater. Chem*. *16*, 4058 (2006).

[18] a) H. Schönherr, F. J. B. Kremer, S. Kumar, J. A. Rego, H. Wolf, H. Ringsdorf, E. Bamberg, *J. Am. Chem. Soc*. *118*, 13051 (1996). b) S. Archambeau, I. Seguy, P. Jolinat, J. Farenc, P. Destruel, T. P. Nguyen, E. Grelet, *Appl. Surf. Sci*. *253*, 2078 (2006). c) T. D. Choudhury, N. V. Rao, R. Tenent, J. Blackburn, B. Gregg, I. I. Smalyukh, J. Phys. Chem. B 115, 609 (2011). d) E. Grelet, H. Bock, *Euro. Lett*. *73*, 712 (2006).

[19] V. Duzhko, E. Aqad, M. R. Imam, M. Peterca, V. Percec, K. D. Singer, *Appl. Phys. Lett*. *92*, 113312 (2008).

[20] a) H. Iino, J. I. Hanna, D. Haarer, *Phys. Rev. B 72*, 193203(2005). b) H. Iino, J. I. Hanna, *J. Phys. Chem. B 109*, 22120 (2005).

[21] a) M. Funahashi, J. I. Hanna, *Phys. Rev. Lett*. *78*, 2184 (1997). b) M. Funahashi, J. I. Hanna, *Adv. Mater*. *17*, 594 (2005). c) M. Funahashi, J. I. Hanna, *Appl. Phys. Lett*. *76*, 2574 (2000).

Chapter 5

Bay-substituted Discotic Liquid Crystalline truxenes

5-1 Introduction

C_3 symmetric truxene (10, 15-dihydro-*5H*-diindeno[1,2-a;1′2′-c]fluorene) shown in Figure 5-1 is a heptacyclic aromatic hydrocarbon. In general, organic compounds based on fluorene exhibit highly fluorescent, which actually also act as fascinating candidates for variety of applications in opto-electronic devices.[1,2] Truxene molecule (Figure 5-1) can be considered to be consisted of three fluorene units, which actually have a same benzene ring in the molecular center and specially appears a planar structure.

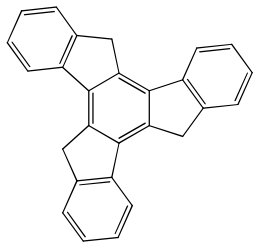

Figure 5-1 The molecular structure of truxene

Compounds based on truxene, even if researches on them could be dated back to more than one century ago [3], had never been studied widely for special usage, however just currently they started to arouse attention when it can be used to be a starting material for preparing organic functional materials, like fullerene derivatives[4]. During the past 10 years, lots of monodisperse dimers [5] and star-shaped oligomers [6], in which truxene was used, have been successfully prepared by using facile synthetic

routes and, presented good research value as functionalized compounds, such as semiconducting materials, nonlinear optical materials, luminescent materials, photochromophores, and so on, as well as applications in the areas of asymmetric catalysis and chiral recognition, fluorescent probes, etc.

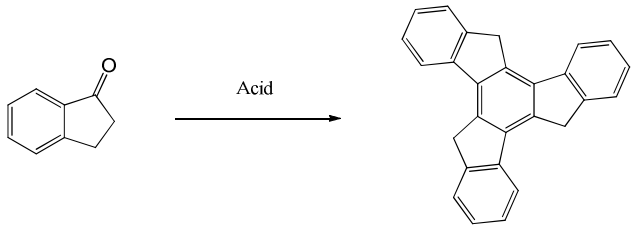

Scheme 5-1 Synthetic route for truxene

Derivatives based on truxene prepared through the acid-catalyzed trimerization always start from 1-indanone (Scheme 5-1), in which Strong acids or Lewis acids, such as hydrochloric acid, phosphorus pentaoxide, phosphorus pentachloride, sulfuric acid, ethyl polyphosphate, polyphosphoric acid, and so on, have generally been employed. Especially, in most cases, introducing aide chains into the peripheral phenyl rings can functionalize it.

Discotic liquid crystals [7] derived from truxene core have been aroused much interests since they display a variety of phase transition and thermal stability and, therefore, recently they were studied extensively in the field of liquid crystalline materials. Truxene discotics with six peripheral chains have been reported to show very abundant phase transition behaviors.

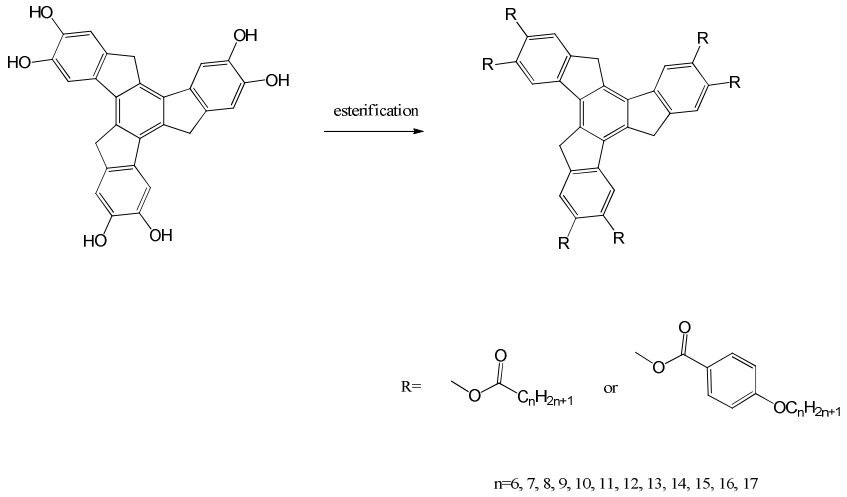

Scheme 5-2 Synthetic route for DLC truxene hexaesters and benzoates

DLC truxene hexaesters and benzoates have been prepared by the introducing flexible alkyl chains to 2, 3, 7, 8, 12, 13- hexahydroxytruxene (Scheme 5-2) [8]. Truxene hexaesters displayed good polymorphism, and all of these compounds showed nematic phase and columnar phases. On the other hand, the homologues of hexabenzoate truxene series exhibited very common phase sequences, that is, Crystal-Columnar-N_D-Isotropic, while other derivatives probably gave rise to both columnar and nematic phases.

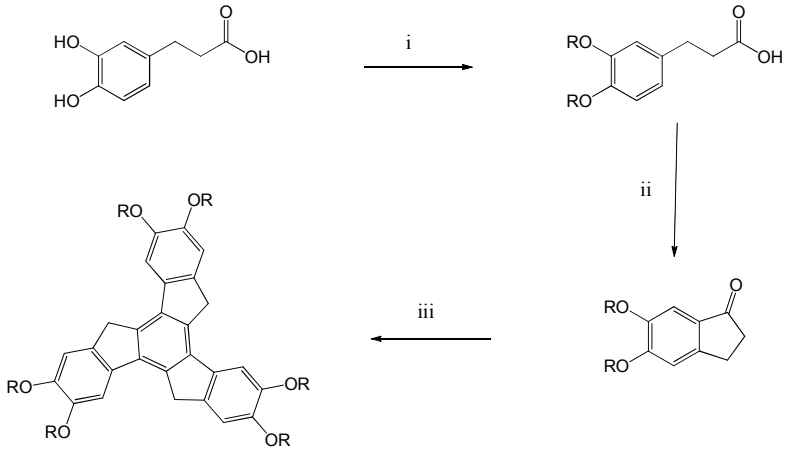

Scheme 5-3 Synthesis of hexaalkoxytruxenes: (i) KOH, ethanol, RBr; (ii) PPA, 110° C; (iii) PPA, 140° C.

Truxene hexaethers previously were synthesized by the route in Scheme 5-3. In this route, Ddihydroxy phenyl propionic acid was alkylated with alkyl halide using KOH in ethanol. The resultant 3-(3,4-dialkoxyphenyl)propionic acids were cyclized to indanone in PPA. A solution of 5,6-dialkoxy-1-indanones when heated at 140 ℃ in PPA produced desired truxene hexaethers in low yield.[7]

In contrast to hexaesters, all of truxene hexaethers were found to show only a hexagonal columnar mesophase, which could be explained based on the consideration of the low steric hindrance from the six ether linkages, which permits a stronger cohesion between cores within a column. Furthermore, clear points decreased gradually on increasing the length of peripheral chains. As expected, the intercolumnar distance rose with both chain length and temperature. The intracolumnar core－core separation in all the compounds was found to be around 3.6 Å.

Researchers in Pei's group recently reported a series of truxene derivatives and their truxenone analogues.[6] They studied how such materials (1, TrO3 and Tr3 in Figure 5-2) could self-assembly into one dimensional microstructures in various solvents. Interestingly, the three compounds also could form liquid crystalline phase during cooling.

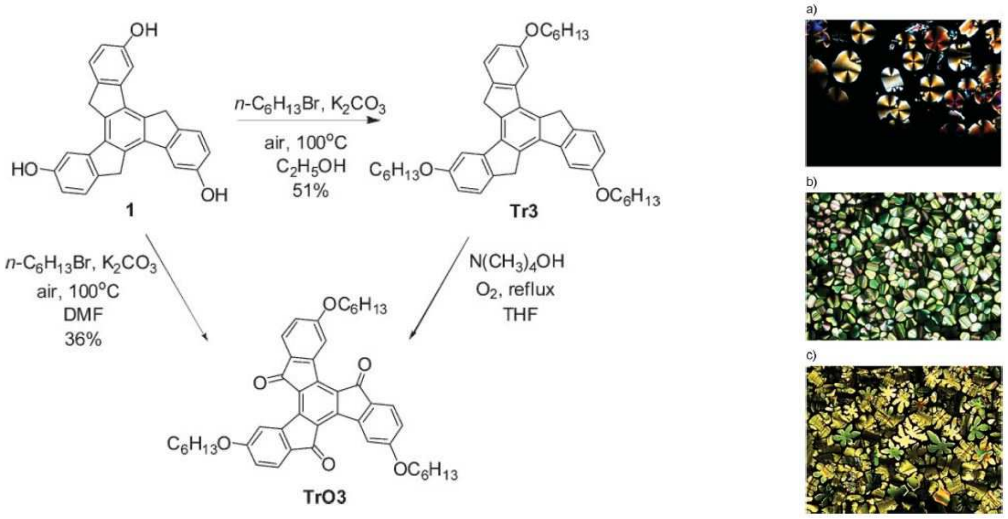

Figure 5-2 Molecular structures and synthetic route, POM graphs for 1, TrO3 and TrO3

Later on, Zhao et al. prepared the type of Tr3 with octoxyl groups (Figure 5-3) according to the same synthetic route reported by Pei, and also studied the phase transition by DSC, POM and XRD to reveal that this material showed highly ordered hexagonal columnar upon heating and cooling. In order to investigate the charge carrier transport in the mesophase of Tr3-octoxy, they tried to measure transient photocurrent through time of flight technique, and finally very high hole mobility up to $10^{-2}cm^2V^{-1}s^{-1}$ was determined.[9]

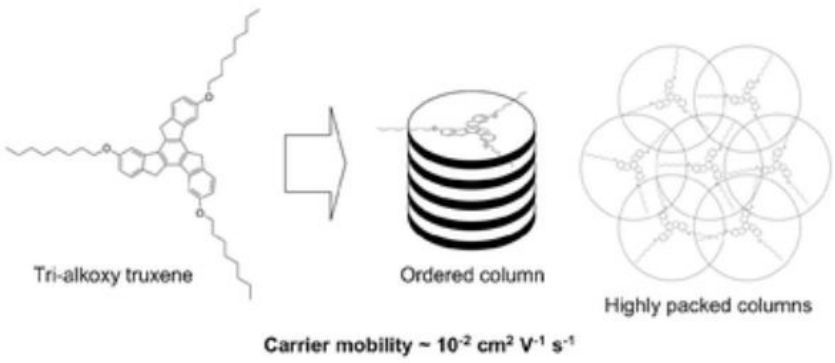

Figure 5-3 The molecular structure and illustration of columnar packing

5-2 Alkoxyl-substituted truxenes

5-2-1 4, 8, 12-trialkoxyltruxene

Tri-peri-substituted truxene was reported to exhibit ordered hexagonal columnar phase and have high hole mobility at the order of 10^{-2} cm^2/Vs in Col_h phase [9]. Here, tri-bay-substituted truxene was synthesized through three-step reaction. In this case, the side chains are located in bay positions of truxene core, which is designed as the concept in this study.

5-2-1-1 Synthesis

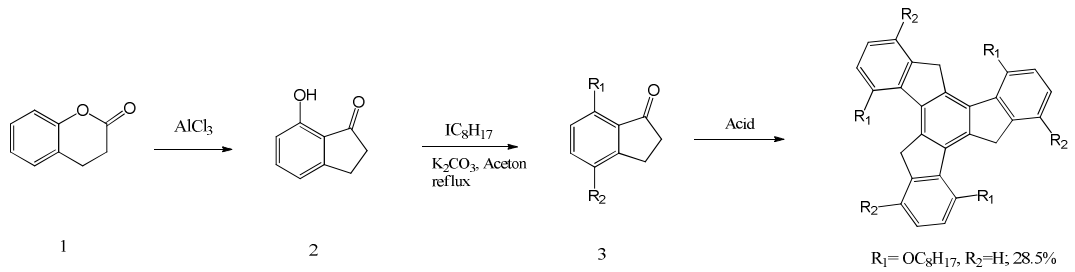

Scheme 5-4 Synthetic route for bay-substitued truxene

Synthesis of 2

A mixture of 4‐chromanone 5 (1) (1 g, 6.8 mmol) and anhydrous, powdered $AlCl_3$ (2.7 g, 20 mmol) was fused at 250 ˚C for 10 min. After allowing the reaction mixture to cool to ambient temperature, dichloromethane (10 mL) and cold hydrochloric acid (10 mL) were added to the mixture. The resulting black miture was extracted with dichloromethane (50mL). Removal of the solvent under reduced pressure followed by flash column chromatography afforded 2 (0.7 g, 5 mmol, 70 %).

^{1}H NMR (500 MHz, $CDCl_3$) δ 9.07 (s, 1H, O*H*), 7.47 (t, *J* = 8.0 Hz, 1H, Ar‐*H*), 6.94 (d, *J* = 7.2 Hz, 1H, Ar‐*H*), 6.75 (d, *J* = 8.0 Hz, 1H, Ar‐*H*), 3.11 (t, *J* = 5.6 Hz, 2H, C*H*$_2$‐CH_2CO), 2.72 (t, *J* = 6.0 Hz, 2H, C*H*$_2$CO);

Synthesis of 3

2 (300mg, 6.8 mmol), anhydrous powdered K_2CO_3 (600mg, 20 mmol), 20ml aceton, and $C_8H_{17}I$ was added into a round bottom flask. This reaction was refluxed for 3 hours. After the reaction was completely finished checked by TLC, the solvent of aceton was removed by vacuum evaporation. Through a simple purification by column chromatography, pure 3 could be obtained.

^{1}H NMR (500 MHz, $CDCl_3$) δ 7.60(d, J=7.5Hz, 1H, Ar-H), 7.40(d, J=7.5Hz, 1H, Ar-H), 7.30(d, J=7.5Hz, 1H, Ar-H), 3.06(t, J = 6.0 Hz, 2H, CH_2-CH_2CO), 2.70(t, J=6.0Hz, 2H, Ar-CH_2-), 1.62(m, 2H, -CH_2-), 1.31-1.40(m, 6H, -CH_2-), 0.88(t, J=7.0Hz, 3H)

Synthesis of 4, 8, 12 trialkoxyltruxene

A suspension of 3 (1 mmol) in the mixture of HOAc and HCl (0.7 mL/0.7 mL) was refluxed at 125℃ for 2 days in a sealed tub. The mixture was poured into a mixture of ice and water. After filtration, the solid was washed with water and acetone to afford the desired product:

^{1}H NMR (500 MHz, $CDCl_3$) δ7.60(d, J=7.5Hz, 1H, Ar-H), 7.40(d, J=7.5Hz, 1H, Ar-H), 7.30(d, J=7.5Hz, 1H, Ar-H), 3.06(t, J = 6.0 Hz, 2H, CH_2-CH_2CO), 2.70(t, J=6.0Hz, 2H, Ar-CH_2-), 1.62(m, 2H, -CH_2-), 1.31-1.40(m, 6H, -CH_2-), 0.88(t, J=7.0Hz, 3H)

5-2-1-2 phase characterization

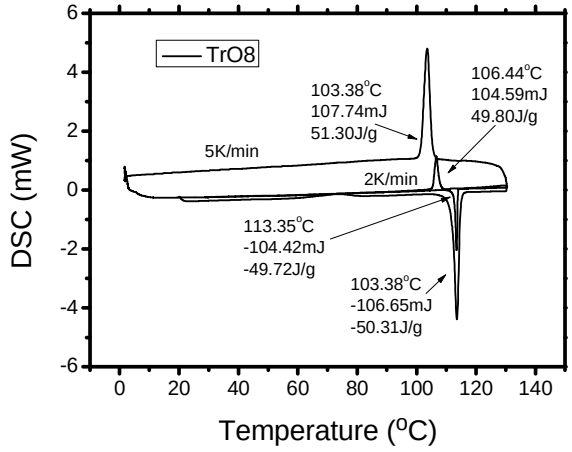

Figure 5-4 DSC curves for 4, 8, 12- trialkoxyltruxene

As shown in Figure 5-4, the compound of 4, 8, 12- trialkoxyltruxene didn't show any mesophase, just exhibited one peak upon heating or cooling. And we can observe that the peak upon cooling always exhibited a left shift, which is typical in crystal non-mesophilic materials.

On the other hand, it is obvious that the endothermic peak (50.3J/g) upon heating exhibited the same enthalpy as the exothermic peak (51.3J/g) upon cooling, indicating that there were only one phase transition in the whole temperature range. So, the compound of 4, 8, 12- trialkoxyltruxene is non-mesophilic.

This conclusion was also supported by the observation of POM textures, which

only one phase transition could be seen. The POM texture in 4, 8, 12-trialkoxyltruxene exhibited feather-like shape shown in Figure 5-5, probably showing a planar columnar alignment between the substrates.

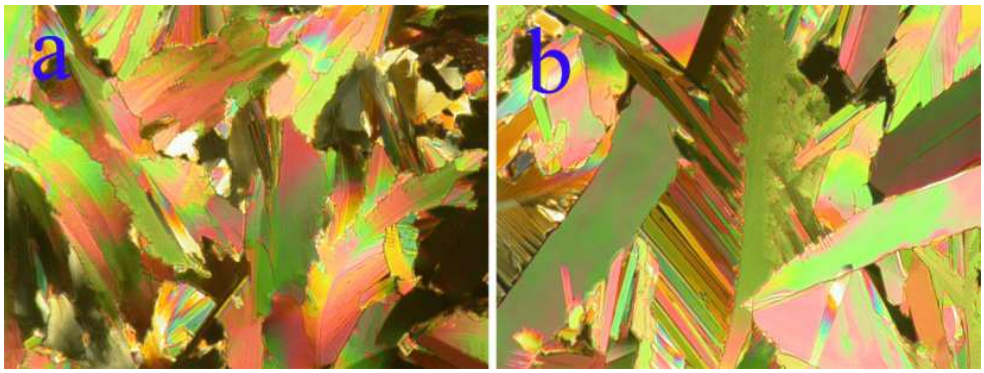

Figure 5-5 POM graphs for 4, 8, 12-trialkoxyltruxene, the cooling rates for the left and the right are 5K/min and 10K/min, respectively.

Although thermal properties characterized by DSC and POM displayed that this compound only had one phase transition with decreasing temperature from isotropic phase, temperature-dependence XRD pots (Figure 5-6) still exhibited a quite unique pattern upon cooling. we can see a high diffraction peak appeared at 23°, which seemly showed a highly ordered columnar phase.

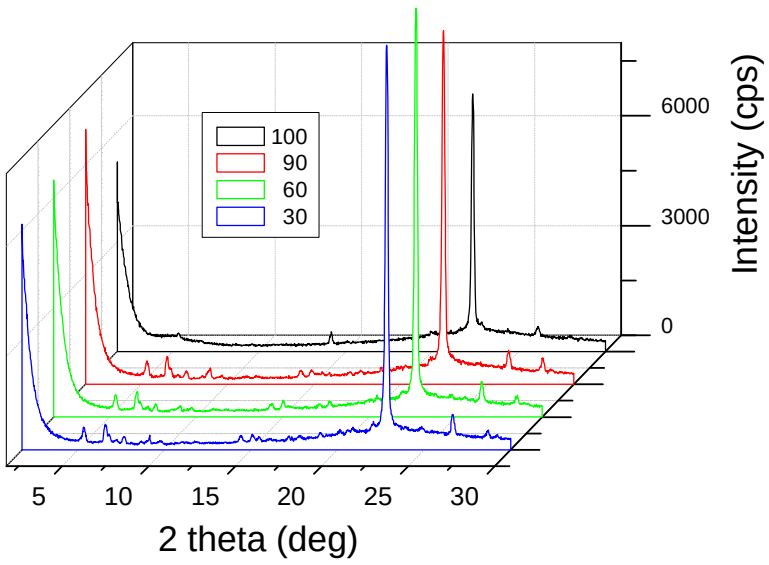

Figure 5-6 XRD patterns for bay-substituted truxene

Furthermore, XRD patterns in crystal phase showed a very high peak at wide angle region, probably suggesting that a very small molecular distance in translational directions.

5-2-1-3 Charge carrier transport

Charge carrier transport measured in TOF is shown in Figure 5-7. Both positive and negative transient photocurrents are dispersive, due to planar molecular alignment[10]. In this case, columnar axis is parallel to the electrodes, leading to much diffusion of charge carrier during the transport.

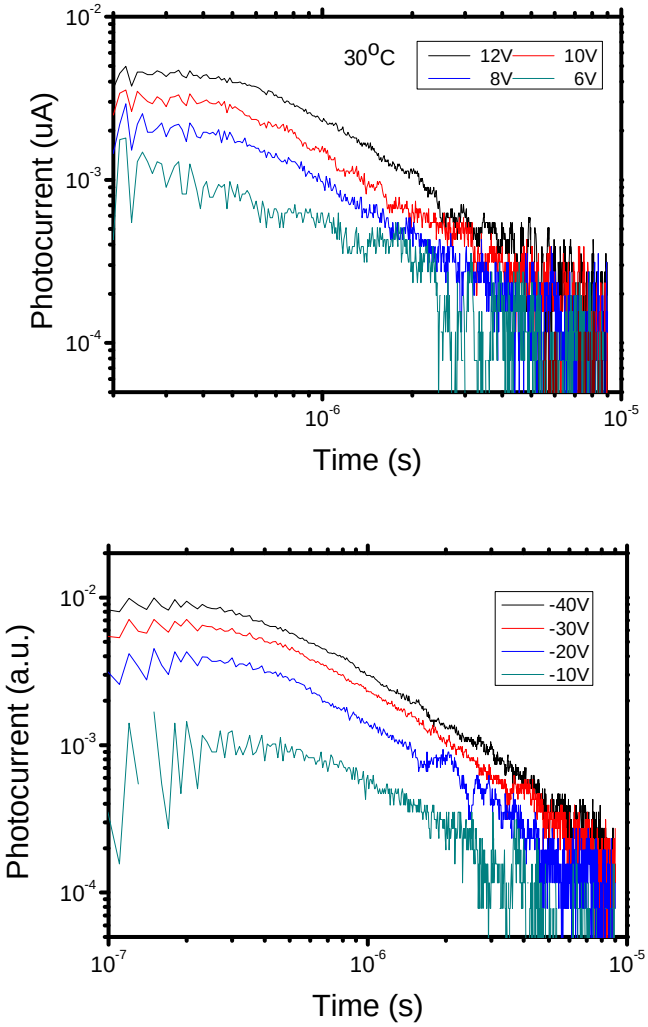

Figure 5-7 Transient photocurrent (double -log scale) of the positive and negative charge carriers at 30℃

5-2-2 1, 5, 9-trialkoxyltruxene

Based on the previous study on the compound of 4, 8, 12- trialkoxyltruxene, its analogue of 1, 5, 9-trialkoxyltruxene was designed and prepared through a similar route, shown in the below Scheme 5-5. In this case, side chains are located at 4, 8, 12 positions of truxene core.

5-2-2-1 Synthesis

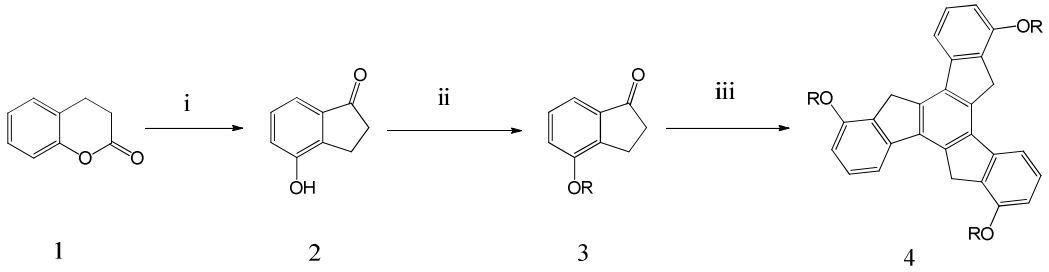

i: $AlCl_3$; ii: IR, K_2CO_3, Aceton; iii: HCl

Scheme 5-5 Synthetic route for 1, 5, 9-trialkoxyltruxene

This synthesis started from 1, the inexpensive dihydrocumarin 1. After an etherization and cyclization, the final product of 1, 5, 9-trilkoxyltruxene could be obtained in a mediate yield.

Synthesis of 2

A mixture of 4 - chromanone 5 (1) (1 g, 6.8 mmol) and anhydrous, powdered $AlCl_3$ (2.7 g, 20 mmol) was fused at 250 ˚C for 10 min. After allowing the reaction mixture to cool to ambient temperature, dichloromethane (10 mL) and cold hydrochloric acid (10 mL) were added to the mixture. The resulting black miture was extracted with dichloromethane (50mL). Removal of the solvent under reduced pressure followed by flash column chromatography afforded 2 (0.7 g, 5 mmol, 70 %).

^{1}H NMR (500 MHz, $CDCl_3$) δ7.60(d, J=7.5Hz, 1H, Ar-H), 7.40(d, J=7.5Hz, 1H, Ar-H), 7.30(d, J=7.5Hz, 1H, Ar-H), 3.06(t, J = 6.0 Hz, 2H, CH_2-CH_2CO), 2.70(t, J=6.0Hz,

2H, Ar-CH_2-), 1.62(m, 2H, -CH_2-), 1.31-1.40(m, 6H, -CH_2-), 0.88(t, J=7.0Hz, 3H)

Synthesis of 3

2 (300mg, 6.8 mmol), anhydrous powdered K_2CO_3 (600mg, 20 mmol), 20ml aceton, and $C_8H_{17}I$ was added into a round bottom flask. This reaction was refluxed for 3 hours. After the reaction was completely finished checked by TLC, the solvent of aceton was removed by vacuum evaporation. Through a simple purification by column chromatography, pure 3 could be obtained.

^{1}H NMR (500 MHz, $CDCl_3$) δ7.60(d, J=7.5Hz, 1H, Ar-H), 7.40(d, J=7.5Hz, 1H, Ar-H), 7.30(d, J=7.5Hz, 1H, Ar-H), 3.06(t, J = 6.0 Hz, 2H, CH_2-CH_2CO), 2.70(t, J=6.0Hz, 2H, Ar-CH_2-), 1.62(m, 2H, -CH_2-), 1.31-1.40(m, 6H, -CH_2-), 0.88(t, J=7.0Hz, 3H)

Synthesis of 1, 5, 9-trialkoxyltruxene

A suspension of 3 (1 mmol) in the mixture of HOAc and HCl (0.7 mL/0.7 mL) was refluxed at 125℃ for 2 days in a sealed tub. The mixture was poured into a mixture of ice and water. After filtration, the solid was washed with water and acetone to afford the desired product:

^{1}H NMR (500 MHz, $CDCl_3$) δ7.60(d, J=7.5Hz, 1H, Ar-H), 7.40(d, J=7.5Hz, 1H, Ar-H), 7.30(d, J=7.5Hz, 1H, Ar-H), 3.06(t, J = 6.0 Hz, 2H, CH_2-CH_2CO), 2.70(t, J=6.0Hz, 2H, Ar-CH_2-), 1.62(m, 2H, -CH_2-), 1.31-1.40(m, 6H, -CH_2-), 0.88(t, J=7.0Hz, 3H)

5-2-2-2 Phase transition

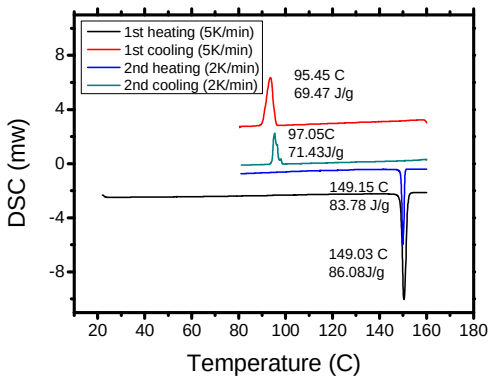

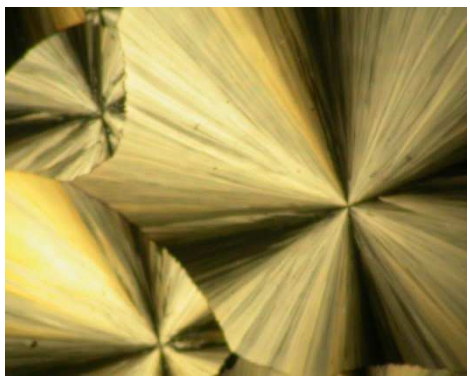

Figure 5-8 DSC curves and POM graph for 1, 5, 9-trialkoxyltruxene

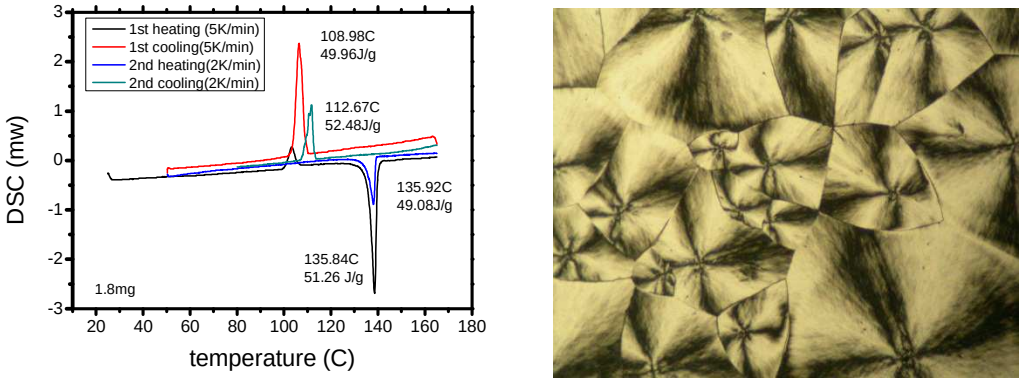

Figure 5-9 DSC curves and POM graph for 1, 5, 9-trialkoxyltruxene

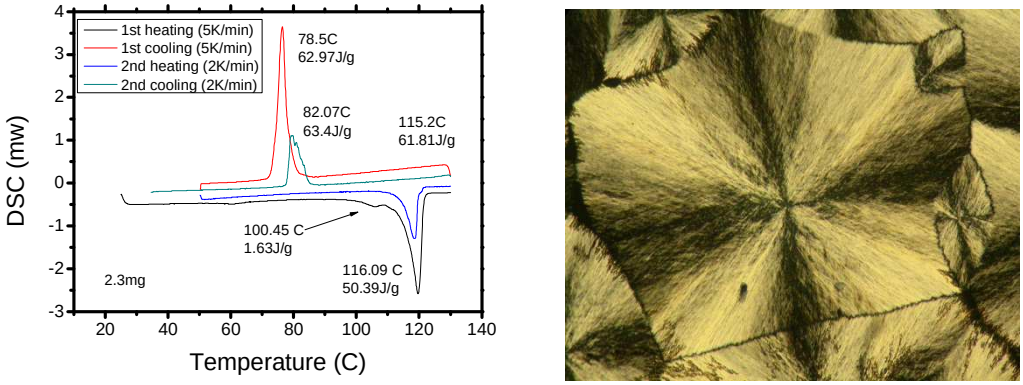

Figure 5-10 DSC curves and POM graph for 1, 5, 9-trialkoxyltruxene

All of these compounds of 1, 5, 9-trialkoxyltruxene also didn't exhibited any mesophase during cooling and heating. Only one phase transition from isotropic phase to crystal phase was observed in DSC plots and POM images (Figure5-8, 5-9 and 5-10). Typically, these images are characteristic for spherulite. Even if these crystals have long range order, their columns align with their columnar axis parallel to substrates, leading to hard determination of non-dispersive transient photocurrent.

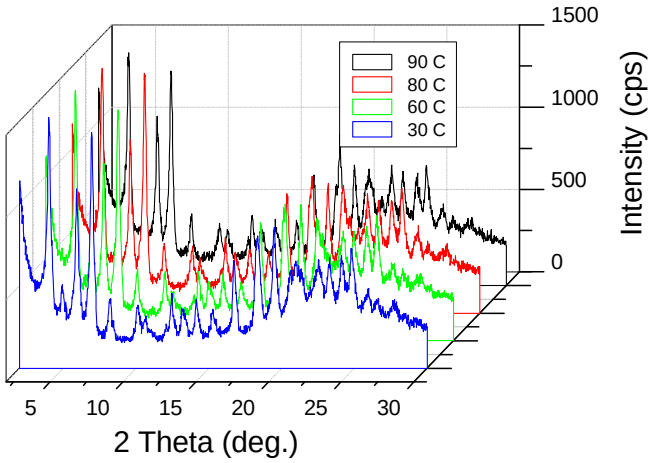

Figure 5-11 XRD patterns of 4, 8, 12-trioctoxytruxene

From temperature-dependence XRD patterns (Figure 5-11), we can see they are quite different with those of 1, 5, 9- trialkoxyltruxene. In the case of 4, 8, 12-trioctoxytruxene, the XRD patterns are typical polycrystalline with disordered structure.

5-2-2-3 Charge carrier transport

In the Figure 5-12, it can be seen that all of these truxene compounds exhibited quite dispersive transient photocurrent, which showed that there were lots of structural defects or chemical impurities.

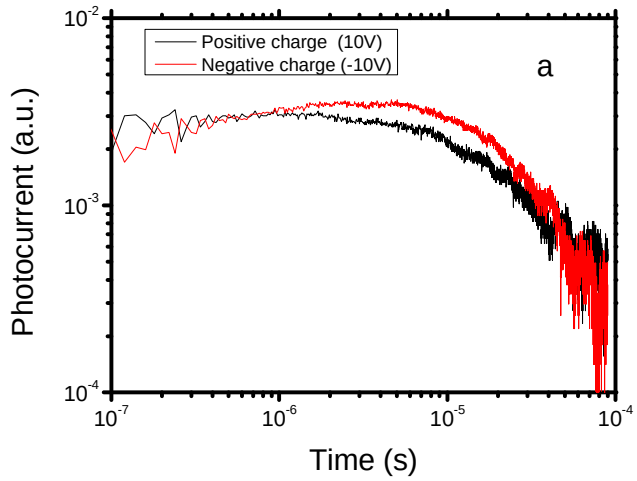

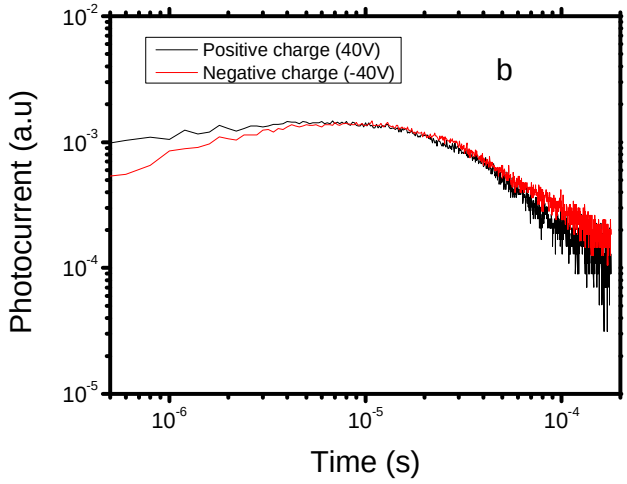

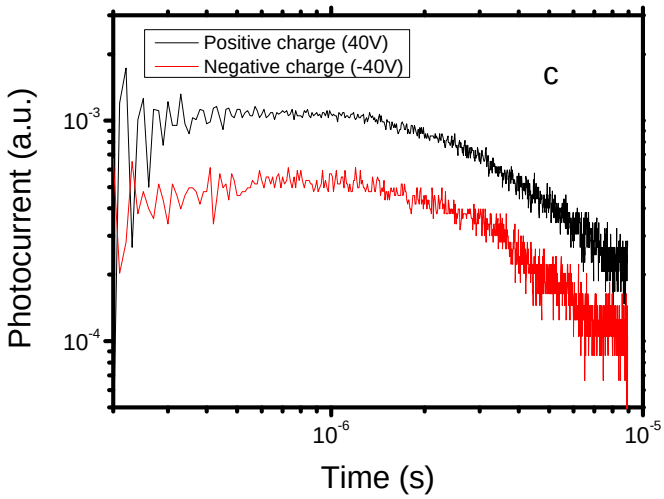

Figure 5-12 Transient photocurrent (double-log scale) of the positive and negative charge carriers at 30℃ (a, b and c: hexyl, decyl and dodecyl, respectively)

5-2-3 Summary

Based on the truxene compound reported, two types of truxene derivatives with bay-located side chains have been synthesized. In this study, alkoxyl groups have been introduced into the bay positions of truxene core, namely, 1, 5, 9-trialkoxyltruxene and 4, 8, 12-trialkoxyltruxene. Both types didn’t exhibited mesophase, and just show the phase transition from isotropic phase to crystal phase upon cooling, which had been confirmed by DSC, POM and temperature-dependence XRD. Moreover, charge carrier transport in their polycrystalline phase was quite dispersive, mainly due to planer columnar alignment.

Based this study, I decided to synthesize bay-substituted truxenes with alkyl side chains. The removal of oxygen atoms probably would bring new insight into the appearance of liquid crystalline behavior, due to possible traps brought by oxygen atoms.

5-3 Alkyl-substituted truxenes

5-3-1 1, 5, 9-trialkyltruxene

5-3-1-1 Synthesis

According to the present strategy, we designed truxene derivatives of 1, 5, 9-trialkyltruxene (Scheme 5-6). The implementation of this strategy began with the multigram-scale synthesis of hydroxyindanone 2 from the inexpensive dihydrocumarin 1 through a literature procedure. [13] The intermediate 2 was triflated to produce 3 with N, N- bis (trifluoromethylsulfonyl) phenylamine at room temperature at a high yield up to 70% prior to the alkylation via Suzuki coupling reaction. At last, intermolecular cyclocondensation reactions were performed under mild conditions by treating a synthetic block, 4 with acid to afford the final truxenes of **Tru4** and **Tru6** at the yields of 63% and 52%, respectively, after purification by column chromatography. It is worth noting that this synthetic pathway for the truxene derivative actually is short and efficient, which might help to avoid contamination of chemical impurities that make it difficult to characterize charge carrier transport by time-of-flight experiments.

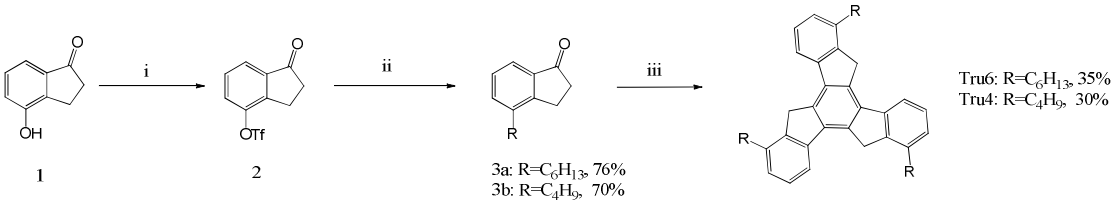

1 2 3a: R=C_6H_{13}, 76% 3b: R=C_4H_9, 70%

i: N,N-Bis(trifluoromethylsulfonyl)phenylamine, Et_3N, DCM, 24h, 95%; ii: Hexylboronic acid, $Pd(dppf)Cl_2$, Ag_2O, K_2CO_3, THF,; iii: HCl, AcOH, 120℃, 2d

Scheme 5-6 Synthetic route for 1, 6, 11-trialkyltruxene

4-hydroxyindan-1-one (2)

A mixture of dihydrocoumarin 1 (3 g, 34 mmol) and anhydrous $AlCl_3$ (13 g, 95 mmol) was fused at 210 ˚C for 1 hour. After the reaction mixture was cooled to room

temperature, ice and cold hydrochloric acid (30 mL) were added to the mixture. The precipitate was collected and washed with EtOH. Recrystallization from absolute EtOH gave 2 (2.1g, 70%) as colorless crystal. Mp 240℃.

Oxoinden-4-yltrifluoromethanesulfonate (3)

N-phenyltrifluoromethanesulphonimide (2.50 g, 7.00 mmol) was added to a solution of 4-hydroxyindan-1-one 2 (1.00 g, 6.75 mmol) and triethylamine (1.05 mL, 7.50 mmol) in dichloromethane (30 mL). The resulting mixture was stirred 24 h at ambient temperature. The mixture was washed with water (30 mL) and brine (30 mL), and extracted with dichloromethane (2 x 50 mL). The organic phase was dried over anhydrous $MgSO_4$. Removal of the solvent under reduced pressure followed by flash column chromatography (eluent: $CHCl_3$/Hexane =1 : 4) afforded the 3-oxoinden-4-yltrifluoromethanesulfonate (1.85 g, 6.61 mmol, 95 %) as colorless solid. ^{1}HNMR (500 MHz, $CDCl_3$) δ 7.80 (t, J= 6.0 Hz, 1H, Ar-H), 7.50 (d, J = 6.0 Hz, 1H, Ar-H), 7.17 (d, J = 8.0 Hz, 1H, Ar-H), 3.20 (t, J = 6.0 Hz, 2H, CH_2-CH_2CO), 2.77 (t, J = 6.0 Hz, 2H, CH_2CO);

7‐7‐Alkylindan‐1‐one (4a and 4b)

A suspension of compound 2 (1mmol), Alkyl boronic acid (3 equiv.), Pd(dppf)Cl_2 (10%mol), powdered K_2CO_3 (3 equiv.), and Ag_2O (2.5 equiv.) in THF (75ml) was stirred under argon at 80°C in a sealed tube. After 48 h, the mixture was cooled to room temperature. The dark solid was filtered, and water was added into the solution. The solution was extracted with $CHCl_3$. After evaporation, chromatography column was carried out to purify the crude product to provide white crystal.

3a: yield 76% ^{1}HNMR (500 MHz, CDCl3) δ 7.60(d, J=7.5Hz, 1H, Ar-H), 7.40(d, J=7.5Hz, 1H, Ar-H), 7.30(d, J=7.5Hz, 1H, Ar-H), 3.06(t, J = 6.0 Hz, 2H, CH_2-CH_2CO), 2.70(t, J=6.0Hz, 2H, Ar-CH_2-), 1.62(m, 2H, -CH_2-), 1.31-1.40(m, 6H, -CH_2-), 0.88(t, J=7.0Hz, 3H)

3b: yield 70% ^{1}HNMR (500 MHz, $CDCl_3$) δ7.65(d, J=7.5Hz, 1H, Ar-H), 7.43(d, J=7.5Hz, 1H, Ar-H), 7.32(d, J=7.5Hz, 1H, Ar-H), 3.13(t, J = 6.0 Hz, 2H,

CH_2-CH_2CO), 2.85(t, J=6.0Hz, 2H, Ar-CH_2-), 1.88(m, 2H, -CH_2-), 1.40(m, 2H, -CH_2-), 0.92(t, J=7.0Hz, -Me)

1, 5, 9-trialkyltruxene (Tru6 and Tru4)

A suspension of 3a/3b (1 mmol) in the mixture of HOAc and HCl (0.7 mL/0.7 mL) was refluxed at 125℃ for 2 days in a sealed tub. The mixture was poured into a mixture of ice and water. After filtration, the solid was washed with water and acetone to afford the desired product:

Tru6

Yield: 63%. Clear point: 172℃

^{1}HNMR (500 MHz, $CDCl_3$) δ 7.79(d, J=7.0Hz, H, Ar-H), 7.44(d, J=7.0Hz, H, Ar-H), 7.21(d, J=7.0Hz, H, Ar-H), 4.11(s, 2H, Ar-CH_2-Ar), 2.83(t, J=7.0Hz, Ar-CH_2-), 1.51(m, 2H, -CH_2-), 1.25(m, 2H, -CH_2-), 0.91(t, J=7.0Hz, -Me). HRMS: Calcd. For $C_{45}H_{54}$ $[M]^+$: 594.4226; Found: 594.4224.

Tru4

Yield: 52%. Clear point: 254℃

^{1}HNMR (500 MHz, $CDCl_3$) δ7.69(d, J=8.0Hz, H, Ar-H), 7.41(d, J=7.5Hz, H, Ar-H), 7.19(d, J=7.0Hz, H, Ar-H), 4.96(s, 2H, Ar-CH_2-Ar), 2.78(t, J=8.0Hz, Ar-CH_2-), 1.72-1.78(m, 2H, -CH_2-), 1.42-1.54(m, 2H, -CH_2-), 1.00(t, J=7.5Hz, -Me). HRMS: Calcd. For $C_{39}H_{42}$ $[M]^+$: 510.3365; Found: 510.3363.

5-3-2-2 Phase transition

The phase transition behaviours of both truxenes were investigated by differential scanning calorimetry (DSC) and polarized optical microscope (POM). Compound **Tru4** didn't show clear mesophase transition upon heating (Figure 5-13), only exhibiting one exothermic peak at 250℃, while exhibited a mesophase from 220℃

to 209℃ with few dendritic textures before crystallization upon cooling (Figure 5-13). The resulting mesophase was identified to be hexagonal columnar phase. In polycrystalline phase, a lot of cracks were observed (Figure 5-15).

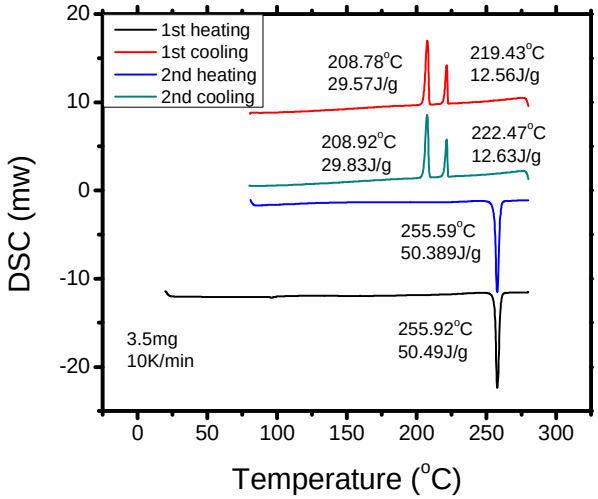

Figure 5-13 DSC curves of 1, 5, 9-tributyltruxene

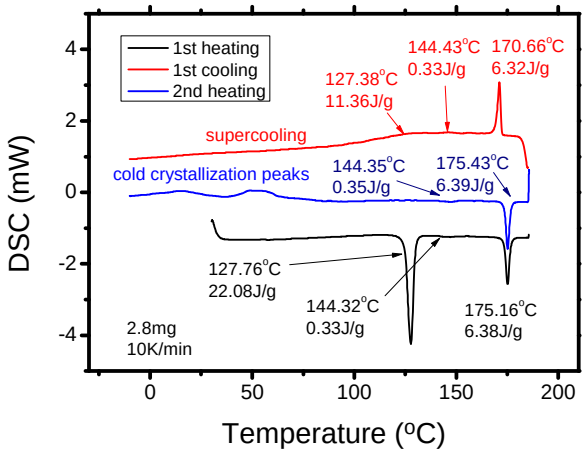

Figure 5-14 DSC curves of 1, 5, 9-trihexyltruxene

In contrast to **Tru4**, **Tru6** exhibited various thermal behaviors (Figure 5-14). The DSC plot indicates that two mesophases appeared in a temperature range from 127℃ to 175℃ in addition to the crystal phase below 127℃ and isotropic phase over 175℃ in the heating process, while upon cooling, the peak (11.36J/g) at 127℃ is quite smaller than that (22.08J/g) in the first heating process, which is usually identified to be the liquid crystal glass transition. [14]

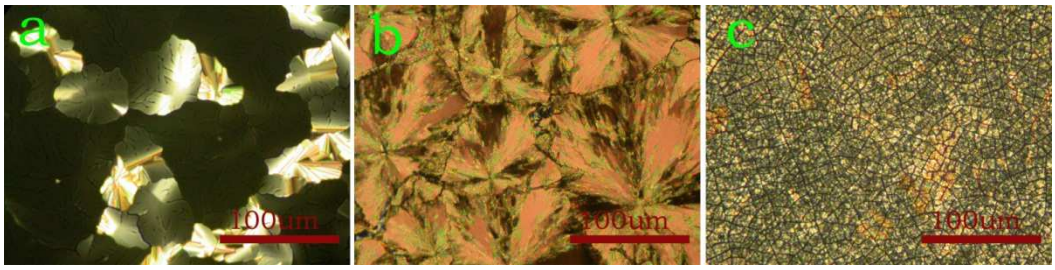

Figure 5-15 POM graphs of 1, 5, 9-tributyltruxene. a) columnar phase, b) polycrystalline phase, c) amorphous phase

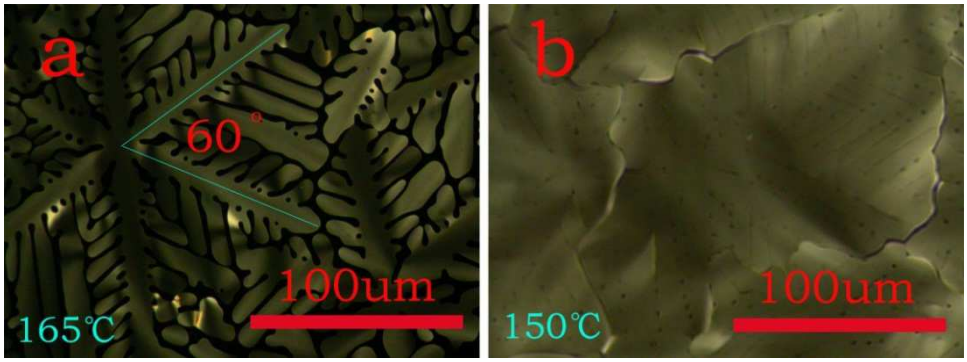

Figure 5-16 POM textures of 1, 5, 9-trihexyltruxene

Through observation of POM images of **Tru6**, its large dendritic textures up to several hundred micrometers (Figure 5-16a) clearly indicated the presence of a highly ordered hexagonal columnar phase in homeotropic alignment. [15] Moreover, the dendritic textures turned to be leaf-like with large domains (Figure5-16b) in the second liquid crystal phase, probably due to the appearance of a higher order structure, and finally this texture was still observed at low temperatures, supporting a liquid crystal glass. When the sample stayed in ambient atmosphere overnight, it was found to crystalize and show clear birefringence in the whole visible region.

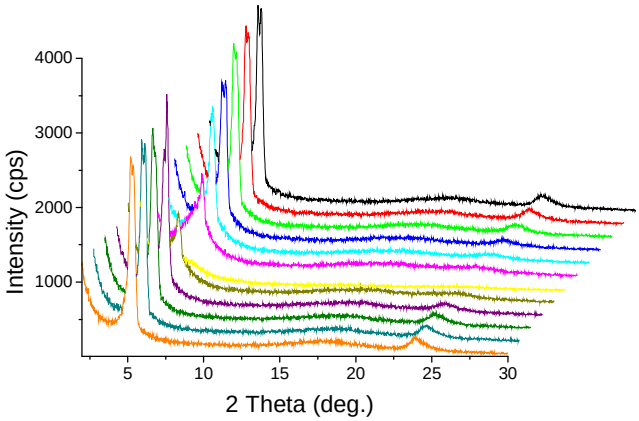

Figure 5-17 Temperature-dependence of XRD patterns of

In order to investigate the microscopic molecular configuration in columnar phases, a study of variable-temperature XRD measurement was conducted in three phases of **Tru6**, i.e., the first mesophase at 160℃, the second one at 140℃ and the glass phase at 30℃ (Figure 5-17) Upon cooling at 160℃ a peak appearing at 23.3º corresponds to the average core-to-core correlation of 3.80 Å, which is assigned to a highly ordered hexagonal columnar phase, combined with the intense low angle peak indexed to (100) that is attributed to a typical hexagonal unit cell with the parameter of a=19.2 Å (Figure 5-18). In particular, the molecular diameter of **Tru6** is calculated to be around 20 Å, which is a good agreement with the small lattice parameter. This indicates that **Tru6** molecules in mesophases tend to arrange tightly to compress intermolecular space, so that they sit in restricted lattice. As expected, the minimum distance among adjacent columns was estimated to be less than 5 Å as schematically illustrated in Figure 1b, which is quite narrow compared with that of peri-substituted DLC truxene (Figure 5-3) [11b, 11c] , which is so close to a typical π-π interaction distance of 3.5 to 4 Å in a column.

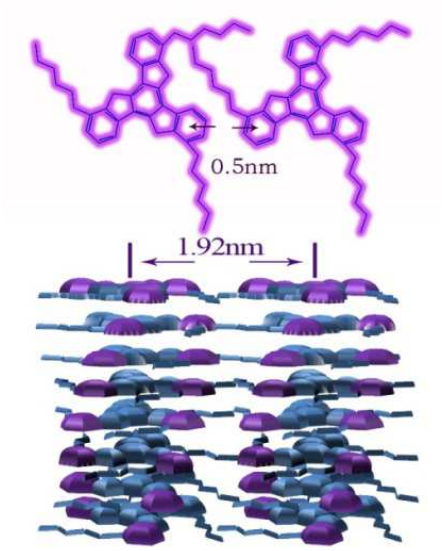

Figure5-18 Schematic illustration

Tru6 exhibited another columnar phase when cooled down to 144℃. Obviously, it is an ordered mesophase because of the appearance of the peak (23.5º) at a wide angle region of XRD pattern at 140℃. At the low angle region of XRD pattern, (100) face in hexagonal lattice split into (200) and (110), which is typical for ordered rectangular columnar phase (Col_{ro}) (Figure 5-17). Indeed, the slight split supports that the phase transition from Col_{ho} phase to Col_{ro} just induced a trivial lattice variation. And also, the π-π interaction distance can be determined to be 3.75 Å, which is little smaller than that in Col_{ho} phase, originated from a tilted molecular conformation in Col_{ro}. This typical Col_{ro} lattice remained to a room temperature range, forming a glass phase, in which the peak at wide angle region of XRD pattern at 30℃ presented a right shift indicating a π-π interaction distance of 3.70 Å narrower than those in the two mesophases (Figure 5-17).

5-3-1-3 Transient state photoconductivity measurement

To characterize charge carrier transport in densely packed columns formed in the windmill-shaped **Tru6**, we measured transient photocurrents by TOF experiments. [16] Samples of **Tru6** were capillary-filled into a 9.3μm thick liquid crystal cell with ITO electrodes at 180℃ in its isotropic phase. As shown in Figure 5-19, well-defined non-dispersive transient photocurrents for positive and negative charges were

observed in the Col_{ho} phases of **Tru6** at 165℃. Each photocurrent exhibited a clear shoulder, which indicates the transit time.

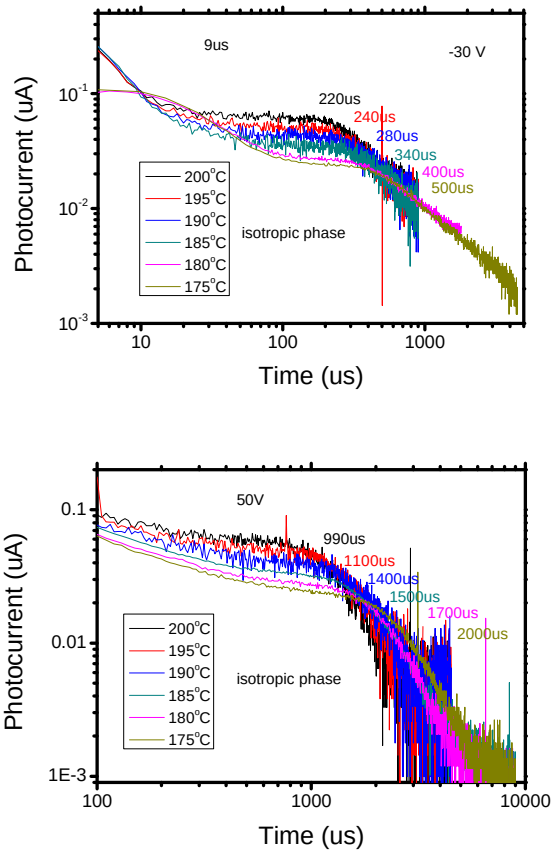

Figure 5-19 Transient photocurrent of Tru-6 in isotropic phase (the upper is negative; the below is positive)

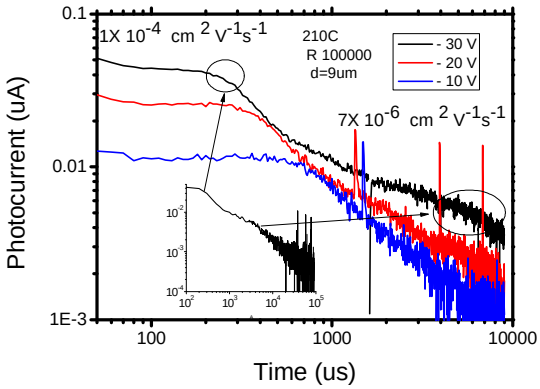

Figure 5-20 Transient photocurrent (electron and ionic) of Tru-6 in isotropic phase

As shown in Figure 5-19, the mobility for positive and negative charges in the

isotropic phase was determined to be 10^{-5}-10^{-4} cm^2 V^{-1} s^{-1}, respectively. Judging from distinguished two kink points at short and long time ranges as shown in Figure 20, we attribute the kink point at the short time range to be electronic conduction for holes and electrons.

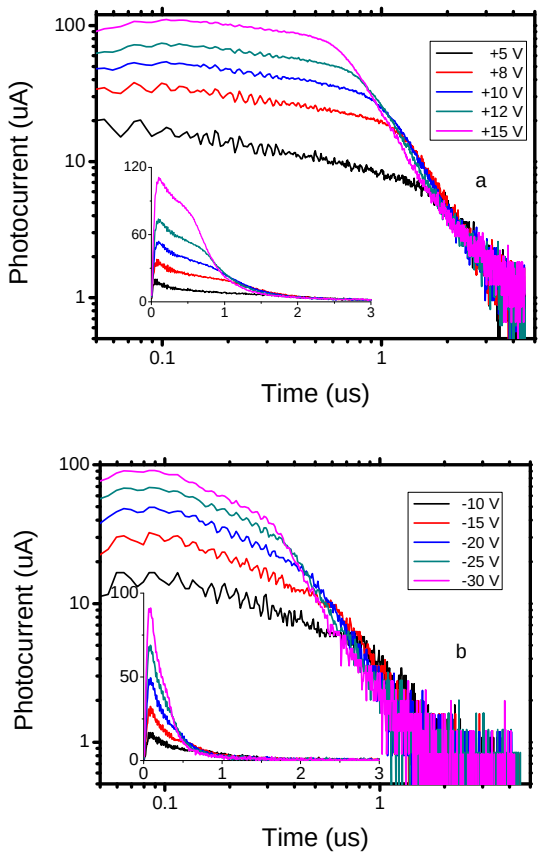

Figure 5-21 Typical transient photocurrent of Tru6 by time of flight at 165℃

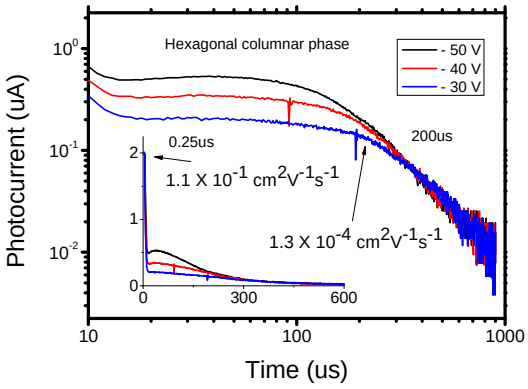

Figure 5-22 Transient photocurrent in hexagonal columnar phase at long time range

In the Col_{ho} phase, the ambipolar transport was enhanced to give hole and electron mobility of 0.11 and 0.1 $cm^2\ V^{-1}s^{-1}$, respectively (Figure 5-21). The ionic transport mobility (in Figure 5-22) was estimated to be 10^{-4} $cm^2V^{-1}s^{-1}$. The hole and electron mobility in the Col_{ro} phase was increased up to 0.12 and 0.11 $cm^2\ V^{-1}s^{-1}$, respectively, which is one order of magnitude higher than those in peripheral-substituted truxene analogues [11] and comparable to that in larger-core liquid crystals as is reported in phthalocyanines [17] and benzoporphyrins [18]. In the glass phase, the mobility of both hole and electron was kept unchanged in the order of 10^{-1} $cm^2\ V^{-1}\ s^{-1}$, even in the room temperatures, implying that such highly ordered columns closely packed hardly changed as temperature was decreased.

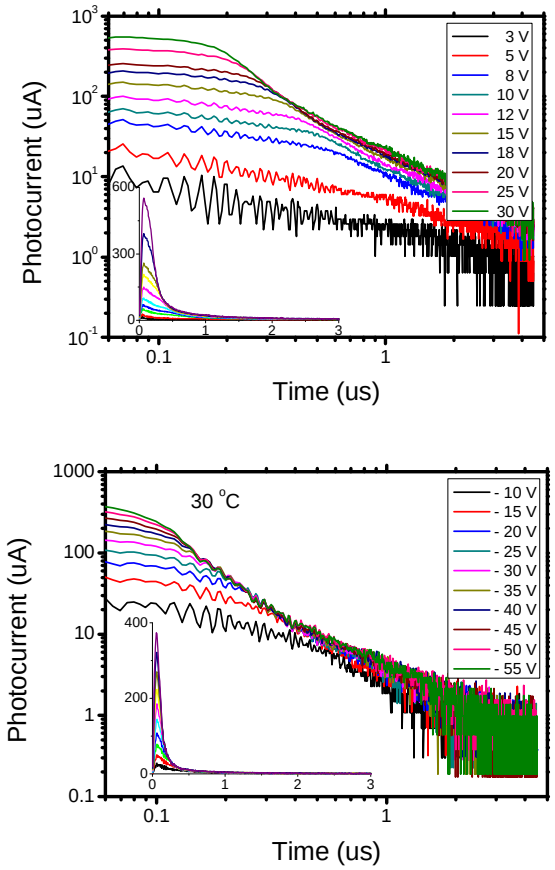

Figure 5-22 Typical transient photocurrent of Tru6 by time of flight in polycrystalline state

This glass state was metastable and turned to be polycrystalline when the cell was kept at a room temperature overnight. In the resulting polycrystalline film, non-dispersive photocurrent could be still observed (Figure 5-22), and enables us to

determine charge carrier mobility in the polycrystalline state to be 0.2 and 0.17 $cm^2 V^{-1} s^{-1}$ for hole and electron, respectively, which are two order of magnitude higher than those of DLC alkyl-substituted-benzocoronene derivatives[8e, 20]. They also hardly depended neither temperature nor electric field (Figure 5-23), and were invariable for several weeks (Figure 5-24). Polycrystalline **Tru4** also showed high ambipolar mobility around 0.3 $cm^2 V^{-1} s^{-1}$ (Figure 5-24), which is the highest in all truxene derivatives[11b, 11c]. It is well known that the non-dispersive charge transport in polycrystalline thin films is rarely observed in non-liquid crystalline organic materials because defective grain boundaries cause deep trap states for charge carriers. Therefore, the fast charge transport in the truxenes is explained by preferential formation of grain boundaries along with the columns[21] and/or possible charge transport among the columns thanks to the small intercolumnar space of 5 Å in the present polycrystalline films.

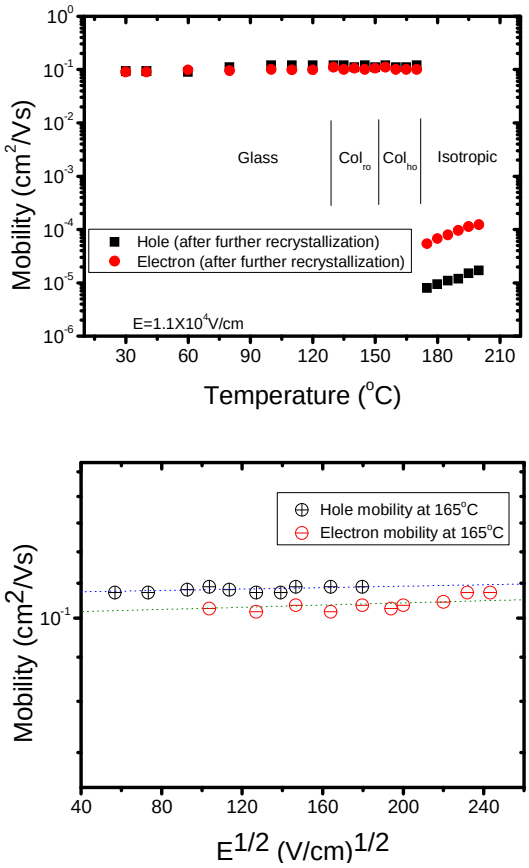

Figure 5-23 Temperature and electric field dependence of charge transport mobility in Tru6

It is noted that mobility of hole and electron is almost constant irrespective of columnar and glassy phase, even if the phase structures are changed slightly as discussed above. In mesophases, the mobility depended on neither temperature nor electric field, respectively, as is often reported in the liquid crystalline phases. This behavior can be well explained by a narrow distribution of the density of states less than 60 meV comparable to kT, where T is the temperature for TOF experiments, [19] and is attributed to less disordered molecular alignment in the column and a small dipole moment of **Tru6**.

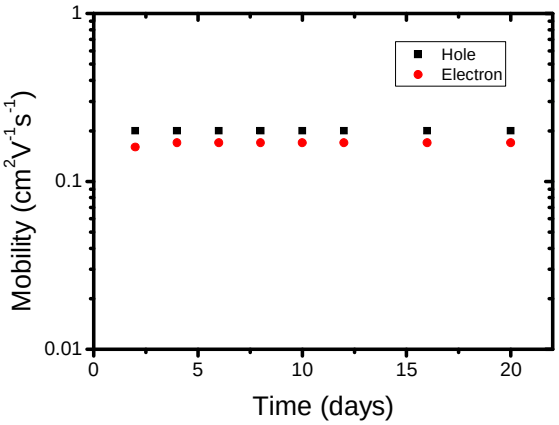

Figure 5-24 Stability of mobility in polycrystalline state

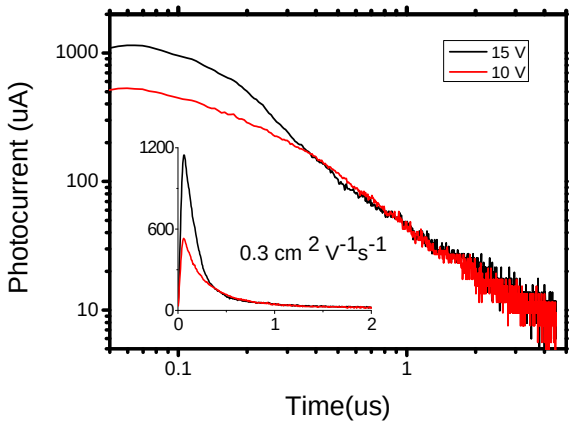

Figure 5-25 Transient photocurrent in polycrystalline phases of **Tru4**, the sample thickness was 9um

5-3-1-4 Summary

In summary, we synthesized novel windmill-shaped discotic liquid crystalline truxenes, i.e., 1, 5, 9-trialkyltruxene substituted with alkyl chains at bay-positions of truxene core. These truxenes showed highly ordered columnar phases with homeotropic alignment upon cooling, in which very narrow intercolumnar space of 5 Å was estimated. The resulting columnar structure was quite stable and so densely packed that molecular motions in mesophases were thought to be confined. Interestingly, these DLC materials showed fast ambipolar carrier mobility over 0.1 $cm^2 V^{-1} s^{-1}$ in both columnar and crystalline phases in spite of a relatively small core size of truxene. These results suggest the windmill-shaped DLC molecules with alkyl substituents at bay positions give densely packed columnar phases, which are advantageous over conventional DLC molecules substituted with peripheral side chains for fast charge carrier transport.[3, 4, 5] The present results may give us a new strategy of molecular design for discotic liquid crystalline organic semiconductors.

5-3-2 3, 8, 13-trialkyltruxene

5-3-2-1 Synthesis

As a reference, a truxene derivative with peri-substituted side chains was synthesized by the route shown in Scheme 5-7. Firstly, using Suzuki coupling to alkylation was achieved at a good yield, and then, the cyclization could be carried out in the condition of acid.

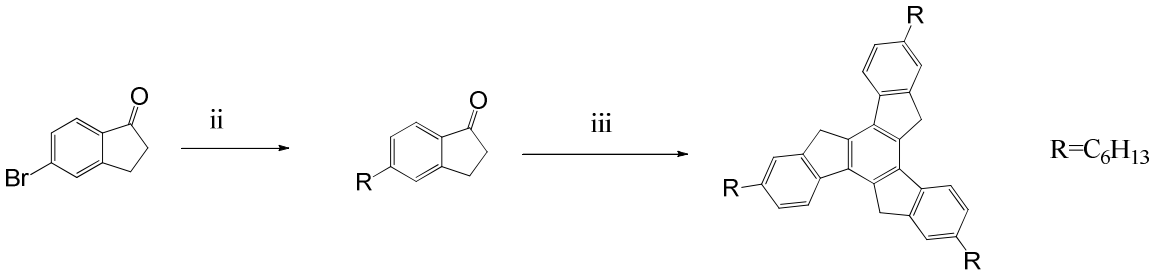

i: Hexylboronic acid, $Pd(dppf)Cl_2$, Ag_2O, K_2CO_3, THF,; ii: HCl, AcOH, 120℃, 2d

Scheme 5-7 Synthetic route for 2, 6, 10-trihexyltruxene

5-3-2-2 Phase transition

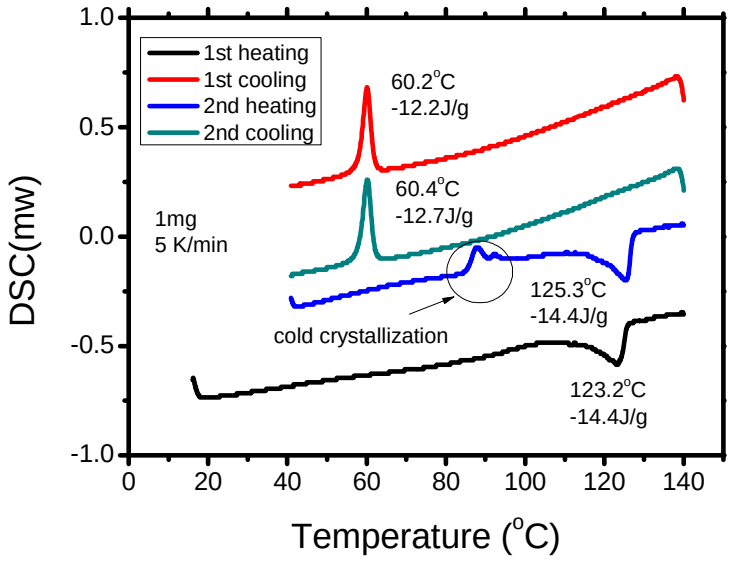

Figure 5-26 DSC curves of 2, 6, 10-trihexyltruxene

DSC plot in Figure 5-26 shows that 2, 6, 10-trihexyltruxene only exhibited one

endothermic peak during heating and one exothermic peak during cooling. And exothermic peak (123℃) upon cooling appears at a lower temperature than that of endothermic peak (60.2℃) upon heating, which always was observed in such discotic materials, mainly originated from fast cooling rate. When 2nd heating was performed, it gave special cold crystallization peaks, which often take place in organic materials with long side chains. This behavior can be explained that such materials have become crystals before arrangement of side chains. So, if such materials are heated again, their side chains first begin to relax with heat release.

In Figure 8, it is observable that 2, 6, 10-trihexyltruxene just showed polycrystalline phase, which exhibited much birefringence in the whole viewable regions in POM image shown in Figure 5-27.

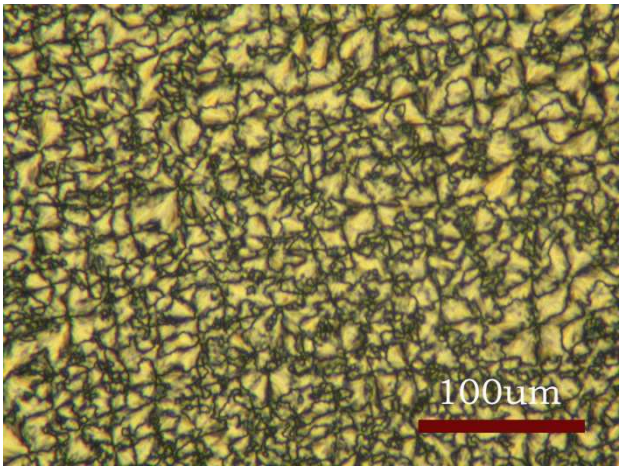

Figure 5-27 POM graph (left) and illustration of discotic nematic phase (right)

5-3-2-3 Charge carrier transport

2, 6, 10-trihexyltruxene does not show liquid crystalline phase. Here, its charge transport was measured in polycrystalline phase upon clooing. It showed bipolar transport with mobility positive and negative charges, respectively.

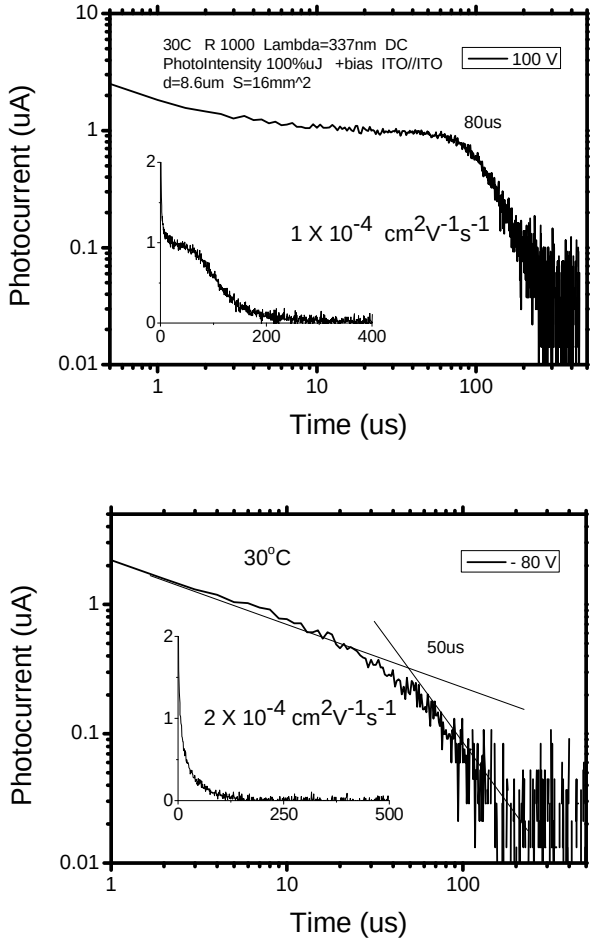

Figure 5-28 Transient photocurrents in polycrystalline phase of 2, 6, 10-trihexyltruxene

In polycrystalline phase, positive charge transport mobility decreased to $1\times10^{-4}cm^2V^{-1}s^{-1}$, probably resulted from the extended moleclular distance, while negative charge transport mobility increased to $2\times10^{-4}cm^2V^{-1}s^{-1}$. This mobility is quite lower than that of bay-substituted truxenes, which reveals the significance of ordered structure for charge carrier transport in discotic liquid crystal.

5-3-2-4 Summary

When introduced by alkyl chains into bay-position, truxenes exhibited columnar mesophases, and showed quite high mobility over $0.1cm^2V^{-1}s^{-1}$. We speculate that such high mobility was originated from the densely packed columnar mesophase, which suppresses the molecular motions.

On the other hand, another truxene derivative with peri-substituted side chains also was prepared, which didn't exhibited any mesophase. The mobility in polycrystalline phase is around $10^{-4}cm^2V^{-1}s^{-1}$, three orders of magnitude lower than the former, which mainly resulted from well-defined one dimensional pathway in the columnar phase of the former.

5-4 Summary of Chapter 6

In this study, bay-substituted truxene derivatives have been prepared through facile synthetic routs. When alkoxyl chains were located at 1, 5 and 9 positions or 4, 8 and 12 positions of truxene core, these compound didn't exhibited any mesophase, and just presented phase transition from isotropic to crystal upon cooling. On the other hand, when alkyl side chains were introduced into 1, 5 and 9 positions of truxene core, the obtained compounds (bearing hexyl and butyl) exhibited ordered columnar pesophases.

In the mesophilic truxene derivatives, namely, 1, 5, 9-trialkyltruxene, very unique phase structure has been revealed, which pointed out the presence of very densely packed columnar lattice with a small intercolumnar space of 5Å.

Charge carrier transport property characterized by TOF showed that very high ambipolar mobility over 0.1 cm2/Vs has been determined in both columnar mesophase and polycrystalline phase. This is the highest mobility in truxene analogues.

This molecular design strategy, incorporation of mono-side-chain in bay position, actually is an extension of the original idea. In the case of windmill-shaped discotic liquid crystals, the intermolecular between two adjacent columns becomes quite smaller than usual, which leads more densely packed columnar structure, thereby enhancing charge carrier transport.

References of Chapter 5

1. K. T. Wong, Y. Y. Chien, R. T. Chen, C. F. Wang, Y. T. Lin, H. H. Chiang, S. M. Peng, Journal of the American Chemical Society, 124, 11576(2002).

2. A. L. Kanibolotsky, R. Berridge, P. J. Skabara, I. F. Perepichka, D. D. Bradley, M. Koeberg, Journal of the American Chemical Society, 126(42), 13695(2004).

3. W. Baker, R. Banks, J. Chem. Soc., 279(1939)..

4. E. M. Pérez, N. Martín, Chemical Society Reviews, 38, 1512(2008)..

5. A. L. Kanibolotsky, R. Berridge, P. J. Skabara, I. F. Perepichka, D. D. Bradley, M. Koeberg, Journal of the American Chemical Society, 126(42), 13695(2004).

6. Y. M. Sun, K. Xiao, Y. Q. Liu, J. L. Wang, J. Pei, G. Yu, D. B. Zhu, Advanced Functional Materials, 15, 818(2005).

7. T. W. Warmerdam, R. J. M. Nolte, W. Drenth, J. C. Van Miltenburg, D. Frenkel, R. J. J. Zijlstra, Liquid Crystals, 3, 1087(1988)..

8. N. H. Tinh, J. Malthete, C. Destrade, Journal de Physique Lettres, 42, 417(1981).

9. K. Q. Zhao, C. Chen, H. Monobe, P. Hu, B. Q. Wang, Y. Shimizu, *Chemical Communications*, *47*, 6290(2011).

10. W. Pisula, M. Zorn, J. Y. Chang, K. Müllen, R. Zentel, *Macromolecular rapid communications*, *30*, 1179(2009).

11. S. Chandrasekhar, D. Demus, J. Goodby, G. W. Gray, H. W. Spiess, V. Vill,. *Handbook of Liquid Crystals Set*, 749(1998).

12. B. R. Kaafarani, *Chemistry of Materials*, *23*, 378(2010).

(13) E. O. Onyango, P. A. Jacobi, *J. Org. Chem*., 2012, **77**, 7411-7427.

(14) J. Wu, T. Usui, J. I. Hanna, *J. Mater. Chem*, 2011, **21**, 8045; K. M. Lee, M. L. Smith, H. Koerner, N. Tabiryan, R. A. Vaia, T. J. Bunning, T. J. White, *Adv. Funct. Mater*., 2011, **21**, 2913.

(15) (a) G. Schweicher, G. Gbabode, F. Quist, O. Debever, N. Dumont, S. Sergeyev, Y. H. Geerts, *Chem. Mater*., 2009, **21**, 5867-5874. (b) T. Kajitani, Y. Suna, A. Kosaka, T. Osawa, S. Fujikawa, M. Takata, T. Aida, *J. Am. Chem. Soc*., 2013, **135**, 14564-14567. (c) R. Kleppinger, C. P. Lillya, C. Yang, *J. Am. Chem. Soc*., 1997, **119**, 4097-4102.

(16) H. Iino, J. I. Hanna, D. Haarer, *Phys. Rev. B*, 2005, **72**, 193203-193206.

(17) H. Iino, J. I. Hanna, R. J. Bushby, B. Movaghar, B. J. Whitaker, M. J. Cook, *App. Phys. Lett*., 2005, **87**, 132102-132104.

(18) X. Y. Liu, T. Usui, H. Iino, J. I. Hanna, *J. Mater. Chem. C*, 2013, **1**, 8186-8193.

(19) A. Ohno, J. I. Hanna, *App. Phys. Lett*., 2003, **82**, 751-753

(20) M. Kastler, F. Laquai, K. Müllen, G. Wegner, *Appl. Phys. Lett*., 2006, **89**, 252103-252105

(21) H. Iino, Y. Takayashiki, J. I. Hanna, R. J. Bushby, *J. J. Appl. Phys*., 2005, **44**, 1310-1312.

Chapter 6

Conclusion and perspective

6-1 Summary of this thesis

In this research, we proposed a new molecular design strategy for discotic liquid crystals, i.e., incorporation of alkyl chains into bay positions of disclike core, so as to achieve densely packed columnar mesophases with hometropic alignment, thereby suppressing molecular motion, which was expected to be beneficial for high-speed charge carrier transport.

Three different types of discotic liquid crystals have been designed and prepared through facile synthetic routes, namely, benzoporphyrin, Hexaazatrinaphthylenes (HATNA) and truxene. Their phase transitions were characterized by using DSC, POM and XRD measurements. Furthermore, the charge carrier transport was measured by time of flight technique.

In the chapter 1, as the background of the present study the research progress on organic semiconductors including amorphous, crystalline, and liquid crystalline small molecules and polymers has been reviewed. And then, it is pointed out that as self-organizing organic semiconductors, liquid crystalline semiconductors are becoming attractive for device application in the future, because of high mobility and controllable molecular alignment. Furthermore, the current problems, what determines the charge transport properties has not been clarified in discotic liquid crystals yet, are also pointed out. The research interests of this thesis were aroused by the recent breakthrough on a bay-substituted phthalocyanine derivative. Based on these results from historical studies, the motivation and purpose of the present study are described: that is, to answer a question about why such high mobility can be achieved in disordered columnar phases of bay-substituted Phthalocyanines and whether high mobility can be observed in other discotic liquid crystals bay-substituted

with long alkyl chains.

In the chapter 2, experimental methods are talked in detail. All compounds were synthesized according to the molecular design strategy. We tried to prepare every compound using short synthetic route to avoid the contamination of chemical impurities. After obtaining the relative compound, its molecular structure was confirmed by ^{1}HNMR and MS spectrum. And then the phase transition could be measured by using DSC and POM, in which molecular orientation was checked by X-ray diffraction. Finally, high-purity samples can be used to transient photocurrent measurements by time of flight technique, and thus the charge carrier mobility can be extracted.

In the chapter 3, we designed a versatile route for synthesis of DLC benzoporphyrin derivatives. Through the new route, we obtained quite high efficiency, mild conditions and functional group tolerance, comparing with the previous one, which was helpful for high-purity sample for measuring charge carrier transport. Such materials were found to exhibit homeotropic columnar alignment. In the hexagonal columnar mesophase, previously people thought that one kind of “disordered” intracolumns have been achieved, meaning that molecules are arranged with a tilt angle to the normal direction. We confirmed that the present actually could be considered as the herringbone configuration by using electronic spectra, which always leads to densely packed lattice and closer stacking in crystal structures.

Furthermore, the intercolumnar distance was estimated to be 21.6Å（the diameter of the core is 16 Å), thereby showing an intercolumnar space about 6Å, quite smaller than that of peri-substituted ones (over 10 Å). This result is consistent with the above mentioned herringbone configuration.

We investigated charge carrier transport and photoconductive behaviours in two discotic liquid crystalline benzoporphyrin derivatives. Interestingly, through time of flight technique, these materials exhibited very high hole mobility over 0.1cm^2/Vs in Col_{hd} and $Col_{rd,}$ while peri-substituted phthalocyanines just showed mobility of 10^{-3} $cm^2V^{-1}s^{-1}$. We contributed this result to a densely packed columnar structure, comparing with peripheral substituted DLCs. Moreover, very high photo-generation

efficiency up to 2% in the columnar phase has been achieved.

In the chapter 4, we have challenged hexaazatrinaphthylene (HATNA) to form molecular columns with out-of-plane orientation for high electron transport. In this research, we discuss facile synthesis of novel hexaazatrinaphthylenes bay-substituted with alkyl, alkylethynyl, and alkylthio groups, i.e., type I, type II and type III, and their phase transition behaviors, as well as feasibility of self-directed molecular orientation on the substrates.

We found that all compounds can form long-range molecular columns with self-directed growth direction. Interestingly, the HATNA substituted with bay alkyl groups (Type I) presented typical “edge-on” molecular alignment to form in-plane-oriented molecular columns on the substrate. On the other hands, the HATNAs with acetylene spacers (type II) exhibited perfect hexagonal lattice patterns: II-a with short side chains showed in-plane molecular columns, while II-b with longer chains obviously resulted in out-of-plane-oriented columns with “face-on” molecular alignment. In the case of III, the HATNA with sulfur atom spacers surprisingly showed molecular columns with rectangular lattices, whose molecular alignment also varied sensitively depending on the alkyl chain length.

Furthermore, CV measurements demonstrated that the introduction of various side chains could not override the electron-deficiency of the HATNA core. More importantly, we also found that the HATNA bay-substituted with octylthio groups showed high electron mobility in the bulk of Colr’ phase and even in polycrystalline phase up to 10^{-3} $cm^2V^{-1}s^{-1}$. This is the first time to determine valid charge carrier mobility through time of flight method in such N-containing compounds.

In the chapter 5, we proposed a new molecular design, i.e., the windmill-shaped molecule based on a disc-like truxene core, which was expected to form a densely packed columnar lattice with a shortened intercolumnar space, thereby suppressing the molecular motions and enhancing charge carrier transport in the discotic columnar mesophases. In addition, mono-side chain is adopted at a bay- position to expose the peripheral phenyl ring, thus leading to possible charge transport among the neighboring columns.

These truxenes showed highly ordered columnar phases with homeotropic alignment upon cooling, in which very narrow intercolumnar space of 5 Å was estimated. The intracolumnar distance of 3.8 Å is larger than other truxene derivatives (3.6 Å) The resulting columnar structure was quite stable and so densely packed that molecular motions in mesophases were thought to be confined.

These DLC materials also showed fast ambipolar carrier mobility over 0.1 cm^2 V^{-1} s^{-1} in both columnar and crystalline phases in spite of a relatively small core size of truxene. Even if the intracolumnar distance is larger than others, densely packed columns can significantly suppress molecular motion, which is advantageous over conventional DLC molecules substituted with peripheral side chains, thereby giving rise to high charge carrier transport.

6-2 General conclusion

Through this study on the synthesis, liquid crystallinity and charge carreri transport of discogens with bay-located side chains, we actually have constructed a new molecular system which can exhibit columnar mesophases with homeotropic aligment, and also further clarified the relationship between molecular orientation and charge carrier transport property. The conclusion is generally summarized:

1) Results from bay-substituted benzoporphyrin derivatives, combined with previous research on bay-substituted phthalocyanines, revealed that the 2D densely packed columnar lattice (herringbone lattice within columns and narrower intercolumnar distance) contributes to the fast charge carrier transport.

The results of bay-substituted benzoporphyrin and phthalocyanines revealed that their unique “disordered” columnar mesophases are quite different from the conventional “disordered” ones. The former actually contains herringbone configuration in the lattice, in which molecules are densely arranged with tilted angle to the normal direction, leading to the absence of peak (π - π interaction) at wide

angle region of XRD patterns. Moreover, herringbone configuration, coupled with narrower intercolumnar spacer (6-8 Å), can effectively confine mobile molecules within columns and maximize the probability for charge hopping, thereby enhancing charge carrier transport.

2) Columnar mesophases could be established through incorporation of alkyl chains into bay positions of various discogens. Previously, only peripheral substituents were widely employed for this purpose.

Incorporation of short side chains into bay positions of discotic cores can be extended to other discotic systems, like tetrabenzoporphyrin, tetraazabenzoporphyrin, HATNA and truxene. All of these compounds with bay-located substituents are able to exhibit columnar mesophases. And also, they show lower isotropic mesophase transition temperature than peripheral-substituted ones. Actually, we construct a new molecular system for discotic liquid crystal.

3) Bay-substituted discotic liquid crystals exhibit more obvious trend to form homeotropic columnar mesophases than peripheral-substituted ones.

Unlike peripheral-substituted discotic liquid crystals which usually show planar alignment in columnar mesophases, the bay-substituted can be easily induced to form homeotropic alignment. However, we still don't understand well about this phenomenon. In addition, in such homeotropic columnar lattice, it was found that the intercolumnar distance is quite smaller than the peripheral cases, which leads to closer stacking.

4) High charge carrier mobility over $0.1 cm^2V^{-1}s^{-1}$ can be achieved in bay-substituted discotic liquid crystals, mainly originated from their densely packed 2D lattices.

First of all, we established discotic liquid crystals, such as phthalocyanine and tetrabenzoporphyrin with bay-located dialkyl chains, which exhibited unique columnar phase showing high mobility over $0.1 cm^2V^{-1}s^{-1}$, as discussed above.

In contrast to phthalocyanine, tetrabenzoporphyrin and HATNA, mono bay-located alkyl chains force truxene to form highly ordered hexagonal columnar mesophase with homeotropic alignment. So, we speculated that the so-called “disorder” is probably caused by the out-of-plane alkyl chains in bay positions, in which strong steric hindrance exists, while the steric effect can be relaxed when only mono alkyl chain is introduced, thus leading to co-facial configuration.

On the other hand, what’ more important is that side chains are located at bay position to purposefully expose the peripheral phenyl ring, and then narrower the intercolumnar distance (around 5 Å) to make charge carrier transport across columns possible, which can help charge carrier to circumvent static defects along quasi one-dimensional columns, and also force a face-to-face stacking of molecular cores to maximize intermolecular couplings, thereby enhancing charge carrier transport within columns. So, combined with the discussion above, it can be concluded that high charge mobility can be obtained in closer packed columnar phase, especially when intercolumnar space is narrow, regardless of the molecular orientation within columns (titled or co-facial), which can be explained that the slow translational movements of the discs on similar and slower time scales than charge carrier transport.

Above all, the present results give us a new strategy of molecular design to obtain discotic liquid crystalline, and also provide an alternative way for establishing homeotropic columnar mesophases which is the requirement for high charge carrier transport. In particular, this concept pushes various discotic liquid crystals into the edge of applicable organic semiconductors.

6-3 Future works

Through this research, we make it quite clear that high charge carrier mobility requires less active motioning molecules in columnar phases. We have found an effective way, i.e., introduction of side chains at bay position, to confine molecular motion.

In the case of bay-substituted benzoporphyrins and truxene, very high charge carrier mobility has been achieved over $0.1 cm^2V^{-1}s^{-1}$. When n-type HATNA derivatives were substituted with bay-located side chains, even if the mobility was just about $10^{-3} cm^2V^{-1}s^{-1}$, probably due to molecular misorientation, these DLC compounds could self-direct form “in-plane” or “out-of-plane” molecular columns, which will be promising for application in OLED and OPv. [1,2]

Actually, for further investigation, we can continue to explore such discotic liquid crystals with bay-located side chains, especially, the type of wind-shaped molecules. This molecular design concept gives us a new insight for more densely packed columnar mesophases.

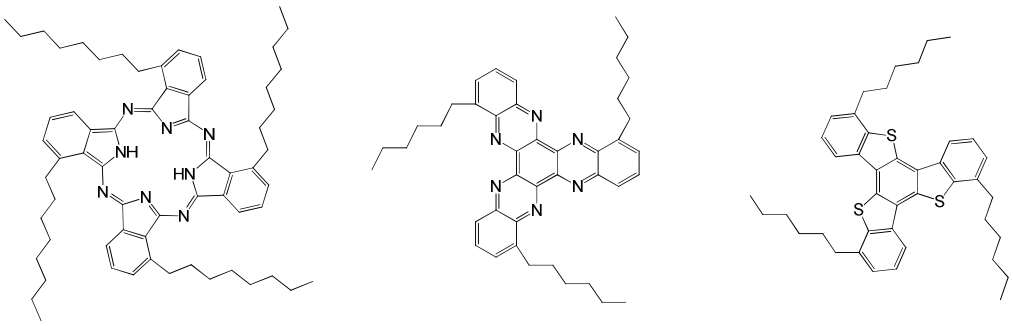

Figure 6-1 Wind-mill shaped discotic liquid crystals for further research

References of Chapter 6

1. L. Schmidt-Mende, A. Fechtenkötter, K. Müllen, E. Moons, R. H. Friend, J. D. MacKenzie, *Science*, 2001, *293*, 1119
2. S. Sergeyev, W. Pisula, Y. H. Geerts, *Chemical Society Reviews*, 2007, *36*, 1902.

Achievements

Journal papers:

1. **Xuying Liu**, Takayuki Usui, Hiroaki Iino, Jun-ichi Hanna, Phase transition, optical and photoconductive properties of bay-substituted benzoporphyrin derivatives, *J. Mater. Chem. C*., **2013**, 1(48), 8186 – 8193.
2. **Xu-Ying Liu**, Takayuki Usui and Junichi Hanna, A windmill-shaped columnar liquid crystal, *To be submitted*.
3. **Xu-Ying Liu**, Takayuki Usui and Junichi Hanna, Self-directed Orientation of molecular columns based on n-type Hexaazatrinaphthylenes (HATNAs) and High Photogenerated Electron Transport, *Chemistry - A European Journal*. In production
4. **Xu-Ying Liu**, Takayuki Usui, Hiroaki Iino, Jun-ichi Hanna. Colored P-type semiconductors: discotic liquid crystalline benzoporphyrin derivatives, Proceedings of 111th Annual Conference of the Imaging Society of Japan, p. 249-252.

Conference:

1) **Xuying Liu**, Jun-ichi Hanna, Inducible Molecular Orientation from “edge-on” to “face-on” Based on Bay-substituted Hexaazatrinaphthylenes (HATNAs), 25th International Liquid Crystal Conference, 29 June - 4 July 2014, Dublin, Ireland. (Poster)
2) **Xuying Liu**, Takayuki Usui, Jun-ichi Hanna, Self-directed Orientation of molecular columns based on n-type Hexaazatrinaphthylenes (HATNAs) and High Photogenerated Electron Transport, 2nd international symposium on self-organized organic molecular semiconductor, 2014/2, Tokyo institute of technology, Japan. (Poster)
3) **Xuying Liu**, Takayuki Usui, Jun-ichi Hanna. Fast Ambipolar Charge Transport in Self-organized Truxene Derivatives, 2nd international symposium on self-organized organic molecular semiconductor, 2014/2, Tokyo institute of technology, Japan. (Oral)

4) **Xuying Liu**, Takayuki Usui, Jun-ichi Hanna. High Electron Mobility in Bay-substituent-induced Columnar Hexaazatrinaphthylenes, CEMS International Symposium on Supramolecular Chemistry and Functional Materials, 2013/11, Tokyo University, Japan. (Poster)

5) **Xuying Liu**, Takayuki Usui, Hiroaki Iino, Jun-ichi Hanna. Colored P-type Semiconductors: Discotic Liquid Crystalline Benzoporphyrin Derivatives, The 111th Annual Conference of the Imaging Society of Japan, 第111回 Japan Imaging Society, Jun. 2013. (Oral)

6) **Xuying Liu**, Takayuki Usui, Jun-ichi Hanna. Synthesis of liquid crystalline Tetrabenzoporphyrins and its charge transport properties, 2012 MRS fall meeting, November 25 – 30, Hynes Convention Center, Boston, MA, USA. (Poster)

7) **Xuying Liu**, Jun-ichi Hanna, High charge carrier mobility in bay-substituted tetrabenzoporphyrin derivatives. G-COE Symposium, 2012, Tokyo Institute of Technology, Tokyo, Japan, May, 2012. (Poster)

Awards

1. 2011.9-2014.9 JASSO scholarship

Acknowledgements

This dissertation doesn't only represent the summary for my research in TIT, and specifically within Hanna-Iino group, but also means a fresh start towards my dream. And also, I am deeply grateful to many nice people for making the time working on my Ph.D. an impressive experience.

First and foremost I have to give my thanks to my advisor Prof. Junichi Hanna. The research supervised by you actually is a real pleasure, which brings me lots of fun and excitement. Hanna sensei also steadily influencs me throughout my PhD course, and orients and supports me with promptness and care, and always encourages me in times of challenges and difficulties; discussions with Hanna sensei frequently gives rise to new insights. Your high scientific standards and hard work set a good example for us. I admire you can make a perfect balance between research interests and personal pursuits, which is quite difficult for others.

I also want to thank Prof. Iino and Prof. Ohno, whose scientific work inspired me a lot. Every time, their thoughtful discussion helped me solve many difficulties met during my study and life. Above all, you made me feel a friend, which I appreciate from my heart. Special thanks and appreciation should be given to Prof. Munekata, Prof. Kajikawa, Prof. Ishikawa and Prof. Shimizu for their important comments and advices for this thesis during my defense.

And then, I greatly appreciate Usui San, Tokayashiki San, Tokoka San, Okamura San and Kuni San for your enormous help and guidance when I met some problems during study and living here throughout these years. They taught me how to use many things in Hanna Lab. and new synthetic methods to prepare my target materials, which promoted my research progress. And I have to give thanks to Nakamura Sensei and Ishigawa San for their consideration about NMR measurement and MS measurement.

In addition, I have been very privileged to get to know and to collaborate with many other great people who became friends over the three years, Wu San, Tao San,

Nitta San, Nakano San, Higuchi San, Zhang San, Matsuto San, Kurosawa San, Kimura San, Matsuno San, Saito San, Izumida San, Yang Kun, Sato Kun, Kudo Kun, Koike Kun, Inoue Kun and Horita Kun. I learned a lot from you about life, research, how to tackle new problems and how to develop techniques to solve them.

Furthermore, I also want to thank Prof. Pu, Prof. Wang, Prof. Zhang (M), Prof. Li, Prof. Zhang (F) and Prof. Wu, who gave me much care and consideration during study in BIGC and TIT. Thank you for your support and encouragement.

I would like to thank Japan Student Services Organization (JASSO) and Global COE (Centers of Excellence) Program for their financial support, which made my study and life in TIT possible.

Last, but not least, I would like to dedicate this thesis to my wife for encouraging me, for her support and the patience. I have to give thanks to my parents and my brothers, for their love, patience, and understanding throughout everything.

Liu Xu-Ying

Suzukakedai Campus

Tokyo Institute of Technology